Paweł Jakuszyk

Differentiating multiple sclerosis and aquaporin-4 antibody-positive neuromyelitis optica spectrum disorders – new insights from non-conventional magnetic resonance imaging

PhD thesis

Completed in the Laboratory of Brain Imaging

of the Nencki Institute of Experimental Biology

Polish Academy of Sciences, Warsaw, Poland

SUPERVISOR:

Dr Maciej Juryńczyk, M.D., Ph.D., D.Sc.

AUXILIARY SUPERVISOR:

Dr Bartosz Kossowski, Ph.D.

Warsaw, 2025

Acknowledgements

During my PhD journey, I have met a lot of wonderful people whose support and contribution to this work should be acknowledged.

First, I would like to thank my supervisors, dr hab. Maciej Juryńczyk and dr Bartosz Kossowski, for giving me the opportunity to expand my scientific horizons and grow within the team we have built over the years. Their constant support and guidance in developing my skills and problem-solving abilities have deeply influenced my perspective, not just on science, but on the world in general.

I would also like to thank all of my colleagues from the Laboratory of Brain Imaging and the Laboratory of Language Neurobiology. The work environment you have created is one of collaboration, inspiration, and mutual respect, which has made this journey all the more enjoyable and enriching.

This chapter of my life has been a rocky road, and I don't think I could have navigated it without my partner, Adrianna. The relationship we have built has been the foundation of my work, helping me through all the twists and turns along the way. Thank you for always being there for me.

I am deeply grateful to my parents, who provided me with the opportunity to learn, explore, and grow. Their sacrifices, belief in my potential, and constant support have shaped who I am today, and I could not have reached this point without their dedication and care. I am forever thankful for everything you have done to help me pursue my dreams.

Lastly, but most importantly, I want to acknowledge all the study participants who dedicated their time and effort to come to the Laboratory of Brain Imaging for a two-hour MRI scan. Without your commitment, none of this would have been possible.

My work was supported by research grants from the Polish National Agency for Academic Exchange ('Polish Returns' programme, PPN/PPO/2020/1/00043/U/00001) and the National Science Centre (providing a research component of the programme 2021/01/1/NZ5/00008).

TABLE OF CONTENTS

ABSTRACT **5**
STRESZCZENIE **7**
LIST OF ABBREVIATIONS **9**
1. INTRODUCTION **11**
1.1. Characterisation of MS and NMOSD 11
1.1.1. Background 11
1.1.2. Epidemiology and demographics 12
1.1.3. Pathophysiology 13
1.1.3.1. Generation of autoimmune response 13
1.1.3.2. Mechanisms of lesion formation 14
1.1.3.3. Chronic active lesions and smouldering inflammation in MS 16
1.1.3.4. Remyelination 16
1.1.3.5. Diffuse white matter damage outside of lesions 17
1.1.4. Disease course and clinical manifestations 20
1.1.4.1. Optic neuritis 21
1.1.4.2. Transverse myelitis 21
1.1.4.3. Brain/brainstem syndromes 22
1.1.5. Blood and cerebrospinal fluid biomarkers 23
1.1.6. Conventional MRI findings 24
1.1.6.1. Brain and optic nerve MRI 24
1.1.6.1.1. White matter lesions 24
1.1.6.1.2. Juxtacortical and cortical lesions 25
1.1.6.1.3. Infratentorial lesions 26
1.1.6.1.4. Optic nerve lesions 26
1.1.6.2. Spinal cord MRI 27
1.1.6.3. Limitations of conventional MRI 29
1.1.7. Treatment 31
1.2. Application of non-conventional MRI to study MS and NMOSD 32
1.2.1. Non-conventional MRI findings 32
1.2.1.1. Brain 32
1.2.1.1.1. Volumetry 32
1.2.1.1.2. T1 relaxometry 33
1.2.1.1.3. Quantitative susceptibility mapping 34
1.2.1.1.4. Diffusion-weighted imaging 35
1.2.1.2. Spinal cord 37
1.2.1.2.1. Volumetry 37
1.2.1.2.2. Diffusion-weighted imaging 38
2. AIMS OF THE WORK **40**

2.1. Rationale for the thesis....40
2.2. Research aims and research questions....40
3. METHODS....41
3.1. Participants....41
3.2. Clinical data acquisition....41
3.3. MRI protocol....41
3.3.1. Brain....42
3.3.2. Cervical spinal cord....42
3.4. MRI data analysis....43
3.4.1. Brain....43
3.4.1.1. Volumetry and lesions assessment....43
3.4.1.2. T1 relaxometry in the cerebral cortex....44
3.4.1.3. Assessment of paramagnetic rim lesions....44
3.4.1.4. Estimation of the NODDI model and lesion-informed tractometry....46
3.4.2. Cervical spinal cord....49
3.4.2.1. Cross-sectional area....49
3.4.2.2. Diffusion tensor imaging....49
3.5. Statistical analysis....50
4. RESULTS....51
4.1. Sample demographics....51
4.2. Analysis of the brain....51
4.2.1. White matter and cortical lesions assessment....51
4.2.2. White matter and grey matter volumetry....53
4.2.3. Lesion-informed tractometry....54
4.2.3.1. NDI differences between MS and AQP4-NMOSD....54
4.2.3.2. NDI differences between MS patients and HC....55
4.2.3.3. NDI differences between AQP4-NMOSD patients and HC....55
4.2.4. Analysis of cortical damage and paramagnetic rim lesions in relation to white matter changes in lesion-free fibres....56
4.3. Analysis of the cervical spinal cord....57
4.3.2. Differences in cross-sectional area....57
4.3.3. Differences in white and grey matter microstructure....58
5. DISCUSSION....59
5.1. Unique cerebrospinal damage patterns in MS and AQP4-NMOSD....59
5.1.1. Assessment of white matter changes in the brain....59
5.1.2. Grey matter abnormalities in the brain....61
5.1.3. The impact of cortical lesions and paramagnetic rim lesions on white matter damage in MS....62
5.1.4. Evaluation of volumetric and microstructural properties in the cervical spinal cord....63
5.2. Strengths and limitations....64

5.3. Future directions.....65
5.4. Concluding remarks..... 66
6. SUMMARY AND CONCLUSIONS.....68
7. REFERENCES..... 70
8. SUPPLEMENTARY MATERIAL.....88
LIST OF FIGURES AND TABLES..... 126
PUBLICATIONS OF THE PhD CANDIDATE..... 127

ABSTRACT

Multiple sclerosis (MS) and neuromyelitis optica spectrum disorders (NMOSD) are distinct autoimmune inflammatory diseases of the central nervous system (CNS), with largely distinct treatment strategies. Both conditions cause recurrent inflammation primarily affecting the optic nerve, spinal cord, and brain. NMOSD is typically associated with aquaporin-4 antibodies (AQP4-IgG) and targets astrocytes, whereas MS is driven by cell-mediated autoreactivity against myelin, leading to demyelination. Diagnosing MS and NMOSD relies heavily on conventional MRI, but overlapping imaging features often complicate differentiation. Although AQP4-IgG detection is the diagnostic gold standard for NMOSD, its availability is limited, and assay sensitivity varies, leading to potential false-negative results. Misdiagnosis remains a challenge, highlighting the need for new, accessible, non-invasive diagnostic tools.

Advanced, non-conventional MRI techniques, such as diffusion-weighted imaging, T1 relaxation rates, quantitative susceptibility mapping, and volumetry, offer deeper insights into CNS pathology by assessing both macro- and microstructural pathological processes, even in regions that appear normal on conventional imaging. This thesis investigates whether such techniques can distinguish relapsing-remitting MS from AQP4-IgG-positive NMOSD (AQP4-NMOSD) by assessing damage in the brain and cervical spinal cord compared to healthy controls.

In the brain, neurite density index (NDI) in white matter tracts was examined, differentiating between lesion-traversing and lesion-free fibres. The cerebral cortex was evaluated based on T1 relaxation rates, identification of cortical lesions, and volumetric analysis. Volumetric analyses were also performed for white matter and deep grey matter. Additionally, in MS, the study explored the relationship between lesion-free white matter fibres and both cortical lesions and paramagnetic rim lesions. In MS, NDI reductions were widespread across both lesion-traversing and lesion-free white matter fibres, along with white matter volume loss. In contrast, AQP4-NMOSD showed NDI reduction only in lesion-traversing fibers and no white matter atrophy. Lower T1 relaxation rates were observed in most cortical regions in MS, but only in a few regions in AQP4-NMOSD. Neither disease showed cortical atrophy, though deep grey matter volume was reduced in MS. Notably, MS exhibited a negative correlation between cortical lesion burden and NDI in

lesion-free white matter fibres, whereas no association was observed with paramagnetic rim lesions.

To assess damage in the cervical spinal cord, cross-sectional area (CSA) and diffusion tensor imaging metrics were used. A significant decrease in CSA was observed in AQP4-NMOSD patients but not in MS patients. Both groups showed a trend toward lower fractional anisotropy in normal-appearing white matter, but no significant differences in grey matter mean diffusivity were found, despite the common presence of spinal cord inflammation in the AQP4-NMOSD group (18/20 AQP4-NMOSD patients had a history of transverse myelitis).

This thesis reveals distinct CNS damage patterns in MS and AQP4-NMOSD. MS exhibits widespread neurodegeneration affecting white matter and cortical/deep grey matter. In contrast, AQP4-NMOSD shows white matter damage most likely originating from axonal disruption by white matter lesions. Additionally, AQP4-NMOSD is marked by extensive cervical spinal cord volumetric changes and potential normal-appearing white matter damage arising from spinal cord attacks. These findings suggest that non-conventional MRI techniques could improve disease differentiation, enhancing diagnostic accuracy. Further validation is necessary before integrating these imaging metrics into clinical practice.

STRESZCZENIE

Stwardnienie rozsiane (SM) i NMOSD (ang. neuromyelitis optica spectrum disorders) to odrębne autoimmunologiczne choroby zapalne ośrodkowego układu nerwowego (OUN) o różnych strategiach leczenia. Powodują nawracające zapalenia nerwów wzrokowych, rdzenia kręgowego i mózgu. NMOSD jest zazwyczaj związane z przeciwciałami przeciw akwaporynie-4 (AQP4-IgG) i prowadzi do uszkodzenia astrocytów, podczas gdy SM wynika z autoreaktywności komórek przeciwko mielinie, prowadząc do demielinizacji. Diagnoza opiera się głównie na konwencjonalnym obrazowaniu metodą rezonansu magnetycznego (ang. magnetic resonance imaging, MRI), lecz nakładające się cechy obrazowe znacznie ją utrudniają. Wykrycie AQP4-IgG jest złotym standardem diagnostycznym NMOSD, jednak dostępność tej metody jest ograniczona, a czułość testów zmienna, co może prowadzić do wyników fałszywie negatywnych. Poprawna diagnoza jest wyzwaniem, co podkreśla potrzebę nowych narzędzi diagnostycznych.

Zaawansowane techniki MRI, takie jak obrazowanie dyfuzyjne (ang. diffusion-weighted imaging), współczynnik relaksacji T1, badanie podatności magnetycznej (ang. quantitative susceptibility mapping) oraz wolumetria, umożliwiają ocenę zmian makro- i mikrostrukturalnych, nawet w obszarach wyglądających na nienaruszone na obrazowaniu konwencjonalnym. W pracy zbadano, czy te techniki mogą odróżnić rzutowo-remisyjne SM od NMOSD z AQP4-IgG (AQP4-NMOSD), analizując uszkodzenia w mózgu i szyjnym odcinku rdzenia kręgowego w porównaniu do grupy kontrolnej.

W mózgu oceniono indeks gęstości neurytów (ang. neurite density index, NDI) w włóknach istoty białej przechodzących przez zmiany oraz wolnych od zmian. Zbadano korę mózgową za pomocą współczynnika relaksacji T1, obecności zmian korowych oraz wolumetrii. Przeprowadzono także analizę wolumetrii istoty białej oraz głębokiej istoty szarej. Dodatkowo, w SM, zbadano związek między włóknami istoty białej wolnymi od zmian a zarówno zmianami korowymi, jak i zmianami z rąbkiem paramagnetycznym. W SM, NDI było obniżone w włóknach istoty białej przechodzących przez zmiany oraz wolnych od zmian, a także zaobserwowano utratę objętości istoty białej. Natomiast w AQP4-NMOSD obniżone NDI zostało zaobserwowane tylko w włóknach przechodzących przez zmiany, bez atrofii istoty białej. Niższe współczynniki relaksacji T1 zaobserwowano w większości obszarów korowych w SM, ale tylko w nielicznych w AQP4-NMOSD. Żadna z chorób nie

wykazała zmian objętości kory mózgowej, choć objętość głębokiej istoty szarej była obniżona w SM. Co istotne, w SM zaobserwowano negatywną korelację między liczbą zmian korowych a NDI w włóknach istoty białej wolnych od zmian, podczas gdy nie stwierdzono takiej zależności w przypadku zmian z rąbkiem paramagnetycznym.

Aby ocenić uszkodzenia w szyjnym rdzeniu kręgowym, zastosowano pomiar wolumetryczny (ang. cross-sectional area, CSA) i obrazowanie za pomocą tensora dyfuzji. Zaobserwowano spadek CSA u pacjentów z AQP4-NMOSD, ale nie u pacjentów z SM. Obie grupy wykazały tendencję do niższej anizotropii frakcyjnej w normalnie wyglądającej istocie białej. Nie stwierdzono różnic w średniej dyfuzyjności w istocie szarej, pomimo obecności stanu zapalnego rdzenia kręgowego w grupie AQP4-NMOSD (18/20 pacjentów z AQP4-NMOSD miało historię zapalenia rdzenia).

Praca ta ukazuje różne wzorce uszkodzeń OUN w SM i AQP4-NMOSD. SM wykazuje rozległą neurodegenerację, która dotyczy istoty białej, kory mózgowej i głębokiej istoty szarej. AQP4-NMOSD pokazuje uszkodzenia istoty białej, najprawdopodobniej wynikające z uszkodzenia aksonów przez zmiany w istocie białej. Dodatkowo AQP4-NMOSD charakteryzuje się rozległymi zmianami objętości szyjnego rdzenia kręgowego oraz potencjalnymi uszkodzeniami normalnie wyglądającej istoty białej wynikającymi z zapalenia rdzenia. Wyniki sugerują, że niekonwencjonalne techniki MRI mogą poprawić różnicowanie tych chorób, zwiększając dokładność diagnostyczną. Dalsza weryfikacja jest niezbędna przed wdrożeniem tych metryk do praktyki klinicznej.

LIST OF ABBREVIATIONS

AD – axial diffusivity

AQP4 – aquaporin-4

BBB – blood-brain barrier

CNS – central nervous system

CSF – cerebrospinal fluid

DIR – double inversion recovery

DTI - diffusion tensor imaging

DWI – diffusion-weighted imaging

EDSS – expanded disability status scale

ETIV – estimated total intracranial volume

FA – fractional anisotropy

FLAIR – fluid-attenuated inversion recovery

HC – healthy controls

IgG – immunoglobulin G

IL-6 – interleukin 6

ISO – isotropic volume fraction

LETM – longitudinally extensive transverse myelitis

MD – mean diffusivity

MEDIC – multi-echo data image combination

MOGAD – myelin oligodendrocyte glycoprotein antibody-associated disease

MP2RAGE – magnetisation prepared 2 rapid acquisition gradient echo

MPRAGE – magnetisation prepared rapid acquisition gradient echo

MRI – magnetic resonance imaging

MS – multiple sclerosis

NAWM – normal-appearing white matter

NDI – neurite density index

NMO – neuromyelitis optica

NMOSD – neuromyelitis optica spectrum disorders

NODDI – neurite orientation density and dispersion imaging

ODI – orientation dispersion index

ON – optic neuritis

ppb - parts per billion

PRL – paramagnetic rim lesions

PSIR – phase-sensitive inversion recovery

QSM – quantitative susceptibility maps

RD – radial diffusivity

SWI –susceptibility-weighted imaging

TM – transverse myelitis

1. INTRODUCTION

1.1. Characterisation of MS and NMOSD

1.1.1. Background

Multiple sclerosis (MS) and neuromyelitis optica spectrum disorders (NMOSD, previously termed neuromyelitis optica, NMO, or Devic's disease) are distinct autoimmune inflammatory demyelinating diseases of the central nervous system (CNS), which typically present with acute attacks of optic neuritis (ON), transverse myelitis (TM) and brain/brainstem inflammation (Juryńczyk et al., 2015). MS, which is more common, was first described in 1838 by a French physician, Jean Martin Charcot, who reported the clinical features of MS in association with disseminated pathological lesions found post-mortem and termed it *la sclérose en plaques* (sclerosis in scattered patches; Charcot & Oliver, 1876). In 1894, another French physician, Eugène Devic, reported a case of a female patient with severe bilateral ON followed by severe TM and death. He referred to the condition as *neuro-myélite optique aiguë* (acute neuromyelitis optica; Jarius & Wildemann, 2013). Based on pathological findings, Devic discussed the relationship of his case with MS, at the same time recognising its unique features, such as the simultaneous ON and TM and the lack of significant cerebral involvement (Jarius & Wildemann, 2013). Following this initial report, NMO was subsequently considered a severe variant of MS, with a particular predilection for involving the optic nerves and spinal cord (Mandler, 2006). The classical NMO phenotype consisted of severe simultaneous or sequential bilateral ON and TM, but further reports described patients who had a milder clinical course, unilateral ON, or ON and TM separated by months or years. After the introduction of MRI to clinical practice, it has been recognised that TM in NMO is characterised by a lesion continuously spanning at least three segments of the spinal cord (longitudinally extensive transverse myelitis, LETM), which is distinct from short-segment lesions observed in MS (Fazekas et al., 1994). A critical milestone in the history of NMO occurred in 2004 when Vanda Lennon and colleagues from Mayo Clinic, Rochester, Minnesota, discovered that approximately 70% of patients with NMO had serum antibodies binding to mouse brain in a characteristic perivascular pattern (Lennon et al., 2004), which subsequently have been identified to be directed against the water channel aquaporin-4 expressed on astrocytic foot processes (Lennon et al., 2005). The high specificity

of serum antibodies against AQP4 facilitated the expansion of the NMO spectrum to include specific forms of the disease, such as isolated ON, isolated TM, and brain or brainstem syndromes. To reflect this broadening, the term NMOSD (NMO spectrum disorders) was introduced (Wingerchuk et al., 2007). By 2015 consensus, the terms NMOSD and NMO have become unified and include both AQP4-IgG positive (AQP4-NMOSD) and AQP4-IgG negative patients as well as patients with unknown AQP4-IgG status for whom serologic testing is currently unavailable (Wingerchuk et al., 2015).

Since MS and NMOSD were first described, considerable advances have been made in understanding the pathogenesis, diagnosis, and treatment of these diseases. This chapter will outline the current state of knowledge on the epidemiology, pathological mechanisms, clinical symptoms, diagnosis, and treatment of MS and NMOSD, emphasising their differences, which may inspire further progress in optimising differential diagnosis. Given that the main focus of this thesis is to implement non-conventional magnetic resonance imaging (MRI) to identify *in vivo* differences between the two diseases relevant to their distinct pathology in the brain and the spinal cord, this section will also delineate MRI techniques previously used to study pathology in MS and NMOSD, their pitfalls and potential ways to overcome them that have been implemented in this thesis. Lastly, the rationale for the thesis and the primary research goals will be defined.

1.1.2. Epidemiology and demographics

According to a global report by Walton et al. (2020), MS is the most common inflammatory/demyelinating disease of the CNS. Approximately 2.8 million people are estimated to have MS worldwide, with a prevalence of 35.9 per 100,000 population. Over the past decade, the prevalence of MS has increased across all world regions. The combined incidence rate from data reported by 75 countries is 2.1 per 100,000 persons per year. The median age of disease onset is 23 to 24 years, with the initial symptoms rarely manifesting before the age of 10 or after the age of 60 (Walton et al., 2020). Women exhibit a twofold higher likelihood of having MS compared with men (Louis et al., 2021).

Before the discovery of AQP4-IgG, epidemiological reports likely underestimated the number of NMOSD cases due to reliance on inadequate diagnostic criteria, leading to worldwide inconsistencies in classification and terminology (Louis et al., 2021). The most

recent international diagnostic criteria (Wingerchuk et al., 2015) have almost doubled the frequency of NMOSD cases as it has allowed for the diagnosis in all AQP4-IgG positive patients, including those with single and isolated attacks. Additionally, screening cases previously diagnosed as MS can now further increase the number of NMOSD cases because of individuals for whom this diagnosis was not previously considered (Louis et al., 2021). A recent report by Hor et al. (2020) states that the prevalence of NMOSD ranges between 0.5 to 4 per 100,000 worldwide, while the incidence is estimated to be around 0.5 to 0.8 new cases per million population per year. Significantly, Asian and black populations are disproportionately affected, with the prevalence in the latter being up to 11.5 per 100,000 population and incidence as high as 7.3 per million. AQP4-NMOSD has a female-to-male ratio of 9 to 1, and its mean age of onset is around 40 years (Hor et al., 2020), which is approximately 10 years older than MS (see Table 1). Nevertheless, AQP4-NMOSD can manifest at any age, with around 4% of cases occurring in children and around 30% in individuals older than 50 (Louis et al., 2021).

1.1.3. Pathophysiology

1.1.3.1. Generation of autoimmune response

MS is a chronic inflammatory disease of the CNS, which is considered to be driven by an autoimmune response directed against myelin. Key myelin proteins, including myelin basic protein, proteolipid protein, and myelin oligodendrocyte glycoprotein, have been proposed as primary autoantigen targets, though their precise roles in disease pathogenesis remain unclear (Dendrou et al., 2015). The immune response is primarily mediated by activated proinflammatory T cells, which migrate across the blood-brain barrier (BBB) and initiate a pathogenic immune response, releasing proinflammatory cytokines, activating resident microglia, and recruiting additional immune cells, ultimately leading to demyelination and axonal damage (Lassmann, 2006). While the role of B-cells in the formation of the autoimmune response in MS has not been fully elucidated, their contribution to MS pathophysiology has been increasingly recognised as crucial. They are thought to advance disease progression through antibody-independent mechanisms, including antigen presentation to T cells, secretion of pro-inflammatory cytokines, and participation in lymphoid structures in the meninges (Comi et al., 2020). Additionally, clinical trials of B-cell depleting therapies, such as anti-CD20 antibodies, have demonstrated their significant

efficacy in reducing disease activity and relapses, further highlighting the essential role of B cells in MS pathogenesis (Hauser et al., 2017; Montalban et al., 2017).

Unlike MS, which is considered a cell-mediated autoimmune disease, AQP4-NMOSD is an antibody-mediated disease with AQP4-IgG being the dominant pathogenic antibody responsible for initiating the autoimmune reaction (Lennon et al., 2004). AQP4-specific immune response is likely generated in the peripheral immune system. The production of AQP4-IgG by B cells is stimulated by interleukin 6 (IL-6), which promotes B cell differentiation into antibody-producing plasmablasts, enhances antibody production, and supports the survival of pathogenic B cells (Bennett et al., 2009). The AQP4-IgG enters the CNS through the BBB, which is thought to be disrupted by AQP4-specific T cells and pro-inflammatory cytokines, or through the cerebrospinal fluid-brain barrier (CSF-brain barrier) at highly permeable sites, including the area postrema (Papadopoulos & Verkman, 2012; Wingerchuk et al., 2015). Since AQP4 is the primary water channel protein in the CNS, with the highest concentration in perivascular and subpial astrocyte foot processes (Vandebroek & Yasui, 2020), its loss due to autoimmune attack disrupts water homeostasis (Gleiser et al., 2016). Furthermore, the binding of the AQP4-IgG triggers a cascade of destructive processes, including complement activation and antibody-mediated cytotoxicity (Hinson et al., 2007). In addition, pro-inflammatory infiltrates, including activated microglia, T cells, and macrophages, contribute to the inflammatory cascade, further exacerbating tissue injury (Jarius et al., 2014). Previously perceived as a primarily demyelinating disease like MS, NMOSD is now recognised as an autoimmune astrocytopathy characterised by patterns of astrocyte damage, dysfunction and loss, which results in secondary demyelination and neurodegeneration (see Figure 1 for a graphical representation of different pathophysiological mechanisms in MS and NMOSD; Carnero & Correale, 2021).

1.1.3.2. Mechanisms of lesion formation

The inflammatory infiltrate within MS white matter lesions primarily includes T cells (both CD4+ and CD8+), B cells, plasma cells, macrophages, and activated microglia (Dendrou et al., 2015). Initially, the inflammatory process starts around postcapillary venules and veins, leading to perivenous demyelinated plaques, which eventually fuse together to form confluent lesions (Barnett & Prineas, 2004). Moreover, myelin-reactive cells in MS lead to the destruction and loss of oligodendrocytes, which causes almost complete loss of myelin with

relative preservation of axons (Kutzelnigg et al., 2005). Apart from white matter lesions, which are the most typical of MS pathology, MS is also characterised by cortical demyelination, which can form in two different ways. Some cortical lesions develop similarly to white matter lesions and form around veins with inflammatory infiltrates, including T cells, B cells, macrophages, and microglia, contributing to local tissue damage (Peterson et al., 2001). Other cortical lesions are likely caused by a CSF soluble factor possibly produced by B cell follicles (Howell et al., 2011). Rather than being intracortical, these lesions are located in the subpial cortex in the proximity of the CSF (Dendrou et al., 2015). Acute active lesions in MS are associated with ongoing, active demyelination and represent the pathologic basis of clinical attack (Filippi et al., 2019). Perivascular and parenchymal inflammatory lymphocyte infiltrates are present in the acute active lesions as well as macrophages recruited to phagocyte myelin debris from destroyed myelin sheaths (Popescu et al., 2013). Oligodendrocyte injury in acute lesions is still considered variable, with both early destruction and relative preservation, and signs of simultaneous remyelination are present (Brück et al., 1995). Despite relative axonal sparing, axonal injury is evident during active inflammatory demyelination and is associated with attack-related disability accumulation (Popescu & Lucchinetti, 2012).

Lesions in NMOSD are distinct from MS (due to complement activation) and contain inflammatory infiltrates consisting primarily of B lymphocytes and macrophages, with relatively small involvement of T lymphocytes (Hinson et al., 2007). Interestingly, unlike MS, NMOSD lesions often contain granulocytes, including eosinophils and neutrophils, which are likely attracted by degradation products from severe inflammation (Huda et al., 2019). These cells exacerbate tissue damage through the release of cytotoxic enzymes and reactive oxygen species. Almost all NMOSD lesions, irrespective of their location or stage of development, are characterised by considerable loss of AQP4 immunoreactivity, which occurs in areas with extensive vasculocentric complement deposition (Misu et al., 2007). However, some lesions associated with clinical recovery in NMOSD do not exhibit immunopathological markers of terminal complement activation despite showing evidence of AQP4 immunoreactivity loss (Kawachi & Lassmann, 2017). It is hypothesised that within these lesions, AQP4-IgG binding triggers the internalisation of AQP4 channels on astrocyte foot processes, disrupting water homeostasis and potentially causing transient dysfunction without sustained complement activation (Misu et al., 2013). This mechanism may contribute

to the observed recovery, as internalised AQP4 may be restored over time. Unlike in MS, cortical lesions are very rarely present in NMOSD patients (Wingerchuk et al., 2015). If present, they are characterised by widespread neuronal loss in cortical layers II to IV as well as loss of AQP4 immunoreactivity on astrocytes in layer I with the absence of complement deposition, microglia activation, and meningeal inflammation (Kawachi & Lassmann, 2017). Neuronal loss in the cortical grey matter of NMOSD patients is partly attributed to anterograde or retrograde axonal degeneration resulting from acute NMOSD lesions or could represent a result of the loss of trophic support following astrocyte damage (Saji et al., 2013).

1.1.3.3. Chronic active lesions and smouldering inflammation in MS

During the course of the disease, active MS lesions can follow different trajectories: they may become inactive, exhibiting a variable degree of microglia activation and reactive gliosis, or they may become chronically active (Lassmann, 2018). Chronic active MS lesions are characterised by a dense presence of activated microglia and macrophages containing myelin degradation products rich in iron. These products are concentrated at the lesion edges and diminish toward the inactive centre. Their presence is a key feature of chronic active lesions, allowing for their identification by MRI, as will be discussed in the section on non-conventional MRI methods. In these so-called smouldering lesions, perivascular proinflammatory infiltrates are present despite the BBB appearing intact, allowing inflammation to persist behind the closed BBB (Popescu et al., 2013). Chronic active lesions are typical of MS (Lassmann, 2018). A recent meta-analysis by Kwong et al. (2021) estimates that the prevalence of chronic active lesions ranges from 47.6% to 88.2% at the patient level and from 2.3% to 41.0% at the level of individual lesions. Smouldering inflammation has not been reported in NMOSD; therefore, its identification strongly points toward MS pathology (Kawachi & Lassmann, 2017).

1.1.3.4. Remyelination

Remyelination is the process through which new myelin sheaths are formed around axons after damage, primarily through the activity of oligodendrocyte precursor cells (Franklin & Ffrench-Constant, 2008). In demyelinating diseases like MS and NMOSD, remyelination is a critical process as it may restore conduction velocity, protect axons from degeneration, and promote functional recovery (Chang et al., 2002). In the early stages of MS, remyelination

often occurs effectively, leading to partial recovery of nerve function (Chari, 2007). However, in chronic MS lesions, remyelination is often incomplete or fails due to inflammation, glial scar formation, and a loss of oligodendrocyte precursor cells' function or recruitment (Kuhlmann et al., 2008). Clinical trials of myelin regeneration in MS have mainly focused on patients with ON, as remyelination in the optic nerve can be accurately quantified using visual evoked potentials and optical coherence tomography (Lubetzki et al., 2020). The trials conducted so far have shown promising results; however, developing remyelination therapies for MS is still ongoing, and further validation is needed (Cadavid et al., 2017; Green et al., 2017).

In NMOSD, remyelination is also typically ineffective and may be inhibited by astrocytopathy, which has been shown to induce changes in microglial morphology, leading to an inflammatory state that can inhibit remyelination (Luo et al., 2023; Yao et al., 2016). Other processes that likely hinder remyelination in NMOSD include oligodendrocyte apoptosis and the ineffective differentiation of oligodendrocyte precursor cells into mature oligodendrocytes (Wrzos et al., 2014). The targeting of oligodendrocyte precursor cell differentiation to generate mature myelinating oligodendrocytes and restore myelin sheaths is considered pivotal for successful remyelination in both MS and NMOSD (Luo et al., 2023).

1.1.3.5. Diffuse white matter damage outside of lesions

Widespread diffuse tissue injury in brain and spinal cord non-lesional white matter is an essential feature of MS pathology. It is characterised by extensive microglia activation, axonal swelling, and neurodegeneration (Kawachi & Lassmann, 2017). Although non-lesional white matter injury is in part thought to originate from anterograde and retrograde neurodegeneration (Dziedzic et al., 2010), it is not only caused by white matter lesions, as it does not appear to be significantly related to white matter lesion load (Kutzelnigg et al., 2005). Another possible mechanism contributing to non-lesional white matter damage in MS is the presence of cortical lesions, where oxidative damage has been linked to oligodendrocyte and neuronal injury, with the latter also impacting axons and dendrites (Fischer et al., 2013). Additionally, studies have demonstrated that meningeal inflammation strongly correlates with diffuse degeneration in non-lesional white matter (Androdias et al., 2010; Haider et al., 2016). These results suggest that cortical damage may play a significant role in driving widespread tissue injury beyond visible lesions.

While it is currently understood that damage in NMOSD is solely secondary to acute attacks, it is still being investigated whether NMOSD is associated with subclinical or non-attack-related pathology, including non-lesional white matter degeneration (Kawachi & Lassmann, 2017). Recent studies have identified dystrophic changes in Müller cells within the retina independent of ON episodes (Oertel et al., 2017; You et al., 2019). Moreover, neurodegeneration in AQP4-deficient regions, such as myelin-preserved periplaque white matter, suggests that demyelination is not essential for neurodegeneration in NMOSD. Abnormalities in astrocytic glutamate transporters and N-methyl-D-aspartate receptor subunits have been observed in AQP4-depleted areas, even with intact myelin, highlighting glutamate imbalance as a key driver of glial-neuronal interactions and neurodegeneration (Hinson et al., 2008). An additional mechanism likely to result in non-lesional white matter injury is anterograde and retrograde degeneration of axons following their transection by lesions (Hokari et al., 2016; Misu et al., 2013). Nevertheless, there appears to be no concrete pathophysiological evidence that non-lesional white matter damage is present in NMOSD, and a direct comparison between MS and NMOSD, analysing the severity of this disease mechanism, is still missing (Kawachi & Lassmann, 2017).

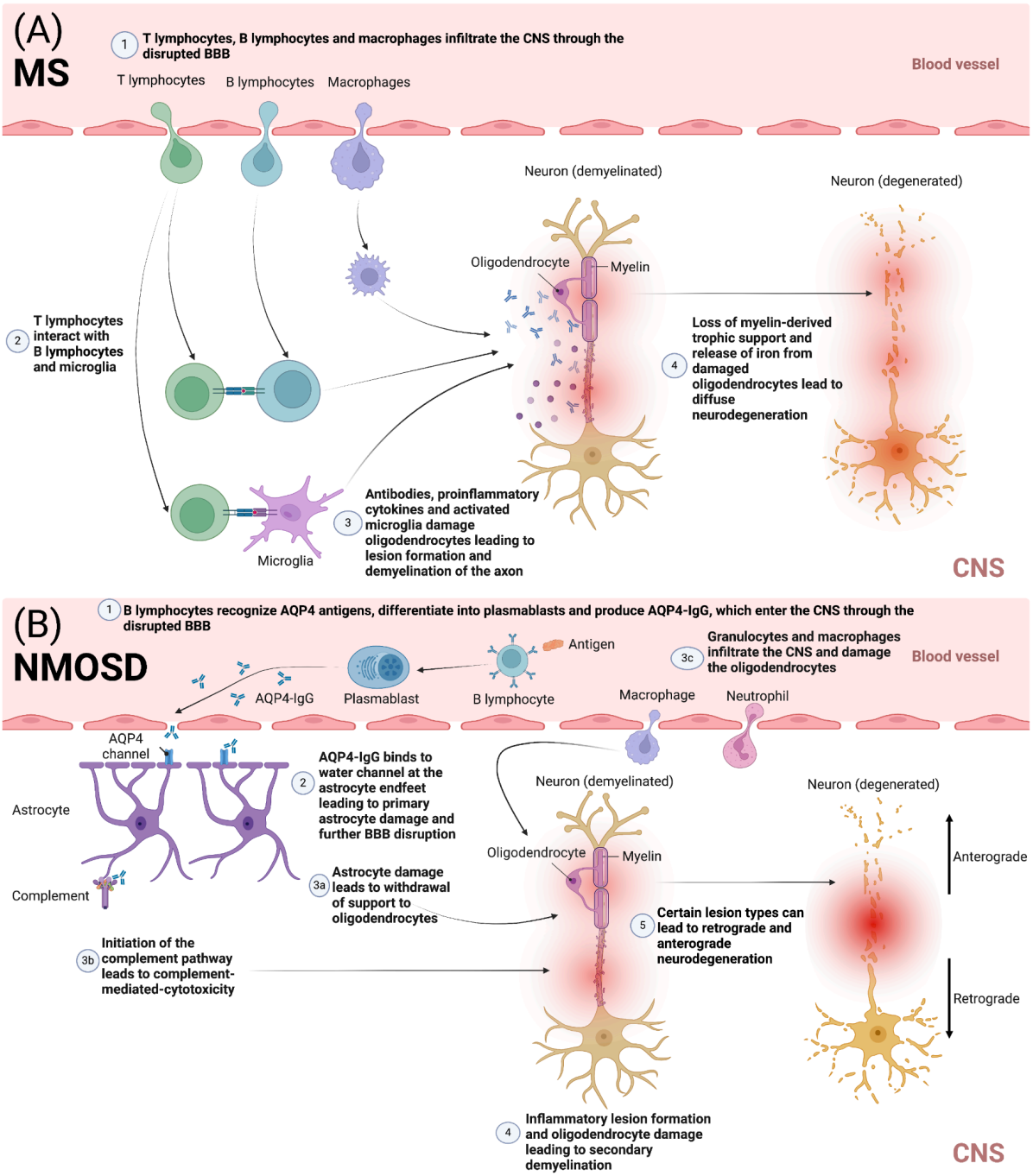

Figure 1. Graphical representation of different pathophysiological mechanisms in MS and NMOSD. (A) In MS, the autoreactive T and B lymphocytes and macrophages infiltrate the CNS through disrupted BBB and cause damage to oligodendrocytes, leading to demyelination and subsequent neurodegeneration. (B) In NMOSD, the B lymphocytes secrete AQP4-IgGs, which disrupt astrocyte functions, leading to their damage, further BBB disruption, complement-mediated cytotoxicity, and proinflammatory infiltrates entering the CNS. This causes secondary demyelination and leads to retrograde and anterograde neurodegeneration. (Original figure created with BioRender.com); MS = multiple sclerosis; NMOSD = neuromyelitis optica spectrum disorders; CNS = central nervous system; BBB = blood brain barrier; AQP4 = aquaporin-4; IgG = immunoglobulin G.

1.1.4. Disease course and clinical manifestations

Most MS patients initially present with acute attacks, typically characterised by good or complete recovery and separated by periods of remission (relapsing-remitting MS, RRMS). These patients might eventually transition into a secondary-progressive MS (SPMS) phase, marked by a gradual accumulation of disability, with or without acute exacerbations. Natural history studies indicate that the rate of progression of RRMS to SPMS is over 50% within 10 years and approximately 90% within 25 years if left untreated (Barzegar et al., 2021). Approximately 15% of MS patients begin the disease with a progressive course known as primary progressive MS (PPMS). Disability progression in PPMS occurs in the absence of relapses from the onset; however, it is not considered pathophysiologically distinct from SPMS (Lublin et al., 2014). The progressive phase is considered highly atypical of NMOSD, which is characterised by a purely relapsing course. While some patients might have a single attack due to a milder disease course, short disease duration, or effective attack-preventing treatment, the disease is always considered as potentially relapsing and requires long-term treatment (Wingerchuk et al., 2015).

While MS attacks can result in inflammation in various regions of the brain, brainstem, cerebellum, optic nerve and spinal cord, NMOSD predominantly affects the optic nerve and the spinal cord, with brain/brainstem attacks being less common and occurring in NMOSD-typical high AQP4 expression sites, such as periependymal, periventricular areas (Juryńczyk et al., 2015). Compared with MS, NMOSD attacks tend to be more severe and can lead to permanent disability, such as blindness or severe motor impairment, even with a single attack (Mealy et al., 2019). A joint UK and Japanese study found that after a median disease duration of 75 months, 18% of studied patients had developed a permanent bilateral visual disability, 34% had a permanent motor disability, 23% had become wheelchair-bound, and 9% had died (Kitley et al., 2012a). Another study reported that in NMOSD, mortality ranges from 9% to 32% and is primarily attributed to respiratory failure in the context of myelitis located in the cervical segment of the spinal cord (Mealy et al., 2018). In NMOSD, neurologic disability typically accumulates with each attack, which makes appropriate and early intervention essential to lessen the severity of an NMOSD relapse and substantially reduce attack-related disability accumulation (Tackley et al., 2016). In MS, the attacks tend to be milder and associated with better recovery (Louis et al., 2021), while disability mainly progresses independently of relapse activity (progression independent of relapse activity),

resulting in a gradual build-up of disability occurring silently between relapses and later (Tur et al., 2023). As stated above, this type of disability progression between attacks does not typically occur in NMOSD and is considered a red flag for the diagnosis (Louis et al., 2021).

Clinical disability in MS is commonly assessed using the Expanded Disability Status Scale (EDSS), a tool developed by Kurtzke to evaluate neurological impairment in MS (Kurtzke, 1983). The EDSS assesses the severity of disability through a comprehensive neurologic examination, focusing on several functional systems, including pyramidal, cerebellar, brainstem, sensory, bladder, visual, and cognitive functions. The scale ranges from 0 (no disability) to 10 (death due to MS), with incremental steps indicating increasing levels of disability. In NMOSD, EDSS serves a similar function in tracking disease progression, as currently, no specific scales exist to assess NMOSD-related disability (Levy et al., 2022).

1.1.4.1. Optic neuritis

ON typically presents with retrobulbar pain associated with visual loss, which is a common presentation in both MS and NMOSD. ON is the first attack in about 20% of MS patients and 64% of NMOSD patients (Balcer, 2006; Jurynczyk et al., 2017). ON attacks in NMOSD are usually more severe when compared with MS-related ON and are associated with poor recovery (Huda et al., 2019). A study by Jiao et al. (2013) estimated that at 5 years from the disease onset, 41% of AQP4-NMOSD patients are blind in either eye and 9% in both eyes. In contrast, in MS, the (2008) study regarding the ON Treatment Trial reported that 77% of MS patients maintained a visual acuity of at least 6/6 even after 15 years following an episode of acute unilateral ON, with only 2 out of 294 patients experiencing a visual acuity below 6/12. Isolated simultaneous bilateral optic neuritis represents another feature predominantly linked with NMOSD, rarely observed in MS. Research on NMOSD indicates that bilateral manifestations at the onset occur in approximately 6–8% of AQP4-NMOSD patients, and it may develop at any point in up to 20% of cases (Jarius et al., 2012). Conversely, in an investigation focusing on the incidence of ON in MS, only 2 out of 472 patients were identified with bilateral presentation (see Table 1; Burman et al., 2011).

1.1.4.2. Transverse myelitis

Inflammation of the spinal cord is most frequently seen in the cervical and thoracic spine segments in both MS and NMOSD (Louis et al., 2021). However, TM presentation in

NMOSD is distinct and more severe than in MS (Wingerchuk et al., 1999). Spinal cord involvement in NMOSD is typically characterised by longitudinally extensive lesions that span more than three contiguous vertebral segments (Ciccarelli et al., 2019). LETM is considered a hallmark of NMOSD (see Table 1) and is thought to be a major cause of severe disability accumulation, which often presents as para- or tetraplegia depending on which spinal cord segment was involved (Huda et al., 2019). In the acute phase, TM in NMOSD can lead to a median EDSS score of 7, which indicates that a patient can no longer walk more than 5 meters without the aid and is essentially restricted to a wheelchair (Cacciaguerra & Flanagan, 2024; Kurtzke, 1983). TM in MS typically affects less than two contiguous vertebral segments (Bot et al., 2004). Only up to 3% of MS patients may present with LETM, and its presence is considered a significant red flag for the diagnosis of MS (Kitley et al., 2012b). Consistent with the greater severity of spinal cord pathology observed in NMOSD compared with MS, patients with NMOSD experience worse motor and sensory outcomes and require assistance with ambulation at earlier disease stages (Juryńczyk et al., 2015).

1.1.4.3. Brain/brainstem syndromes

Brain attacks are typical for MS and less common in NMOSD, which classically is a disease of the optic nerve and the spinal cord (Louis et al., 2021). MS brain attacks may present with a wide spectrum of symptoms, including hemiparesis, sensory loss, and cerebellar symptoms, including tremor, ataxia, or dysarthria (Wilkins, 2017). While MS attacks predominantly affect the white matter around the lateral ventricles, NMOSD attacks typically occur in regions with high AQP4 expression (see Table 1), including periependymal areas around the third and fourth ventricles (such as the area postrema and hypothalamus) and the aqueduct of Sylvius (Pittock et al., 2006). Area postrema syndrome, characterised by unexplained, persistent hiccups, nausea, or vomiting, is often associated with lesions in the dorsal medulla and affects approximately 20% of NMOSD patients at disease onset and up to 40% over the disease course (Louis et al., 2021). Similar to LETM, area postrema syndrome is a hallmark of NMOSD and is not typically observed in MS (Qiu et al., 2011). Interestingly, while AQP4 is also highly expressed in the cerebellum, cerebellar attacks are rare in NMOSD, which indicates that AQP4 expression patterns in the brain do not fully explain the location of lesions (Kermode, 2008). A more detailed description of the topology and characteristics of brain and brainstem, and spinal cord lesions in MS and NMOSD will be presented in the subchapter, which is related to conventional MRI findings.

1.1.5. Blood and cerebrospinal fluid biomarkers

While MRI is the most important diagnostic tool in MS, CSF examination can also provide valuable insights, as IgG abnormalities are common. More than 95% of patients exhibit oligoclonal bands on CSF gel electrophoresis (Louis et al., 2021). However, it is worth noting that oligoclonal bands are not specific to MS and can be observed in up to 30% of patients with other neurological inflammatory diseases, including NMOSD (see Table 1; Wingerchuk et al., 2007). The revised 2017 McDonald criteria have facilitated early detection of MS by incorporating CSF oligoclonal bands testing as markers of disease progression over time (McNicholas et al., 2019).

In NMOSD, AQP4-IgG detected in the patient's serum serves as a sensitive (~70%) and highly specific (~100%) biomarker (Jeyalatha et al., 2022). A cell-based assay, whether fixed or live, is the most accurate method for its detection (Waters et al., 2016). The detection of AQP4-IgG has become an integral part of the diagnostic process as reflected by the current criteria by Wingerchuk et al. (2015), which stratify the diagnosis into AQP4-NMOSD patients and patients who were either AQP4-IgG negative or with unknown serostatus. It is commonly accepted that AQP4-IgG negative NMOSD patients are a highly heterogeneous cohort, likely composed of different distinct diagnoses involving atypical MS and NMOSD mediated by yet undiscovered antibodies (Juryńczyk et al., 2022). In those patients, diagnosis presents significant challenges, as evidenced by the high level of disagreement among experts when evaluating individual cases (Juryńczyk et al., 2016).

Notably, the test for AQP4-IgG is currently the gold standard for NMOSD diagnosis. However, the most recent report by Holroyd et al. (2019), which assessed the assay's availability in 60 participating countries from all WHO world regions, states that low-income countries had poor availability of the assay compared with high-income countries and that 48% of African and Eastern Mediterranean countries had no access to the test at all. Additionally, it has been reported that antibody levels may decline during periods of NMOSD remission and that different types of antibody assays have variable sensitivity and can produce false-negative results (Waters et al., 2012). As evidenced, the diagnosis of NMOSD is highly reliant on serologic testing; however, due to significant variability in the availability and quality of these tests, it is not possible to differentiate MS from NMOSD based on serologic testing alone.

1.1.6. Conventional MRI findings

The diagnosis of MS and NMOSD is critically reliant on MRI, which serves as a cornerstone for identifying characteristic lesion patterns and distributions, alongside clinical evaluation, CSF/blood analysis, and the exclusion of mimicking conditions (Louis et al., 2021). Current MS diagnostic criteria (2018) focus on the importance of two crucial elements in MS diagnosis (i.e., dissemination in space and time). Dissemination in space describes the involvement of at least two anatomically different CNS locations, illustrating a multifocal process. On the other hand, dissemination in time denotes that disease activity is recurring and exacerbations/relapses have occurred at different dates. Dissemination in time and space can be demonstrated using MRI, with dissemination in time being evident with one new T2 or contrast-enhancing lesion on any follow-up scan or the presence of both contrast-enhancing and non-enhancing lesions at any time. Dissemination in space is characterised by one or more T2 lesions in at least two of four specified areas (i.e., periventricular, juxtacortical or cortical, infratentorial, spinal cord).

In NMOSD, the most recent criteria by Wingerchuk et al. (2015) state that in AQP4-NMOSD patients, only a single core clinical characteristic (e.g., ON, TM, area postrema syndrome, or brainstem syndrome) is necessary for the diagnosis. For diagnosing patients negative for AQP4-IgG or those with undetermined serostatus, a minimum of two core clinical characteristics manifesting in at least two distinct regions are required (Wingerchuk et al., 2015). Additionally, one of these characteristics must include ON, LETM, or area postrema syndrome (Wingerchuk et al., 2015). MRI plays a crucial role in supporting these clinical criteria by providing detailed imaging of the affected regions, which can help distinguish NMOSD from other conditions (Kim et al., 2015).

1.1.6.1. Brain and optic nerve MRI

1.1.6.1.1. White matter lesions

Brain lesions are present in more than 95% of MS patients (Louis et al., 2021) and in approximately 50% to 89% of AQP4-NMOSD patients (Kim et al., 2015). MRI sequences used for clinical evaluation in MS and NMOSD primarily include T1-weighted, T2-weighted, fluid-attenuated inversion recovery (FLAIR), and contrast-enhanced sequences (Geraldes et al., 2018). Focal lesions are typically identified by hyperintensity on T2-weighted/FLAIR

images and, if acute, appear as contrast-enhanced foci on T1-weighted images (Filippi et al., 2019).

MS brain lesions are typically round or ovoid, well-demarcated, with asymmetric distribution in both cerebral hemispheres (Filippi et al., 2019). They are located in the periventricular, juxtacortical, cortical, and infratentorial regions. Periventricular MS lesions adjacent to the lateral ventricles (see Figure 2A) usually follow the path of deep medullary veins, resulting in their primary orientation being perpendicular to the lateral ventricles (Filippi et al., 2016). These lesions typically have an ovoid shape when viewed on the axial plane and are commonly referred to as *Dawson's fingers* (see Figure 2B), a term derived from Dawson's original pathological characterisation (see Table 1; Dawson, 1916). Most lesions in MS are centred around a vein, which can be detected by overlaying T2/FLAIR images and susceptibility-weighted imaging (SWI) sequences, providing good contrast from the veins (Sati et al., 2016). These lesions, known as the central vein sign, are commonly observed in periventricular areas and are a distinguishing MRI feature of MS. They are characterised by a small vein centrally located within white matter lesions, reflecting perivenular inflammation.

Brain lesions in NMOSD can be both nonspecific and specific. Nonspecific lesions typically appear as dot-like or patchy lesions, are less than 3 cm in diameter, and are usually located in the deep white matter, brainstem, or cerebellum (Kim et al., 2010). Lesions typical of NMOSD occur primarily during the acute cerebral attacks and include periependymal lesions surrounding the lateral ventricles (see Figure 3A), extensive hemispheric lesions (see Figure 3B), and long corticospinal tract lesions (see Table 1; Kim et al., 2015; Kim et al., 2012). NMOSD lesions usually lack the central vein sign. A recent study evaluating the diagnostic performance of the central vein sign estimated that the median proportion of CVS-positive lesions was 62.1% in MS and 10.7% in AQP4-NMOSD (Cagol et al., 2024).

1.1.6.1.2. Juxtacortical and cortical lesions

Cortical lesions typically present as small focal abnormalities confined to or spanning the cortical width and are difficult to detect using routine sequences like FLAIR (Calabrese et al., 2010). To improve sensitivity in detecting cortical lesions, advanced sequences that enhance the contrast between the cortex and white matter, such as double inversion recovery (DIR) or phase-sensitive inversion recovery (PSIR), have been proposed (Sethi et al., 2012). Cortical lesions are strongly suggestive of an MS diagnosis, occurring in approximately 60% of MS

patients compared with 5% of AQP4-NMOSD patients (Cagol et al., 2024). In MS, juxtacortical (i.e., at the junction between the white matter and grey matter) and cortical lesions (see Figure 2C) can be observed in all cortical areas, including the cerebellum (Pareto et al., 2015). What is more, juxtacortical lesions with a U–fibre–type morphology (see Figure 2D) are highly specific for MS and are not typically seen in NMOSD (Matthews et al., 2013). If present, cortical lesions in NMOSD are typically juxtacortical and are more commonly observed during the acute phase (Kim et al., 2012, 2016).

1.1.6.1.3. Infratentorial lesions

An infratentorial lesion is characterised by a T2-hyperintense anomaly located in the brainstem, cerebellar peduncles, or cerebellum. In MS, infratentorial lesions can occur in the pons, midbrain, and cerebellar white matter, including the cerebellar peduncles (Filippi et al., 2019). Similar to white matter lesions, they are typically round or ovoid in shape and well-demarcated. In NMOSD, infratentorial lesions are characteristically located in areas rich in AQP4, occurring around the cerebral aqueduct and in the dorsal brainstem adjacent to the fourth ventricle, including regions such as the area postrema and the solitary tract (Cacciaguerra et al., 2019). Interestingly, medullary lesions in NMOSD can also be contiguous with cervical spinal cord lesions (Wingerchuk et al., 2015).

1.1.6.1.4. Optic nerve lesions

Optic nerve imaging is less widely used in MS due to its limited clinical utility for differential diagnosis, as optic neuropathy in MS can often be diagnosed clinically, and MRI findings may not significantly alter management decisions in most cases (Sastre-Garriga et al., 2024). Optic nerve lesions in MS are typically focal, short, and tend to involve the anterior segments of the optic nerve, often sparing the optic chiasm (Filippi et al., 2019). On MRI, these lesions may be associated with inflammation and mild swelling during episodes of acute ON, with gadolinium enhancement indicating active demyelination (Toosy et al., 2014). In contrast, ON in NMOSD is typically associated with longitudinally extensive optic nerve lesions (involving more than 50% of the length of the nerve), which have a predilection to locate in the posterior segments of the optic nerve, including the optic chiasm (Khanna et al., 2012).

1.1.6.2. Spinal cord MRI

The inflammatory process in the spinal cord is typically identified by hyperintensity on T2-weighted images and hypointensity on T1-weighted images (Filippi et al., 2019). In MS, spinal cord lesions are detected in 75% to 90% of patients (Ciccarelli et al., 2019). They appear hyperintense on T2-weighted sequences and can occur along the entire spinal cord, although they are most commonly located in cervical spine segments (see Figure 2E). What is more, MS spinal cord lesions have a predisposition to involve peripheral white matter in the lateral and posterior columns with frequent involvement of adjacent grey matter. Spinal cord lesions in MS are often small, multiple, take up less than half of the cord cross-sectional area, and do not exceed two vertebral segments (Ciccarelli et al., 2019).

Spinal cord involvement in patients with AQP4-NMOSD who have TM presents with distinct radiological appearances from MS. LETM, characterised by spinal cord lesions extending over three or more vertebral segments (see Figure 3C), is one of the hallmark radiological features of NMOSD (Wingerchuk et al., 2015). However, the longitudinal extension of spinal cord lesions in NMOSD is typically more pronounced, with the median lesion length spanning seven vertebral segments and reaching a maximum of up to 16 segments (Ciccarelli et al., 2019; Murchison et al., 2015). Additionally, spinal cord lesions in NMOSD are commonly observed in the cervical and upper thoracic segments rather than in the lower thoracic and lumbar regions, with a predilection for the AQP4-rich central gray matter (Kim et al., 2015).

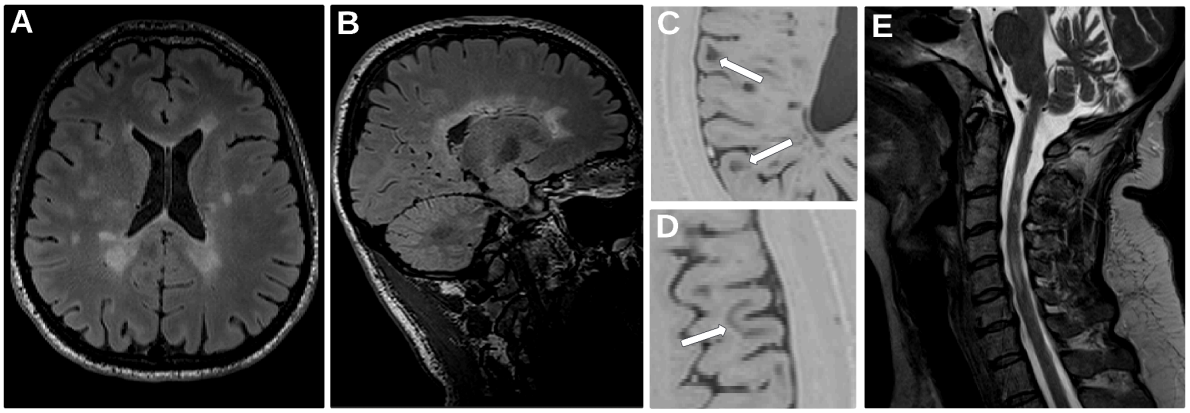

Figure 2. Examples of conventional MRI findings in MS. (A) Axial FLAIR showing periventricular and subcortical lesions. (B) Sagittal FLAIR showing *Dawson's fingers* type lesions. (C) Axial PSIR showing juxtacortical lesions. (D) Axial PSIR showing juxtacortical lesion with a U-fiber–type morphology. (E) Sagittal T2 showing multiple small spinal cord lesions. (Original figure based on MRI images obtained at the Laboratory of Brain Imaging, Nencki Institute of Experimental Biology); MS = multiple sclerosis; MRI = magnetic resonance imaging; FLAIR = fluid attenuated inversion recovery; PSIR = phase sensitive inversion recovery.

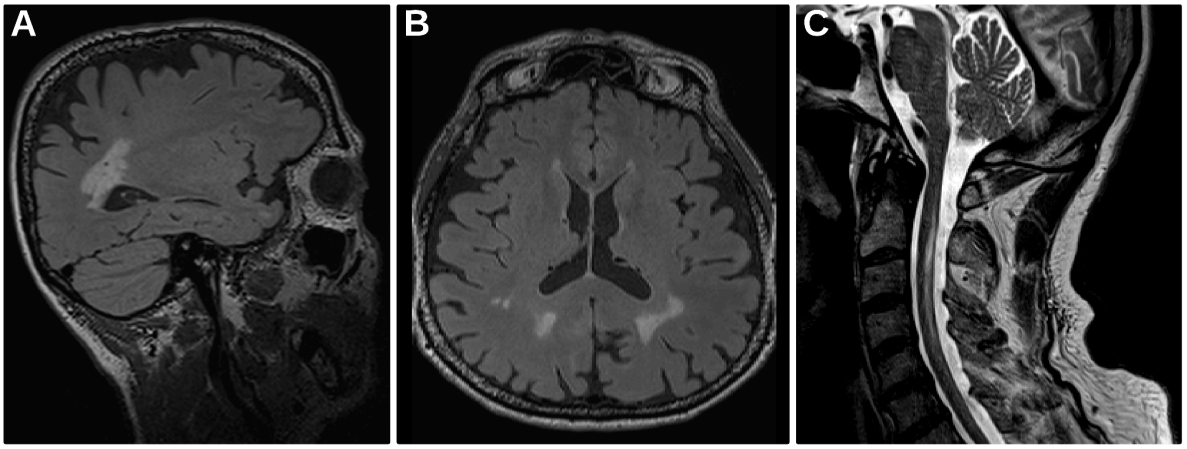

Figure 3. Examples of conventional MRI findings in NMOSD. (A) Sagittal FLAIR showing periependymal lesion surrounding the lateral ventricle. (B) Axial FLAIR showing extensive and confluent hemispheric lesions. (C) Sagittal T2 showing LETM. (Original figure based on MRI images obtained at the Laboratory of Brain Imaging, Nencki Institute of Experimental Biology) NMOSD = neuromyelitis optica spectrum disorders; MRI = magnetic resonance imaging; FLAIR = fluid-attenuated inversion recovery; LETM = longitudinally extensive transverse myelitis.

1.1.6.3. Limitations of conventional MRI

Conventional MRI sequences are routinely used in clinical practice for diagnosing and distinguishing inflammatory demyelinating diseases of the CNS. These sequences rely on basic lesion characteristics such as shape, location, and number (see Table 1), but they fail to reflect the microstructural differences that underpin distinct pathologies. Studies, such as Matthews et al. (2013), have shown that certain MRI findings, like *Dawson's fingers* type lesions or subcortical U-fibre lesions, can help differentiate MS from NMOSD with high specificity. In contrast, abnormalities like LETM or extensive, bilateral optic nerve lesions are strongly suggestive of NMOSD. However, similarities in imaging findings are common as MS and NMOSD share clinical features, including episodes of ON, TM, and brain or brainstem attacks, which correspond with inflammatory lesions visible on MRI. It was shown that around 27% of NMOSD patients presented with brain lesions that met diagnostic criteria for MS (Matthews et al., 2013). This overlap, present not only in the brain but also in the spinal cord, complicates diagnosis, particularly in early or atypical cases where lesion characteristics may not be distinct. Lesion size and distribution in the spinal cord can resemble MS in some NMOSD cases, with LETM resolving into smaller, MS-like lesions over time (Smith et al., 2023). Additionally, the timing of the MRI examination can influence interpretation, as short spinal cord lesions may represent the early evolution of LETM, causing NMOSD to resemble MS (Jarius et al., 2023). These complexities highlight the limitations of conventional MRI in distinguishing MS from NMOSD, particularly in cases where clinical and radiological features overlap is more pronounced (Juryńczyk et al., 2022; Matthews & Palace, 2014).

Because conventional MRI cannot assess macro- and microstructural properties such as axonal integrity, myelin loss, or volume changes, it fails to capture the subtle tissue changes that precede or coincide with visible lesions and contribute to disease progression. This gap in imaging capability becomes especially important in conditions like MS and NMOSD, where damage patterns may display subtle differences that are not easily detectable by conventional methods. Therefore, moving beyond conventional MRI to incorporate more advanced, non-conventional imaging techniques is crucial for capturing a more comprehensive view of disease mechanisms, enabling better differentiation between MS and NMOSD, and allowing for earlier intervention that could slow or even prevent irreversible damage.

Table 1. Key features of MS and NMOSD facilitating differential diagnosis

	MS	NMOSD
Most prevalent ethnicity	Caucasian	Caucasian with over-representation of Afro-American and Asian
Age of onset	20 - 40 y/o	30 - 50 y/o
Disease course	Relapsing or progressive	Relapsing
Female to male ratio	3:1	9:1
Brain involvement on MRI	95%	50 - 89%
Brain lesions	Ovoid, well-demarcated Periventricular *Dawson finger* type lesions Cortical lesions	Mainly non-specific If specific – located in the area postrema, solitary tract, or corticospinal tracts
Optic nerve involvement	Commonly unilateral	Bilateral in up to 20% of cases
Spinal cord lesions	<2 vertebral segments Predilection for peripheral white matter	>3 vertebral segments Predilection for central grey matter
Disability progression	Largely independent of relapses and progressive	Relapse dependent Progressive disability is a red flag
Attack severity	Commonly mild with good recovery	Commonly severe with poor recovery
Oligoclonal bands in CSF	Most cases (95%)	Typically absent, but may be present in <30% of cases
AQP4-IgG in serum	Absent	Present in the majority of patients (60 - 90%)

y/o = years old.

1.1.7. Treatment

The mainstay of MS and NMOSD therapy is the management of acute attacks and the prevention of relapses (Louis et al., 2021). In both conditions, treatment of acute attacks consists of using intravenous steroids as they provide short-term clinical benefit by reducing the severity and shortening the duration of the attacks (Ontaneda & Rae-Grant, 2009; Sherman & Han, 2015). In patients who are resistant or refractory to steroids, plasma exchange can be used as a second-line treatment (Berkovich, 2016). However, in NMOSD, due to severe disability associated with the attacks, there is a lower threshold, compared with MS, for using plasma exchange if the patient does not respond well to standard steroid treatment (Bonnan et al., 2018).

Despite both MS and NMOSD being autoimmune demyelinating conditions, long-term treatment preventing relapses is almost completely exclusive in both conditions (Kümpfel et al., 2024). In MS, disease-modifying therapies reduce the progression of the disease by suppressing or modulating immune function (Louis et al., 2021). Their primary anti-inflammatory effects are observed in the relapsing phase of MS, leading to a decrease in the frequency of the relapses, reducing the accumulation of MRI lesions, and stabilising, delaying, or occasionally modestly improving disability (Robertson & Moreo, 2016). Evidence supports that disease-modifying therapies are most effective when introduced in the initial stages of the disease (Hauser & Cree, 2020). Therefore, current clinical approaches often recommend early treatment with highly effective medications, including 1) ocrelizumab (Hauser et al., 2017), 2) rituximab (Salzer et al., 2016), 3) alemtuzumab (Cohen et al., 2012; Coles et al., 2012), 4) natalizumab (Polman et al., 2006; Rudick et al., 2006), or 5) cladribine (Cohen et al., 2012; Coles et al., 2012). Currently, available MS-modifying medications are far less effective in progressive MS stages (Louis et al., 2021). Nevertheless, if patients with progressive MS still exhibit notable disease activity like new MRI lesions or clinical exacerbations, the use of certain drugs may be warranted. Therapies are limited and include siponimod, approved for SPMS, and ocrelizumab approved to use in PPMS (Kappos et al., 2018; Montalban et al., 2017). At present, treatment of MS progression remains an unmet need and requires a greater understanding of the neurodegenerative component of the disease.

Recent studies elucidating the immune system pathomechanisms driving AQP4-NMOSD have identified the complement system, the IL-6 pathway, and the B

lymphocyte-mediated damage as possible new therapeutic targets for managing the disease. These observations prompted the development of three new AQP4-NMOSD-specific therapies, which until 2019 did not exist: 1) inebilizumab (Cree et al., 2019), 2) eculizumab (Pittock et al., 2019), and 3) satralizumab (Yamamura et al., 2019). Before the development and approval of these therapies, off-label drugs (e.g., rituximab, mitoxantrone), which were also used for treating MS, were widely available for use in NMOSD (Kimbrough et al., 2012). However, certain drugs effective in treating MS (beta-interferon, fingolimod, natalizumab) have been linked to ineffectiveness or exacerbation of symptoms in NMOSD, resulting in significant visual, motor, and sphincter disability (Juryńczyk et al., 2013; Palace et al., 2010), as well as the development of extensive brain lesions (Juryńczyk et al., 2015).

1.2. Application of non-conventional MRI to study MS and NMOSD

1.2.1. Non-conventional MRI findings

Compared with conventional MRI, novel non-conventional MRI techniques offer several advantages: 1) they can identify subtle lesion characteristics, such as the presence of iron or vessels within or around the lesions; 2) they enable quantitative measurements of metrics related to demyelination and axonal loss, both within lesions and in normal-appearing brain tissue, as well as in specific white and grey matter regions; and 3) they allow the assessment of brain volume loss, including regional atrophy, all of which may serve as useful discriminators in diseases with attack-related damage that show a predilection for specific brain regions (Cortese et al., 2024; Granziera et al., 2021).

1.2.1.1. Brain

1.2.1.1.1. Volumetry

MRI-based brain volumetry is increasingly being used in the clinical setting to assess macrostructural brain volume changes from structural MRI sequences like T1-weighted, T2-weighted, and FLAIR images, which are present in most standard MRI protocols for demyelinating diseases. Volumetric measures of brain structures, including white matter, cortical grey matter, and deep grey matter, have been shown to be valid biomarkers of the clinical state and disease progression in neurodegenerative, demyelinating diseases (Giorgio & De Stefano, 2013).

Brain atrophy is a well-recognized feature of MS (Cagol et al., 2022), with an estimated annual rate of approximately 0.7 – 1%, compared with 0.2 – 0.3% in the healthy population (Rocca et al., 2017). It affects both grey matter and white matter structures throughout the CNS (Andravizou et al., 2019). In MS, deep grey matter atrophy is present early in the disease and is associated with the fastest volume loss rate, which correlates with disability progression (Eshaghi et al., 2018). Moreover, cortical grey matter atrophy has been shown to be strongly linked with cognitive impairment, even more so than the volume of white matter lesions (Lie et al., 2022). Although white matter atrophy in MS is less prominent compared with deep grey matter or cortical atrophy, it is still considered to contribute to disability progression and cognitive impairment (Sanfilipo et al., 2006).

Studies regarding brain atrophy in NMOSD are scarce and often report contradictory findings. A recent study found that NMOSD patients had lower, though not statistically significant, global brain, white matter, and grey matter volumes (Messina et al., 2022). However, the study did find significantly lower cortical and brainstem volumes and optic chiasm atrophy, particularly in patients who had experienced at least one episode of ON. Other studies using volumetrics and voxel-based morphometry either found reduced white matter and grey matter volumes in NMOSD compared with healthy controls (HC; Chanson et al., 2013; Ota et al., 2015; von Glehn et al., 2014) or showed no evidence of atrophy at all (Matthews et al., 2015).

1.2.1.1.2. T1 relaxometry

Quantitative T1 mapping measures the T1 relaxation times, which are influenced by changes in water content and macro/micro molecules within tissues, such as those caused by demyelination and axonal loss in the brain (Laule et al., 2007). Whole-brain T1 mapping offers a personalised approach assessing the extent of diffuse pathology by quantifying T1 changes relative to the normal distribution of T1 relaxation times in healthy individuals (Bonnier et al., 2019). To date, T1 relaxometry has not been included in routine clinical protocols in MS, partly due to the complexity of acquisition techniques, often leading to reproducibility issues (Granziera et al., 2021). However, new, promising T1 mapping approaches like magnetisation prepared 2 rapid acquisition gradient echo (MP2RAGE) sequences have managed to provide highly reproducible T1 maps (Voelker et al., 2016). Despite the difficulty in image acquisition and isolating the impact of macro/micro molecules

on T1 measurements, research has demonstrated a strong correlation between T1 relaxation values and myelin content in white matter and lesions in MS (Mottershead et al., 2003).

In a recent study by Rahmanzadeh et al. (2022b), T1 relaxation was shown to distinguish between MS focal white matter lesions and cortical pathology from peri-plaque white matter. Additionally, it demonstrated high sensitivity to normal-appearing grey matter pathology, surpassing methods like quantitative susceptibility mapping (QSM), myelin water fraction, and magnetisation transfer ratio (Rahmanzadeh et al., 2022b). What is more, T1 relaxation rates have been reported to decrease in the cortex of MS patients with disease progression, which is attributed to an increase in iron deposition associated with demyelination and neuronal degeneration (Steenwijk et al., 2016).

In NMOSD, assessment of T1 changes in lesion-free periependymal regions showed no significant differences compared with HC (Pasquier et al., 2019). However, another study demonstrated decreased T1 relaxation in the normal-appearing white matter (NAWM) of patients with NMOSD compared with HC, but not when compared with patients with MS (Chou et al., 2019).

1.2.1.1.3. Quantitative susceptibility mapping

QSM involves imaging techniques used to measure the absolute concentrations of substances based on their changes in local magnetic susceptibility, offering an improvement over standard SWI by providing quantitative rather than qualitative susceptibility measurements (Liu et al., 2015). In QSM, magnetic susceptibility is determined from local frequency shifts in MRI signals obtained from phase images of gradient echo sequences using deconvolution with a dipole kernel. QSM maps enable the quantification of paramagnetic trace elements like iron in ferritin, deoxygenated haemoglobin in blood, and diamagnetic calcium (Kim et al., 2023; Liu et al., 2015). Additionally, myelin and the microstructural anisotropy of white matter can also cause local shifts in magnetic susceptibility due to the diamagnetism of proteins and lipids (Granziera et al., 2021).

Susceptibility imaging, including SWI and QSM, has led to a breakthrough in the understanding of the MS disease process (as studied in vivo) and has demonstrated a unique potential of non-conventional imaging to provide clinically relevant information (Calvi et al., 2022). A key finding is the paramagnetic rim observed at the edge of some MS chronic active lesions (termed paramagnetic rim lesions, PRL), which an MRI-pathology correlation study

has linked to activated iron-laden microglia/macrophages representing ongoing inflammation and demyelination (Galbusera et al., 2023). The detection of PRL is a promising biomarker for predicting disease progression and monitoring treatment efficacy while also being useful in diagnosis. In a multinational study involving 438 individuals with diverse neurological conditions, PRL were identified in 52% of MS patients, in contrast to only 7% of patients with non-MS diagnoses, demonstrating a high specificity of 93% in distinguishing MS from non-MS conditions (Maggi et al., 2020). Notably, paramagnetic rims were rarely observed (less than 5%) in lesions associated with NMOSD (Sinnecker et al., 2012, 2016).

The possibility of applying QSM into clinical protocols is facilitated by existing protocols utilising 2D or 3D gradient-echo sequences for T2*-weighted or susceptibility-weighted imaging, which can also serve for QSM reconstruction if phase images are available. However, widespread clinical implementation of QSM is hindered by the absence of necessary algorithms on commercial scanners and the lack of consensus on the optimal reconstruction algorithm (Langkammer et al., 2018).

1.2.1.1.4. Diffusion-weighted imaging

Diffusion-weighted imaging (DWI) enables the characterisation of water motion within the human body. In DWI, applying carefully structured diffusion gradients designed to dephase and subsequently rephase spins of hydrogen atoms in the water molecules makes the MRI signal sensitive to water movement in between the turning on and off of the gradients. Additionally, by applying gradients in different directions, DWI is capable of assessing the directionality of said movement. By applying mathematical models that use both signal strength and direction, it is possible to assess the underlying tissue microstructure properties (Le Bihan & Johansen-Berg, 2012).

Multiple DWI-based models are available to choose from, with diffusion tensor imaging (DTI) being the most commonly used. The DTI model describes the Gaussian process of anisotropic diffusion and can be depicted as an ellipsoid with three principal directions, represented by eigenvectors and corresponding eigenvalues (O'Donnell & Westin, 2011). DTI can assess white matter fibre characteristics by quantifying parameters such as fractional anisotropy (FA), mean diffusivity (MD), axial diffusivity (AD), and radial diffusivity (RD). Importantly, FA and MD were validated as markers of microstructural integrity in an MRI-postmortem study. A study by Schmierer et al. (2007) showed strong

correlations between FA and MD in NAWM with myelin content and, to a lesser extent, axon count, with FA being particularly sensitive to white matter integrity, showing significant differences between myelinated and unmyelinated fibres. Currently, DTI protocols are accessible on the majority of clinical scanners and could potentially be integrated into clinical practice (Granziera et al., 2021). Nevertheless, DTI measurements may be unreliable in brain regions with crossing fibres, which are estimated to affect between 30% and 90% of white matter in the brain, as DTI cannot accurately represent multiple independent intra-voxel orientations (Landman et al., 2010; Schilling et al., 2017).

To overcome the limitations of the DTI model, Neurite Orientation Dispersion and Density Imaging (NODDI) was developed as a novel diffusion MRI biophysical model, offering a more specific approach to studying brain tissue microstructure (Zhang et al., 2012). NODDI utilises multi-shell diffusion MRI data to create a three-compartment model composed of 1) an intracellular compartment with restricted anisotropic non-Gaussian diffusion (i.e., neurite density index, NDI), 2) an extracellular compartment with hindered anisotropic Gaussian diffusion, and 3) a free water compartment with free isotropic Gaussian diffusion (i.e., isotropic volume fraction, ISO). Additionally, NODDI allows for calculating the orientation dispersion index (ODI), which represents neurite directionality. Similar to DTI metrics, NODDI measures have been validated by histopathological studies, which demonstrated good correlation between ODI and histological measures of neurite orientation dispersion in brain and spinal cord, and NDI, representing the density of axons and dendrites in a given voxel, to correlate strongly with myelin and moderately with histology-derived neurofilament density measures (Grussu et al., 2017; Mollink et al., 2017). Since the NODDI model requires multi-shell data acquisition, its routine clinical application is challenging. However, NODDI measurements are feasible in clinical settings with modern scanners that support multi-shell diffusion protocols. Further studies are needed to assess reproducibility and establish reference cut-offs for HC (Kamiya et al., 2020).

DTI has been used in MS to study both lesions and NAWM. When compared with white matter from HC, white matter lesions typically exhibit increased MD and decreased FA (Alshehri et al., 2022; Cercignani et al., 2000; Filippi et al., 2000; Hagiwara et al., 2019). Interestingly, DTI has demonstrated abnormalities not only within lesions but also in NAWM, where a similar yet less pronounced pattern of lower FA and higher MD (compared with HC) has been observed (Filippi et al., 2000; Margoni et al., 2022; Tedone et al., 2023; Yu et al.,

2019). Studies utilising the newer NODDI model support the presence of damage within lesioned tissue as well as widespread abnormalities in NAWM. Similar to DTI findings, MS patients exhibit lower NDI and ODI values in white matter lesions, with a less pronounced reduction observed in NAWM compared with HC (Collorone et al., 2020; Hagiwara et al., 2019; Schneider et al., 2017; Spanò et al., 2018; Storelli et al., 2022). Additionally, when the DTI and NODDI models were compared, NDI was shown to detect more pronounced and widespread abnormalities than FA (Collorone et al., 2020; Granberg et al., 2017; Spanò et al., 2018).

DWI-based studies in patients with NMOSD are limited. Similar to MS, NMOSD white matter lesions exhibit lower FA and higher MD and ISO when compared with healthy white matter (Boaventura et al., 2025; Kato et al., 2022). Interestingly, findings on NAWM damage in NMOSD remain inconclusive, with some studies reporting evidence of diffuse injury evidenced by increased MD or decreased NDI within the whole brain NAWM (Cacciaguerra et al., 2021; Liu et al., 2012; Nakaya et al., 2024; Sun et al., 2023), selective damage (lower FA, lower NDI) to white matter tracts in visual, sensory, and motor systems (Kato et al., 2022; Messina et al., 2022; Pichiecchio et al., 2012), or no damage at all (Aboul-Enein et al., 2010; Matthews et al., 2015). Potential explanations for these inconsistencies possibly include small sample sizes, methodological differences, and the under-examined relationship between lesions and the surrounding white matter (Matthews et al., 2015).

1.2.1.2. Spinal cord

1.2.1.2.1. Volumetry

Spinal cord volume is typically assessed using a 3D T1 or T2-weighted sequence with isotropic resolution less than 1 mm in order to minimise the partial volume effect from the surrounding CSF (Ciccarelli et al., 2019). The most common quantitative measure to evaluate the spinal cord is the cervical spinal cord cross-sectional area (CSA; Casserly et al., 2018). 3D T1 or T2-weighted volumetric scans and spoiled T2*-weighted sequences can be used to obtain high-quality images of the spinal cord with good tissue contrast, allowing for grey matter segmentation and its volumetric assessment. Nowadays, automated methods utilising registration of scans over time are thought to enhance the precision of spinal cord volume

measurements, thereby allowing for the detection of treatment effects, which may facilitate the inclusion of spinal cord atrophy assessment in clinical trials (Ciccarelli et al., 2019).

In MS, the majority of recent studies investigating spinal cord volume found significantly lower CSA measures in MS patients compared with HC and significant links between spinal cord atrophy and disability progression (Mina et al., 2021; Tsagkas et al., 2018). Another study found a significant reduction in the volume of grey matter rather than the whole cord in MS patients (Mariano et al., 2021). The rate of volume decrease in RRMS is thought to be faster in the brain than in the spinal cord, which is likely due to the high degeneration of cortical regions (Ciccarelli et al., 2019).

Interestingly, NMOSD patients are reported to experience larger volume decreases in the spinal cord than in the brain, suggesting different pathogenic mechanisms than in MS (Ciccarelli et al., 2019; Liu et al., 2015). The literature on spinal cord pathology in NMOSD is scarce, and the exact relationship between cord atrophy and disability accumulation remains unknown (Ciccarelli et al., 2019). Recent studies have reported significantly lower CSA values in both cervical and thoracic cord segments in NMOSD as compared with HC and found a significant negative relationship between CSA and EDSS (Lersy et al., 2021; Mariano et al., 2021). These results suggest that spinal cord volumetry could have a role in NMOSD diagnosis and disease monitoring.

1.2.1.2.2. Diffusion-weighted imaging

In most clinical settings, the DTI model is a feasible option for imaging the spinal cord, providing valuable insights into underlying microstructural changes (Wheeler-Kingshott et al., 2014). However, obtaining DWI with the high b-values required for NODDI model estimation is challenging due to the low signal-to-noise ratio and pronounced motion artefacts (Grussu et al., 2015). While DTI is currently used primarily to investigate disease mechanisms, a future possibility is that it could assist in prognosis and therapy planning, offering a more personalised approach to patient care (Shim et al., 2020; Vedantam et al., 2014).

Like brain lesions, white matter spinal cord lesions in MS are characterised by lower FA than HC (Lersy et al., 2021; Mariano et al., 2021). Additionally, MS's spinal cord white matter shows lower FA and higher MD values when compared with HC. Similar alterations in FA and MD were observed when only non-lesional spinal cord white matter was assessed

(Margoni et al., 2022). Importantly, a study aimed at evaluating the tissue integrity of major cervical cord white matter tracts using DTI found that both FA and RD correlated with clinical measures of disability, suggesting that DTI could serve as an imaging biomarker for spinal cord tissue injury in MS (Naismith et al., 2013).

In NMOSD, DTI studies of the spinal cord consistently demonstrate alterations in tissue integrity, including decreased FA in white matter and increased MD in both lesions and whole cord white matter (Mariano et al., 2021; Rivero et al., 2014). Interestingly, higher RD was observed in spinal cord white matter lesions in NMOSD patients compared with lesions in MS patients, suggesting a distinct pattern of tissue destruction characterised by radial expansion of water molecules, and was proposed as a potential diagnostic biomarker for NMOSD (Klawiter et al., 2012). The non-conventional MRI methods described in this subchapter are summarised in Figure 4.

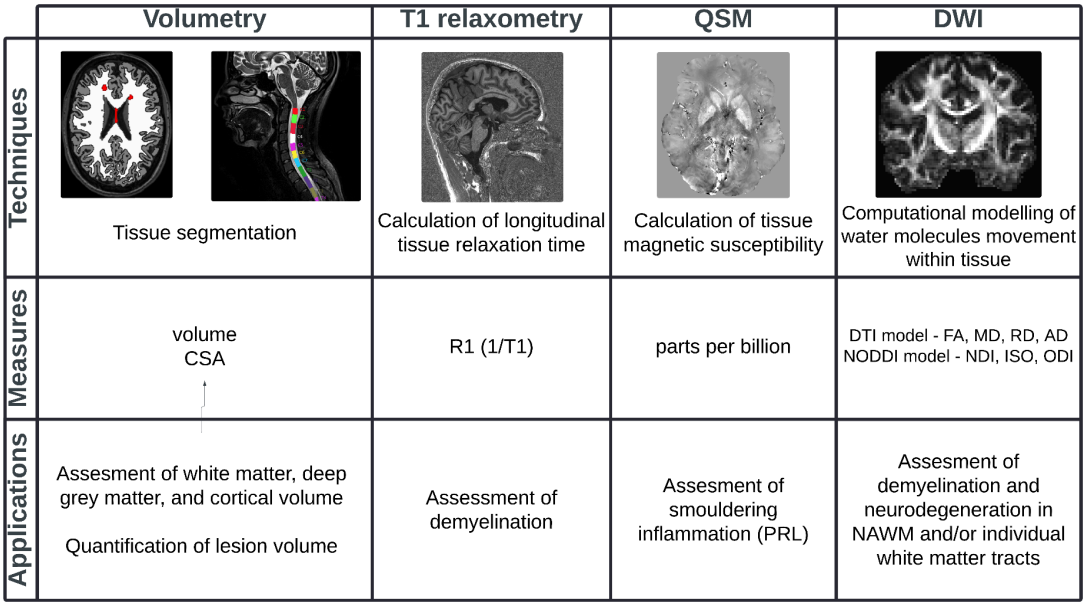

Figure 4. Graphical overview of non-conventional MRI methods. (Original figure); CSA = cross-sectional area; QSM = quantitative susceptibility mapping; PRL = paramagnetic rim lesions; DTI = diffusion tensor model; FA = fractional anisotropy; RD = radial diffusivity; AD = axial diffusivity; NODDI = neurite orientation dispersion and density imaging; NDI = neurite density index; ISO = isotropic volume fraction; ODI = orientation dispersion index; NAWM = normal-appearing white matter.

2. AIMS OF THE WORK

2.1. Rationale for the thesis

MS and NMOSD are two separate CNS inflammatory/demyelinating diseases with different and largely mutually exclusive management. NMOSD is a mimic of MS, which may lead to misdiagnosis. Despite the clinical and radiological overlap, MS and NMOSD are driven by distinct pathomechanisms, which lead to differences in brain and spinal cord pathology characteristics. While useful in many clinical situations, routine MRI identifies only a subset of these features, mainly relating to the lesion shape, number, and location. The aim of this work was to study whether non-conventional MRI of the brain and cervical spinal cord, allowing for the assessment of processes at the microstructural level, may identify novel discriminators between MS and NMOSD based on their distinct pathology.

2.2. Research aims and research questions

Primary aim: To prospectively and cross-sectionally explore patterns of cerebral and cervical spinal cord damage using non-conventional MRI in patients with MS and AQP4-NMOSD compared with HC.

Secondary aims:

1. To identify and characterise patterns of cerebral white matter damage in MS and AQP4-NMOSD by investigating: 1) damage in white matter fibres that traverse and do not traverse through white matter lesions, and 2) white matter volume.
2. If white matter damage is identified in either MS or AQP4-NMOSD in fibres that do not traverse through white matter lesions, explore other potential causes beyond typical white matter lesions, including cortical lesions and chronic active lesions.
3. To assess cerebral grey matter abnormalities in MS and AQP4-NMOSD by investigating: 1) T1 relaxation rates in the cortex, 2) cortical volume, and 3) deep grey matter volume.
4. To evaluate patterns of cervical spinal cord damage in MS and AQP4-NMOSD across: 1) the whole cord, 2) white matter, and 3) grey matter.

3. METHODS

3.1. Participants

This prospective cohort study received approval from the bioethics committee at the Institute of Psychiatry and Neurology in Warsaw, Poland (nr 8/2021). All participants signed a written informed consent form. Twenty MS patients were enrolled from a disease-modifying treatment clinic in the Department of Neurology, Wolski Hospital, Warsaw. Twenty NMOSD patients were recruited from NMOSD clinics at the Wolski Hospital and the Department of Neurology at the Warsaw Medical University. All MS patients met the revised McDonald's criteria for RRMS (Thompson et al., 2018). All NMOSD patients met the revised 2015 NMOSD criteria (Wingerchuk et al., 2015) and tested positive for AQP4-IgG on a fixed cell-based assay. All MS and NMOSD patients were scanned at least two months post their last disease attack. Twenty HC, matched for sex and age with the AQP4-NMOSD cohort, were recruited through social media channels of the Laboratory of Brain Imaging, Nencki Institute of Experimental Biology, Polish Academy of Sciences in Warsaw. The exclusion criteria included any contraindications to research MRI scanning, such as claustrophobia, metal implants, or pregnancy. Additionally, HC were screened for conditions that may confound the findings (i.e., neurological conditions). Recruitment of all participants occurred between September 2021 and July 2022.

3.2. Clinical data acquisition

Clinical data of MS and AQP4-NMOSD patients were obtained from clinical records provided by treating neurologists at referring centres. This data included information on the number of disease attacks and their phenotypes, the EDSS score at the time of the study scan, and the current disease-modifying therapy.

3.3. MRI protocol

All study participants underwent scanning at the Laboratory of Brain Imaging, Nencki Institute of Experimental Biology, Polish Academy of Sciences in Warsaw. MRI data were collected using a 3T Siemens Trio scanner (Siemens Erlangen, Germany). Prior to the MRI scan, all participants were instructed to remain as still as possible while lying down in the scanner. The MRI protocol consisted of two imaging sessions (brain and cervical spinal

cord), with the brain scan lasting approximately 43 minutes and the cervical spinal cord scan lasting approximately 23 minutes, all conducted during a single visit. Participants were given breaks of approximately 15 minutes between the sessions. A standard operation procedure was used to ensure consistent acquisition in terms of participant positioning and set-up of sequences. Data quality was evaluated following each acquisition, and the acquisition was repeated if necessary.

3.3.1. Brain

During the brain imaging session, all participants were scanned using a 32-channel array head coil. The protocol included: 1) T1 weighted magnetization-prepared rapid acquisition gradient echo (MPRAGE): repetition time/echo time/inversion time = 2530/3.32/1100 ms, acquisition time = 6 min; 2) FLAIR: repetition time/echo time/inversion time = 5000/388/2100 ms, both with 1 mm3 isotropic spatial resolution, acquisition time = 7 min; 3) multi-shell DWI: repetition time/echo time/resolution = 3660/101 ms/2x2x2 mm3 isotropic with b-values of 0/500/1250/2500 s/mm2 and 13/18/36/53 measurements per shell, respectively, and an additional diffusion acquisition with 7 measurements of b-value 0 s/mm2 with reversed phase encoding direction to correct for susceptibility-induced distortions, acquisition time = 8 min; 4) T1 weighted magnetization-prepared rapid acquisition gradient echo with 2 separate readouts at different inversion times (MP2RAGE): repetition time/echo time/inversion time 1/inversion time 2 = 5000/2.96/700/2500 ms, and 1 mm3 isotropic spatial resolution, acquisition time = 8 min; 5) T2*-weighted gradient echo, multi-echo QSM sequence with repetition time/echo times = 27/4.65, 9.15, 13.65, 18.15, 18.15, 22.65 ms and 0.7×0.7×1.0 mm3 spatial resolution, acquisition time = 8 min; (6) PSIR sequence: repetition time/echo time/inversion time = 4000/381/380 ms, with 0.9 mm3 isotropic spatial resolution, acquisition time = 6 min. The whole scanning session lasted approximately 43 min. Due to technical difficulties, the MP2RAGE sequence could not be acquired for three MS patients, and the QSM sequence was not obtained for two HC and one MS patient.

3.3.2. Cervical spinal cord

During the cervical spinal cord imaging session, all participants were scanned using a 12-channel array head and neck coil. The protocol included: 1) T2 weighted sequence: repetition time/echo time = 2800/83 ms, with 0.8×0.6×3.0 mm^3 spatial resolution, acquisition time = 4.5 min; 2) T1 weighted sequence: repetition time/echo time = 2000/3.21 ms, with 1

mm^3 isotropic spatial resolution, acquisition time = 5 min; 3) T2 weighted sequence: repetition time/echo time = 2000/118 ms, with 0.8 mm^3 isotropic spatial resolution, acquisition time = 4.5 min; 4) DWI: repetition time/echo time/ = 600/99 ms, 0.9x0.9x5 mm^3 spatial resolution, with b-values of 0/800 s/mm^2, 1/64 measurements per shell respectively, and an additional diffusion acquisition with four measurements of b-value = 0 s/mm^2 with reversed phase encoding direction to correct for susceptibility-induced distortions, acquisition time = 4 min; 5) spoiled T2* Multi-Echo Data Image Combination (MEDIC) sequence: repetition time/echo time = 600/13 ms, with 0.5 mm^3 isotropic spatial resolution, acquisition time = 5 min. Due to the participant's resignation, the cervical spinal cord protocol was not obtained for one participant from the HC cohort.

3.4. MRI data analysis

3.4.1. Brain

3.4.1.1. Volumetry and lesions assessment

Segmentations of white matter lesions were obtained by manually tracing hyperintense lesions on FLAIR images using FSLeyes software (McCarthy, 2022), following the guidelines outlined by Filippi et al. (2019): 1) round to ovoid in shape, 2) ranging from a few millimetres to more than one or two centimetres in diameter, with a minimum long-axis length of 3 mm, 3) visible on at least two consecutive slices. Created binary lesion masks were then coregistered with MPRAGE images using a rigid body transformation algorithm. Subsequently, the lesion-filling function from FSL software was used to estimate intensity values from surrounding white matter and fill in signal dropouts in MPRAGE images to improve the registration and segmentation process. Each patient's T2-hyperintense white matter lesion volume was calculated based on their respective lesion mask. Lesion-filled MPRAGE images were fed to segmentation algorithms implemented in Freesurfer software (Dale et al., 1999) to obtain the volumes of cerebral white matter, cerebral cortex, and deep grey matter. All obtained volumetric measures were normalised by dividing them by the estimated total intracranial volume (ETIV) to adjust for differences in cranium sizes. The resulting value was then multiplied by 100 to represent a percentage of the ETIV.

PSIR and the corresponding FLAIR images were used to determine the number of cortical lesions. Similar to the assessment of white matter lesions, the images were visually

examined, and lesions were identified based on the guidelines provided by Filippi et al. (2019). On PSIR, cortical lesions were defined as focal hypointense abnormalities relative to the surrounding normal cortex, either confined entirely within the cerebral cortex or extending into the subjacent white matter, and identified on at least two consecutive slices.

3.4.1.2. T1 relaxometry in the cerebral cortex

Cortical segmentation was performed using Freesurfer on the standard MPRAGE images. Quantitative T1 relaxation rate maps for the cerebral cortex were calculated using the MP2RAGE sequences. The MP2RAGE T1 relaxation rate maps were registered to FreeSurfer's reconstructed image using the denoised UNIFIED images. The Ciftify utility from the Human Connectome Project was employed to generate the grey matter ribbon and project voxels with coordinates situated between the white and pial surfaces for sampling and smoothing the T1 relaxation rate values (Glasser et al., 2013). Averaged estimates were then extracted for the Destrieux atlas, which includes 150 regions of the cerebral cortex (Destrieux et al., 2010).

3.4.1.3. Assessment of paramagnetic rim lesions

QSM maps were computed from multi-echo phase and magnitude T2*-weighted images using the SEPIA Matlab toolbox. The Morphology Enabled Dipole Inversion algorithm (Liu et al., 2011) was applied to unwrap phase data and estimate susceptibility maps, with CSF used as a reference value. The QSM images were visually inspected for the presence of PRLs and cross-referenced with the corresponding FLAIR images (see Figure 5). A lesion was classified as a PRL if a hyperintense rim was visible on QSM on at least two consecutive slices.

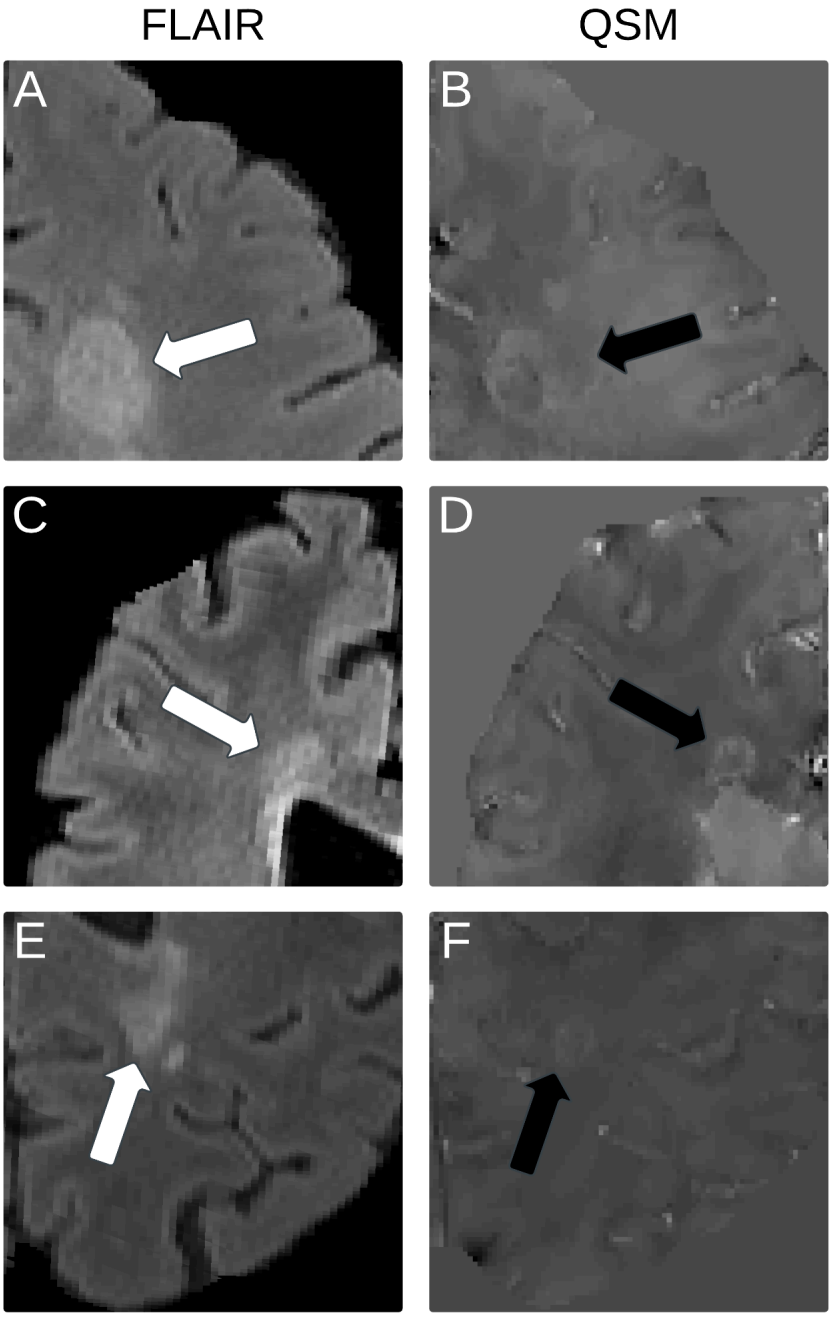

Figure 5. Examples of PRL visible on FLAIR (depicted by white arrows) and corresponding QSM images (depicted by black arrows). (A, B) A 29-year-old male with RRMS. (C, D) A 42-year-old female with RRMS. (E, F) A 45-year-old female with RRMS. (Original figure based on MRI images obtained at the Laboratory of Brain Imaging, Nencki Institute of Experimental Biology); FLAIR = fluid-attenuated inversion recovery; QSM = quantitative susceptibility mapping; RRMS = relapsing-remitting multiple sclerosis; MRI = magnetic resonance imaging.

3.4.1.4. Estimation of the NODDI model and lesion-informed tractometry

DWI pre-processing followed the standard MRtrix3 pipeline (Tournier et al., 2019), including denoising, Gibbs artefact removal, motion correction, eddy-currents correction, EPI distortions correction based on the opposite phase-encoded b0 images, and intensity bias correction. Additionally, the mean image calculated from b0 shells was created for registration purposes. Quality control assessment for the DWI images was performed with an automated EDDY QC framework (Bastiani et al., 2019). NDI maps were generated by fitting the nonlinear three-compartment NODDI model to preprocessed DWI data using the NODDI Matlab Toolbox (Zhang et al., 2012).

To perform tract segmentation, response functions for white matter, grey matter, and CSF were estimated, and a multi-tissue constrained spherical deconvolution (CSD) algorithm was used to obtain white matter fibre orientation distribution (Dhollander & Connelly, 2016). CSD peaks, representing the dominant fibre orientations within a voxel, served as an input into TractSeg to generate white matter tract segmentations (Wasserthal et al., 2018). For each subject, TractSeg utilised the CSD-derived orientation data to generate 50 white matter tracts, with 5,000 streamlines approximating fibre bundles computed for each tract. To exclude the influence of lesions on the reconstruction of physiological white matter tracts, the accuracy of tract segmentation performed by TractSeg was visually reviewed for any anomalies, but no issues were identified.

The acquired tracts were segmented based on the binary lesion masks, which were used as input for the MRtrix3 *tckedit* command with the following criteria:

1. Only streamlines that passed through the lesion mask were retained.
2. Streamlines that intersected any region defined by the lesion mask were discarded.

As a result, two types of tract parts were obtained, with fibres appropriately selected to represent the part of the tract traversing through and not traversing through white matter lesions. To ensure robust analysis and minimize bias from incomplete data, any segmented tract part containing fewer than 50 out of 5000 total streamlines was excluded from further analysis (Wasserthal et al., 2020). For example, for a given tract, if the vast majority of fibers

traversed a lesion, only the lesion-traversing part was used; conversely, if tract fibers did not traverse a lesion, only the lesion-free part was analysed.

The NDI values along specific tracts were obtained with TractSeg's tractometry module (Wasserthal et al., 2020). The algorithm computed a central line for each tract and divided the tract's streamlines into 100 segments. NDI values were then sampled at each segment and aggregated (mean of all 100 segments) to yield a single value per tract. Mean NDI values were obtained for whole unsegmented tracts (without division into fibres traversing and not traversing through white matter lesions) as well as for tract fibres that traversed and did not traverse through white matter lesions separately. To exclude focally decreased NDI values within white matter lesions from the tract fibers passing through them, an in-house algorithm was used to identify lesion locations along each tract. NDI values associated with these focal lesion points (i.e., tracts segments directly affected by a lesion) were then removed from calculating the mean.

To evaluate differences in lesion burden across individual tracts in MS and NMOSD, bundle load (defined as the volume of streamlines passing through lesions divided by the total volume of the tract of interest) was calculated for each of the 50 examined tracts (see Figure 6 for a detailed flowchart representing analysis steps in the brain-related dataset; Chamberland et al., 2021).

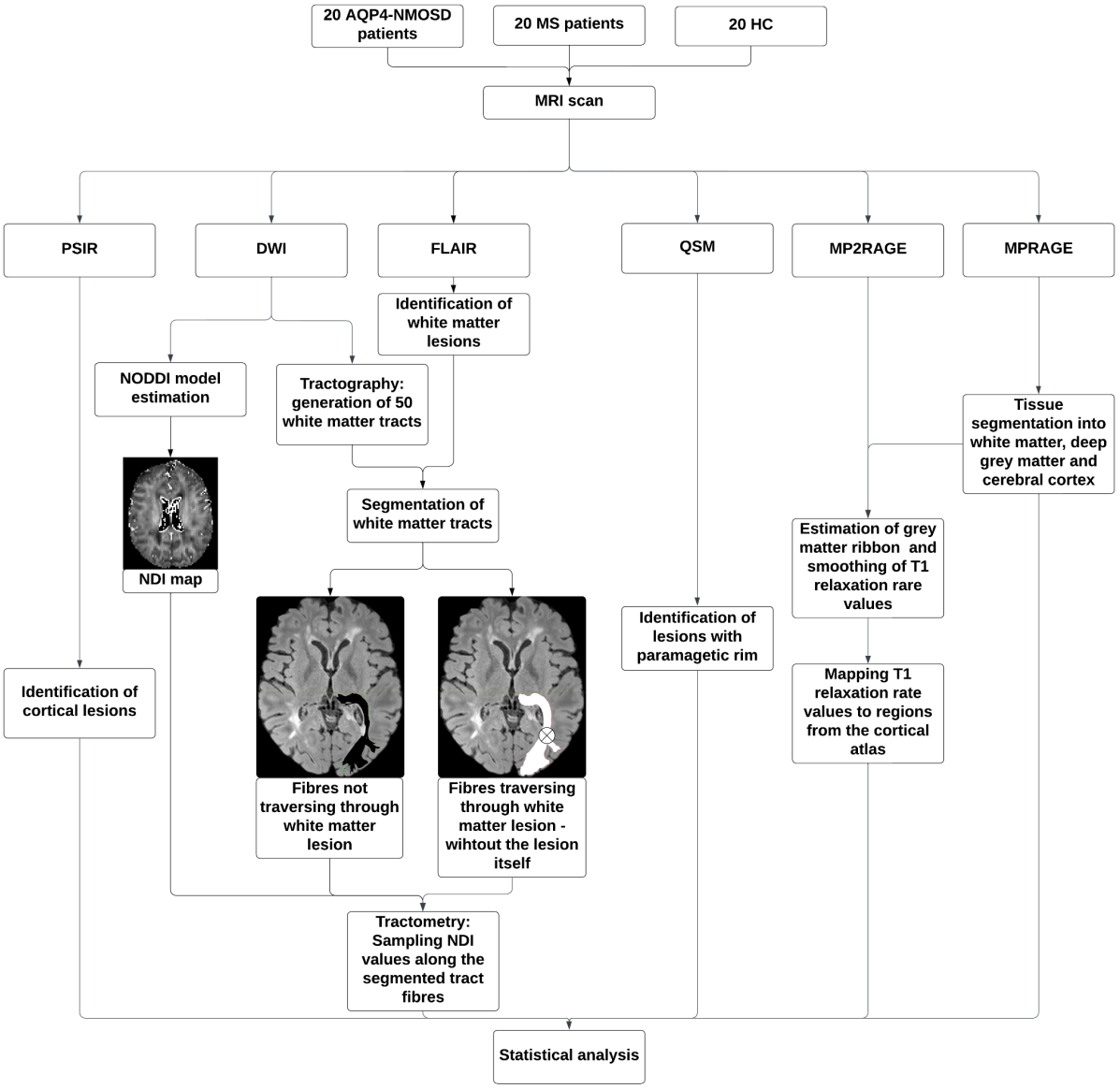

Figure 6. Flowchart of the brain-related dataset analysis process. Optic radiation is an example of a segmented white matter tract - the white area represents fibres traversing through a white matter lesion (depicted as a crossed circle). In contrast, the black area represents lesion-free fibres. (Original figure); AQP4 = aquaporin-4; NMOSD = neuromyelitis optica spectrum disorders; HC = healthy controls; MRI = magnetic resonance imaging; MPRAGE = magnetization prepared rapid gradient echo; DWI = diffusion-weighted imaging; FLAIR = fluid-attenuated inversion recovery; QSM = quantitative susceptibility mapping; MP2RAGE = magnetization prepared 2 rapid gradient echo; PSIR = phase sensitive inversion recovery; NODDI = neurite orientation dispersion and density imaging; NDI = neurite density index.

3.4.2. Cervical spinal cord

3.4.2.1. Cross-sectional area

Cervical cord T2-weighted images were used to obtain mean CSA values between C2 - C7 spinal segments. T2 images were automatically segmented to generate a binary spinal cord mask using the DeepSeg tool (Gros et al., 2019) from Spinal Cord Toolbox (SCT; De Leener et al., 2017), and, if necessary, manually adjusted using FSLeyes. Subsequently, images were manually labelled at the intervertebral level (posterior tip of each disc). Segmented spinal cord and vertebral labels were then used to straighten and transform the images to the PAM-50 spinal cord template (De Leener et al., 2018). Quality of the segmentation and registration process was ensured by visually inspecting each step using the quality control tool provided by SCT. CSA was computed for each vertebral level, and the average CSA from C1 - C7 was employed for statistical analysis.

3.4.2.2. Diffusion tensor imaging

Spinal cord DWI preprocessing was carried out according to standard SCT protocol and involved correction for susceptibility-induced distortions and motion. Subsequently, the DWI images were registered to the PAM-50 template using a multimodal registration algorithm (De Leener et al., 2018). The DTI model was then fitted to the preprocessed DWI data, resulting in the generation of FA and MD maps.

To evaluate the DTI metrics within NAWM of the cervical spinal cord, binary lesion masks were generated using the DeepSegLesion algorithm on axial MEDIC images, which were coregistered to DWI images (Gros et al., 2019). Additionally, T2-weighted and T1-weighted images were inspected to confirm the lesion location in the cervical spine, and in some cases, manual mask adjustment was performed in FSLeyes. The resulting lesion masks were then subtracted from the coregistered white matter atlas provided by the SCT (Lévy et al., 2015) to create NAWM masks. Grey matter masks of the cervical spinal cord were obtained using MEDIC images, which were segmented using the DeepSeg tool and manually adjusted if necessary (grey matter masks of the cervical spinal cord were not obtained for 1 HC, 3 AQP4-NMOSD patients, and 4 MS patients due to substantial artefacts on MEDIC images). Mean FA in the NAWM and mean MD in grey matter were calculated for each participant in the cervical spinal cord.

3.5. Statistical analysis

Normality and equality of variance were tested for all variables. Differences in demographic and volumetric characteristics were assessed with one-way Analysis of Variance (ANOVA) with *post hoc* pairwise t-tests (Bonferroni correction for multiple comparisons), Welch's t-test, or Mann-Whitney U test. Welch's t-tests were used to assess between-group NDI differences in individual tracts (Benjamini-Hochberg correction (p = 0.05) for multiple comparisons). Pairwise Spearman's Rank correlation was used to study the relationship between lesion count (PRL, cortical lesions) and NDI in individual tracts (Benjamini-Hochberg correction for multiple comparisons, p = 0.05). Between-group comparisons for the cervical spinal cord analysis were done using one-way ANOVA with *post hoc* pairwise t-tests (Bonferroni correction for multiple comparisons) or Welch's ANOVA with *post hoc* Games-Howell tests (Tukey correction for multiple comparisons). *P*-values were two-tailed, and statistical significance was set at 0.05.

4. RESULTS

4.1. Sample demographics

The female-to-male ratio was 18:2 in each study group. The effect of diagnosis was significant for age, $F(2, 57) = 12.22$, $p < 0.001$. *Post hoc* comparisons indicated that at the study scan, MS patients were younger ($M = 35.4$, $SD = 9.4$ years old) when compared with both AQP4-NMOSD patients ($M = 50$, $SD = 13.2$), $p < 0.001$, and HC ($M = 48.8$, $SD = 7.9$), $p < 0.001$. MS patients had significantly lower EDSS compared with AQP4-NMOSD patients ($M = 2.1$, $SD = 2.2$ vs. M = 3.8, $SD = 1.9$) $U = 297.5$, $p = .008$. There were no statistically significant differences in disease duration or time from the last attack to the study scan between MS and AQP4-NMOSD (see Table 2).

4.2. Analysis of the brain

4.2.1. White matter and cortical lesions assessment

MS patients had significantly higher white matter lesion volume when compared with AQP4-NMOSD patients ($M = 0.69$, $SD = 0.86$ vs $M = 0.23$, $SD = 0.36$), $t(25.29) = -2.18$, $p = 0.04$ (see Table 2). Three AQP4-NMOSD patients did not present with any brain lesions. In AQP4-NMOSD patients, two white matter tracts did not have any lesion load in any patient (right inferior cerebellar peduncle and right superior cerebellar peduncle). However, no statistically significant differences in bundle load were observed in any white matter tract between MS and AQP4-NMOSD ($p > 0.05$ for each tract; see Figure 7). At least one cortical lesion was identified in 16 MS patients and 4 AQP4-NMOSD patients. MS patients had significantly more cortical lesions than AQP4-NMOSD patients ($M = 7.8$, $SD = 12.5$ vs. $M = 0.45$, $SD = 1.2$), $t(19.34) = -2.6$, $p = 0.02$. At least one PRL was identified in 7 MS patients (between 1 and 5 PRL per patient) and none of the AQP4-NMOSD patients.

Table 2. Demographics and clinical/MRI characteristics of patients and controls

	MS	AQP4-NMOSD	HC
Sex, *n* (male/female)	20 (2/18)	20 (2/18)	20 (2/18)
Age, years, mean ± SD	35 ± 9***	50 ± 13	49 ± 8
EDSS score, median (range)	1 (0 - 6.5)**	3.7 (1 - 7.5)	-
Disease duration years, mean ± SD	4.7 ± 5.5	8.4 ± 7.5	-
Time from last attack to study scan, mean ± SD (months)	18.8 ± 34.7	35.9 ± 29.5	-
Brain lesions present, *n*	20	17	-
Normalised white matter lesion volume (%), mean ± SD	0.69 ± 0.86**	0.23 ± 0.36	-
PRL count, mean ± SD (*n*)	1.1 ± 1.7 (7)	-	-
Cortical lesions count, mean ± SD (*n)*	7.8 ± 12.5* (16)	0.45 ± 1.2 (4)	-
Disease-modifying therapy at the time of the scan, (*n*)	Dimethyl fumarate (11) Glatiramer acetate (1) Interferon-beta (2) Ocrelizumab (2) Untreated (4)	Azathioprine (2) Azathioprine + Methylprednisolone (1) Azathioprine + Prednisolone (1) Inebilizumab (3) Intravenous immunoglobulin (1) Methotrexate + Methylprednisolone (1) Prednisolone (3) Rituximab (4) Satralizumab (4)	-
Number of patients who had previous TM, *n*	11	18	-
Cervical cord lesion present, *n*	10	6	-

*$p < 0.05$, **$p < 0.01$, ***$p < 0.001$; *n* = number of participants

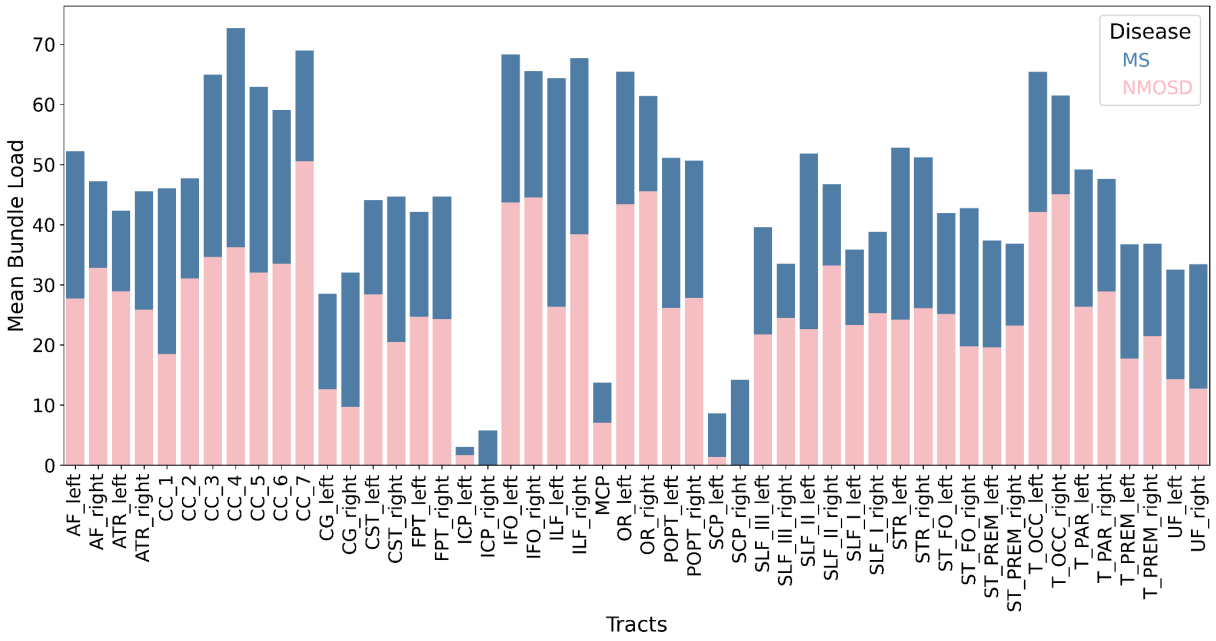

Figure 7. Mean bundle load in MS and AQP4-NMOSD. The AQP4-NMOSD bundle load bar (pink) is overlaid on the MS bundle load bar (blue). The y-axis represents the percentage of fibres in each tract with lesion involvement. Mean bundle load did not significantly differ between diseases in any of the investigated white matter tracts ($p > 0.05$). MS = multiple sclerosis; NMOSD = neuromyelitis optica spectrum disorders; AQP4 = aquaporin-4; AF = arcuate fascicle; ATR = anterior thalamic radiation; CC = corpus callosum; CC_1 = rostrum; CC_2 = genu; CC_3 = rostral body; CC_4 = anterior midbody; CC_5 = posterior midbody; CC_6 = isthmus; CC_7 = splenium; CG = cingulum; CST = corticospinal tract; FPT = fronto-pontine tract; ICP = inferior cerebellar peduncle; IFO = inferior occipito-frontal fascicle; ILF = inferior longitudinal fascicle; MCP = middle cerebellar peduncle; OR = optic radiation; POPT = parieto‑occipital pontine tract; SCP = superior cerebellar peduncle; SLF_I = superior longitudinal fascicle I; SLF_II = superior longitudinal fascicle II; SLF_III = superior longitudinal fascicle III; STR = superior thalamic radiation; ST_FO = striato-fronto-orbital; ST_PREM = striato-premotor; T_OCC = thalamo-occipital; T_PAR = thalamo-parietal; T_PREM = thalamo-premotor; UF = uncinate fascicle.

4.2.2. White matter and grey matter volumetry

The effect of diagnosis was significant for normalised white matter volume, $F(2, 57) = 4.89$, $p = 0.01$. *Post hoc* comparisons indicated that the normalised white matter volume in MS patients ($M = 28.36$, $SD = 2.52$) was significantly lower than HC ($M = 31.3$, $SD = 3.05$), $p = 0.008$. No significant differences were found between AQP4-NMOSD patients ($M = 29.8$, $SD = 3.29$) and both HC and MS patients.

The effect of diagnosis was also significant for normalised subcortical grey matter volume, $F(2, 57) = 8.83$, $p < 0.001$. *Post hoc* comparisons indicated that the normalised subcortical grey matter volume in MS patients ($M = 3.35$, $SD = 0.31$) was significantly lower

than HC (M = 3.83, SD = 0.4), $p < 0.001$. No significant differences were found between AQP4-NMOSD patients (M = 3.59, SD = 0.36) and both HC and MS patients.

No significant differences in normalised cortical volume were found between the studied groups, $F(2, 57) = 0.72$, $p = 0.49$.

4.2.3. Lesion-informed tractometry

4.2.3.1. NDI differences between MS and AQP4-NMOSD

When examining unsegmented white matter tracts, 17 out of 50 tracts showed significantly lower NDI values in MS compared with AQP4-NMOSD (see Supplementary Table 1).

In white matter fibres traversing through white matter lesions, NDI was reduced in MS for only one of the 48 assessed tracts (two white matter tracts did not have any lesion load in any AQP4-NMOSD patient) when compared with AQP4-NMOSD (isthmus of the corpus callosum, M = 0.58, SD = 0.05 vs. M = 0.63, SD = 0.04), $t(31.66) = -2.56$, $p = 0.04$. (see Figure 8A; see Supplementary Table 2).

In white matter fibres not traversing through white matter lesions, MS patients exhibited significantly lower NDI values in 6 of 50 tracts compared with AQP4-NMOSD patients. These included: isthmus of the corpus callosum (M = 0.58 SD = 0.04 vs. M = 0.62 SD = 0.05), $t(37.73) = -2.70$, $p = 0.04$; left corticospinal tract (M = 0.67, SD = 0.03 vs. M = 0.70 SD = 0.03), $t(37.98) = -3.08$, $p = 0.02$; left inferior cerebellar peduncle (M = 0.68, SD = 0.04 vs. M = 0.72, SD = 0.02), $t(36.14) = -3.40$, $p = 0.01$; left inferior longitudinal fascicle (M = 0.52, SD = 0.03 vs. M = 0.54, SD = 0.04), $t(34.90) = -2.99$, $p = 0.02$; middle cerebellar peduncle (M = 0.72, SD = 0.03 vs. M = 0.75, SD = 0.04), $t(31.67) = -3.11$, $p = 0.02$; left parieto-occipital pontine tract (M = 0.64, SD = 0.02 vs. M = 0.67, SD = 0.03), $t(36.08) = -2.73$, $p = 0.04$. (see Figure 8B; see Supplementary Table 3).

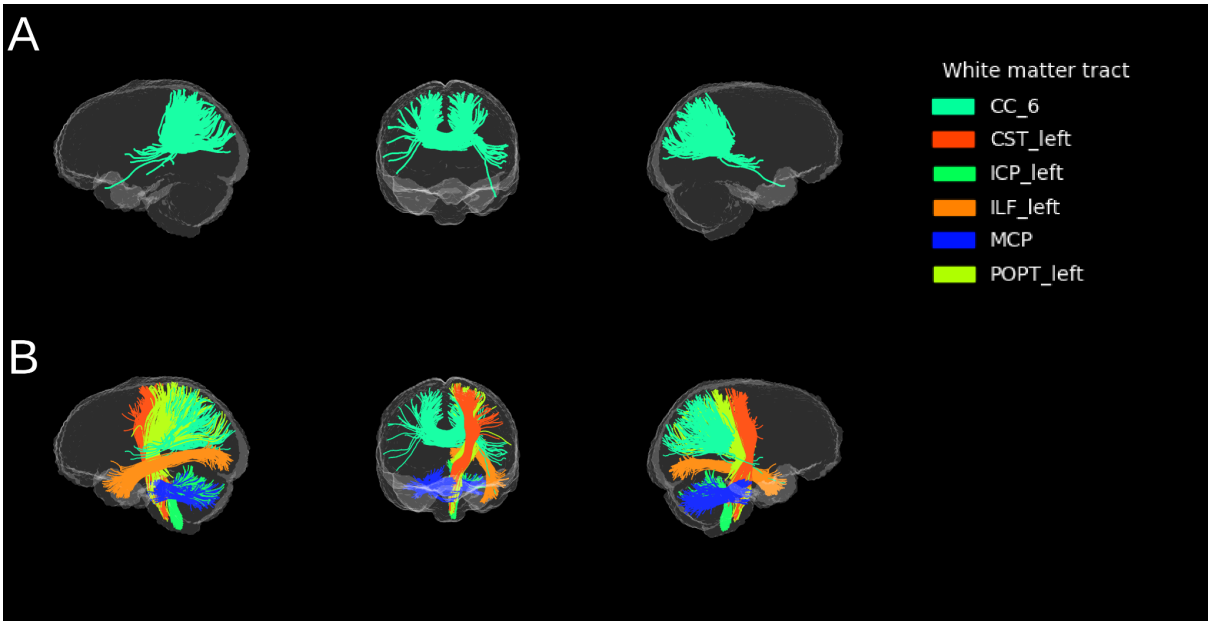

Figure 8. Significant differences in mean NDI between MS and AQP4-NMOSD. (A) White matter fibres traversing through white matter lesions show significantly lower NDI values in MS patients when compared with AQP4-NMOSD patients. (B) White matter fibres not traversing through white matter lesions show significantly lower NDI values in MS patients when compared with AQP4-NMOSD patients. MS = multiple sclerosis; NMOSD = neuromyelitis optica spectrum disorders; AQP4 = aquaporin-4; CC_6 = isthmus; CST = corticospinal tract; ICP = inferior cerebellar peduncle; ILF = inferior longitudinal fascicle; MCP = middle cerebellar peduncle; POPT = parieto‑occipital pontine tract.

4.2.3.2. NDI differences between MS patients and HC

In the evaluation of unsegmented tracts, 48 out of 50 white matter tracts in MS patients demonstrated a significant reduction in NDI compared with the corresponding tracts in HC (see Supplementary Table 4).

After segmenting tracts based on lesion location, a decrease in NDI was identified in 40 out of 50 tracts in fibres traversing through white matter lesions and in 34 out of 50 tracts in fibres not traversing through white matter lesions when compared with whole tracts from HC (see Supplementary Table 5; see Supplementary Table 6).

4.2.3.3. NDI differences between AQP4-NMOSD patients and HC

In AQP4-NMOSD patients, the assessment of unsegmented tracts showed no significant differences in NDI when compared with HC (see Supplementary Table 7).

Among tract fibres traversing through white matter lesions, 9 out of 48 white matter tracts in AQP4-NMOSD patients showed a significant decrease in NDI compared with whole tracts in HC. However, when assessing lesion-free fibres, no significant differences in NDI were identified between AQP4-NMOSD patients and HC in any white matter tract (see Supplementary Table 8; see Supplementary Table 9).

4.2.4. Analysis of cortical damage and paramagnetic rim lesions in relation to white matter changes in lesion-free fibres

Next, cortical damage in MS and AQP4-NMOSD patients was evaluated using T1 relaxation rates. In MS, the relationship between the count of cortical lesions as well as the count of PRL and NDI in white matter fibres, not traversing through white matter lesions, was examined separately. Compared with HC, cortical T1 relaxation rates were significantly lower in 103 out of 150 cortical regions in MS patients (see Supplementary Table 10; see Figure 9A) and in 4 out of 150 in AQP4-NMOSD patients (see Supplementary Table 11; see Figure 9B). In AQP4-NMOSD these regions included: right central sulcus (M = 0.75, SD = 0.01 vs. M = 0.77, SD = 0.01), $t(32.25) = -3.26$, $p = 0.01$; left central sulcus (M = 0.74, SD = 0.02 vs. M = 0.76, SD = 0.02), $t(30.37) = -2.84$, $p = 0.03$; right superior occipital gyrus (M = 0.73, SD = 0.02 vs. M = 0.75, SD = 0.01), $t(30.25) = -2.73$, $p = 0.04$; right superior occipital sulcus and transverse occipital sulcus (M = 0.73, SD = 0.02 vs. M = 0.75, SD = 0.01), $t(29.09) = -2.60$, $p < 0.05$. Also, MS patients had significantly lower T1 relaxation rates in 28 out of 150 cortical regions compared to AQP4-NMOSD (see Supplementary Table 12; see Figure 9C). In MS patients, the cortical lesion count showed a statistically significant negative correlation with NDI in fibres not traversing through white matter lesions in 38 out of 50 white matter tracts (see Supplementary Table 13). However, no significant correlation was found between PRL count and NDI values in any such tract.

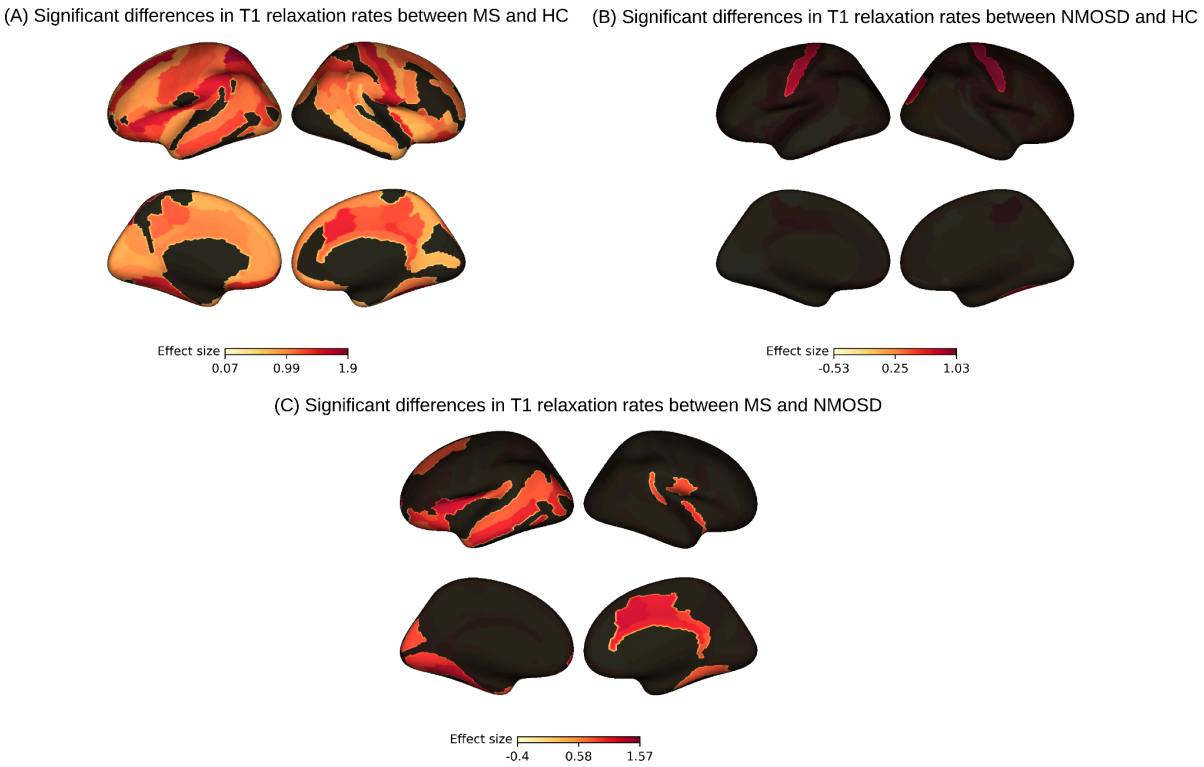

Figure 9. Significant differences in mean T1 relaxation rates observed between the studied groups. (A) Among cortical regions, 103/150 exhibited significantly lower T1 relaxation rates in MS patients compared with HC. (B) 4/150 cortical regions showed significantly lower T1 relaxation rates in AQP4-NMOSD patients compared with HC. (C) 28/150 cortical regions exhibited significantly lower T1 relaxation rates in MS patients compared with AQP4-NMOSD patients. MS = multiple sclerosis; HC = healthy controls; NMOSD = neuromyelitis optica spectrum disorders; AQP4 = aquaporin-4.

4.3. Analysis of the cervical spinal cord

4.3.1. Assessment of lesions

Six AQP4-NMOSD and ten MS patients had at least one residual T2-hyperintense lesion in the cervical spinal cord on the research scan (see Table 2).

4.3.2. Differences in cross-sectional area

The effect of diagnosis was significant for the spinal cord CSA, $F(2, 56) = 3.58$, $p = 0.03$. *Post hoc* comparisons indicated that AQP4-NMOSD patients ($M = 63.78$, $SD = 9.0$) had significantly lower whole cord CSA than HC ($M = 70.75$, $SD = 6.54$), $p = 0.04$. No significant differences between AQP4-NMOSD and MS patients ($M = 68.85$, $SD = 9.51$) or between MS patients and HC were found (see Figure 10).

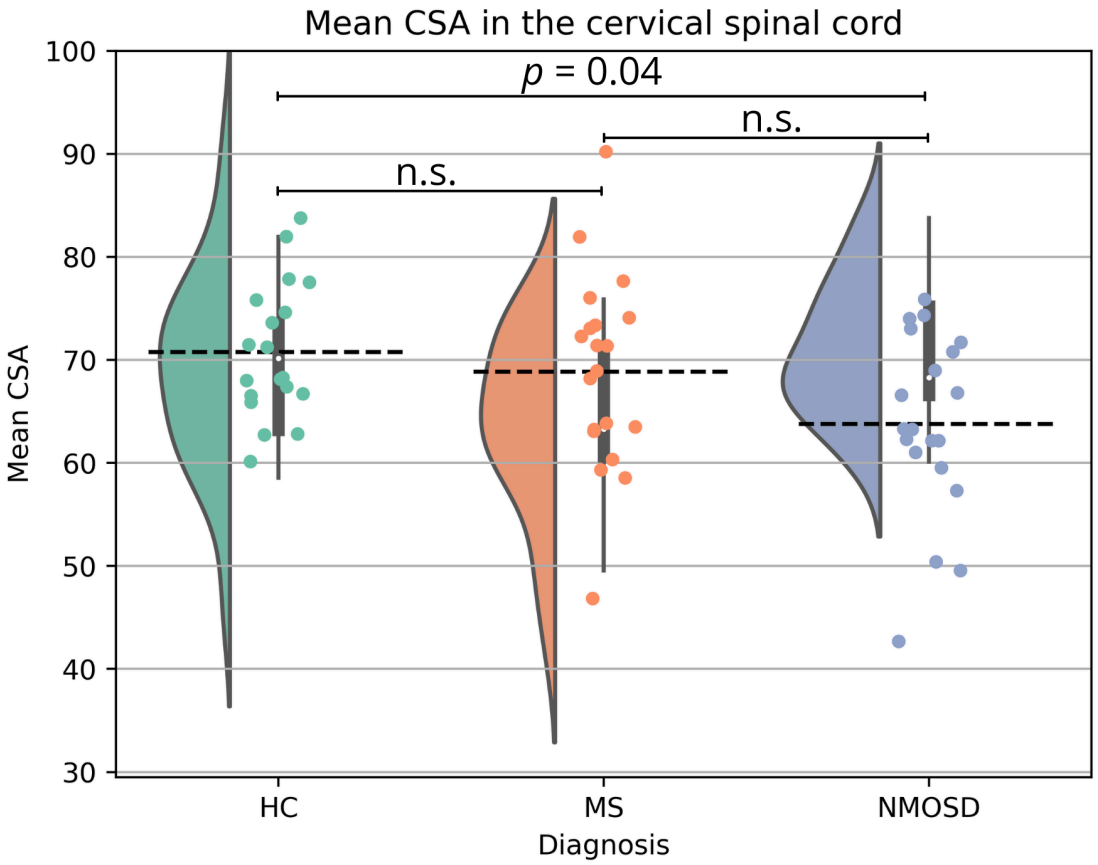

Figure 10. Between-group differences in mean CSA of the cervical spinal cord. Each data point represents a value from a single participant. CSA = cross-sectional area; HC = healthy controls; MS = multiple sclerosis; NMOSD = neuromyelitis optica spectrum disorders; n.s. = not significant.

4.3.3. Differences in white and grey matter microstructure

The effect of diagnosis was significant for the FA in NAWM, $F(2, 33.46) = 4.72$, $p = 0.02$. *Post hoc* analysis showed trends toward significance in comparison between AQP4-NMOSD patients ($M = 0.60$, $SD = 0.07$) with HC ($M = 0.65$, $SD = 0.03$), $p = 0.057$, and MS patients ($M = 0.61$, $SD = 0.05$) with HC, $p = 0.063$. No significant differences between AQP4-NMOSD and MS patients were found.

No significant between-group differences were observed when assessing cervical spinal cord grey matter MD, $F(2, 48) = 1.07$, $p = 0.35$.

5. DISCUSSION

While traditional approaches like conventional MRI are generally reliable in typical MS and AQP4-NMOSD cases, they often fall short in atypical or borderline presentations. These cases carry a significant risk of misdiagnosis and consequent inappropriate treatment, leading to long-term disability. New non-conventional MRI techniques have the potential to identify distinctive features that could improve the characterisation and differentiation of MS and AQP4-NMOSD, ultimately leading to more accurate diagnoses and better patient outcomes.

This thesis prospectively and cross-sectionally evaluated in vivo brain and cervical spinal cord characteristics in MS and AQP4-NMOSD patients using non-conventional MRI methods. Grey and white matter features were comprehensively assessed in both disorders and compared with benchmark measurements from the HC group. In the brain, the study examined NDI in white matter tracts, distinguishing between fibres that traverse through T2-hyperintense white matter lesions and those that do not. The cerebral cortex was evaluated using T1 relaxation rates, cortical lesion identification, and volumetry, with volumetric analyses also performed for white matter and deep grey matter. Additionally, in MS, the relationship between lesion-free white matter fibres and both cortical lesions and chronic active lesions marked by a paramagnetic rim was investigated. In the cervical spinal cord, FA in NAWM, MD in grey matter, and whole cord CSA were analysed to identify damage patterns unique to each disorder.

This chapter will discuss the main findings of this research, address its strengths and limitations, and explore potential directions for future studies. The concluding remarks will provide key insights and contributions of the thesis.

5.1. Unique cerebrospinal damage patterns in MS and AQP4-NMOSD

5.1.1. Assessment of white matter changes in the brain

No statistically significant differences in lesion burden were found between MS and AQP4-NMOSD across any white matter tract. When examining whole (unsegmented) white matter tracts, MS patients exhibited a significant reduction in NDI across most tracts (48 out of 50 tracts) when compared with HC. In contrast, no such reductions were observed in AQP4-NMOSD patients. However, a more distinctive pattern emerged when the tracts were

segmented into fibres traversing and not traversing through white matter lesions. In MS, NDI reductions were widespread, affecting the majority of tract fibres regardless of whether they traversed through white matter lesions (40 out of 50 tracts) or remained lesion-free (37 out of 50 tracts). In contrast, AQP4-NMOSD patients exhibited a more localised damage pattern, with lower NDI occurring only in tract fibres traversing through white matter lesions (9 out of 48 tracts) and never in lesion-free fibres. Moreover, normalised white matter volume was significantly lower in MS patients when compared with HC, while no such effect was observed in AQP4-NMOSD patients.

These findings provide further evidence that diffuse, non-lesional white matter injury in MS cannot be solely attributed to anterograde and retrograde neurodegeneration from white matter lesions (Kawachi & Lassmann, 2017). This conclusion is supported by the observation that the majority of white matter fibres not traversing through any white matter lesions at any location still exhibited decreased NDI values compared with whole tracts in the cerebral white matter of HC, which suggests the involvement of additional, white matter lesion-independent mechanisms driving neurodegeneration in MS. Conversely, in AQP4-NMOSD patients, significant NDI reductions were observed in several tract fibres traversing through white matter lesions, while fibres anatomically independent of these lesions showed no such reductions. This pattern may reflect a lack of widespread neurodegenerative mechanisms in white matter in AQP4-NMOSD, further supporting the idea that axonal loss is primarily secondary to inflammatory attacks. Moreover, the extent of neurodegenerative changes in AQP4-NMOSD lesions varies, with some white matter lesions remaining asymptomatic (Kim et al., 2012), while others, particularly those presenting as hypointense on T1-weighted images, are associated with more pronounced tissue destruction and worse patient outcomes (Ghazanfari et al., 2024). This lesion heterogeneity in AQP4-NMOSD could explain why only some lesion-traversing fibres show altered microstructural integrity, while others remain unaffected.

The current study suggests that chronic neurodegenerative processes present in MS (observed even at the individual tract level) and potentially absent in AQP4-NMOSD can be used to discriminate between the two diseases. In a direct comparison between MS and AQP4-NMOSD patients, six tracts with fibres not traversing through white matter lesions were found to have significantly lower NDI in MS compared with AQP4-NMOSD. These tracts are associated with pyramidal (left corticospinal tract), cerebellar (middle cerebellar

peduncle, left inferior cerebellar peduncle, left parieto-occipital pontine tract), and cognitive (left inferior longitudinal fascicle, isthmus of the corpus callosum) functions. The cerebellar findings are especially noteworthy, as previous studies have demonstrated that loss of FA in the cerebellum can occur even in the absence of white matter lesions. This change has been observed in patients with early or mild MS, despite no detectable reduction in cerebellar volume (Deppe et al., 2016; Rocca et al., 2004). Additionally, FA loss in the cerebellum has been observed in patients with clinically isolated syndrome who had no infratentorial lesions, and this loss was associated with shorter conversion times to clinically definite MS. (Kugler & Deppe, 2018). Furthermore, when comparing MS and AQP4-NMOSD patients, one tract (the isthmus of the corpus callosum) was identified in which fibres traversing through white matter lesions exhibited significantly lower NDI in MS. This particular finding could be attributed to heterogeneity in focal lesion demyelination and neurodegeneration severity in MS (Lucchinetti et al., 2000). It is possible that the observed tract was affected by a heavier load of chronic active lesions in the MS patient cohort. As these lesions exhibit severe tissue demyelination with microglia activation, they may lead to more pronounced neurodegeneration in the affected tract (Rahmanzadeh et al., 2022a).

5.1.2. Grey matter abnormalities in the brain

In this study, cortical lesions were more commonly found in MS patients than in AQP4-NMOSD patients, in whom these lesions were mostly absent. Although no normalised cortical volume loss was identified in MS and AQP4-NMOSD patients compared with HC, the T1 relaxation rates for the cerebral cortex were lower in the majority (103 out of 150) of cortical regions in our MS patients compared with HC. This finding was observed in only 4 out of 150 cortical regions in AQP4-NMOSD patients. Moreover, MS patients showed significantly lower T1 relaxation rates in 28 out of 150 cortical regions when compared with AQP4-NMOSD patients. Subcortical grey matter volume was also found to be lower in MS, compared with HC, which was not the case in AQP4-NMOSD patients.

The results further confirm that MS is characterised by extensive cortical and deep grey matter changes, which likely reflect widespread cortical demyelination and neurodegeneration (Calabrese et al., 2015; Rahmanzadeh et al., 2022b). They also suggest that microstructural changes may be evident even when macrostructural (volumetric) changes are not, demonstrating their potential value in the diagnostic process. In AQP4-NMOSD, the

absence of widespread cortical alterations aligns with the understanding that the disease primarily affects astrocytic function and perivascular tissue, sparing cortical grey matter to a greater extent (Kawachi & Lassmann, 2017).

Interestingly, significant bilateral alterations in T1 relaxation times were observed in the central sulcus (sensorimotor cortical areas) of AQP4-NMOSD patients, which could indicate that neurodegeneration following severe TM attacks may extend to the brain via anterograde and/or retrograde mechanisms. This issue remains underexplored, with only one study by Papadopoulou et al. (2019) investigating volume changes in the ventral posterior thalamic nucleus, which receives afferent white matter fibres from the spinal cord and projects the information further to the cortex. Notably, no significant volume changes were observed in AQP4-NMOSD patients with a history of TM.

5.1.3. The impact of cortical lesions and paramagnetic rim lesions on white matter damage in MS

In MS, significant negative correlations were identified between the number of cortical lesions and NDI in the majority of lesion-free white matter tracts (38 out of 50). This relationship suggests that cortical pathology may contribute to diffuse neurodegeneration in white matter, independent of white matter lesion burden. The findings also indicate that a reduction in NDI within tract fibres not traversing through white matter lesions is more closely associated with measures of cortical damage rather than chronic active lesions, as PRL count showed no such relationship. This potential link between cortical lesions and widespread white matter damage aligns with emerging evidence that cortical pathology plays a critical role in the pathogenesis of MS, particularly in its progressive forms, and with previous studies showing that meningeal inflammation correlates with diffuse NAWM degeneration (Androdias et al., 2010; Haider et al., 2016). Cortical demyelination and neurodegeneration may create a pro-inflammatory and neurotoxic environment, mediated by mechanisms such as retrograde and anterograde degeneration of axons connecting cortical and subcortical structures (Calabrese et al., 2015; Kolasinski et al., 2012). Moreover, studies have suggested that cortical damage in MS can disrupt functional and structural connectivity, which may further exacerbate white matter integrity loss, even in regions without visible lesions (Krijnen et al., 2024; Tahedl et al., 2018). While these findings highlight the importance of cortical pathology as a distinct and potentially significant driver of diffuse

white matter changes in MS, the directionality of the relationship between cortical and white matter damage remains to be further investigated.

5.1.4. Evaluation of volumetric and microstructural properties in the cervical spinal cord

Analysis of CSA in the cervical spinal cord showed that AQP4-NMOSD patients had significantly lower CSA compared with HC, highlighting substantial structural changes in this group. This finding aligns with previous studies, which have demonstrated pronounced spinal cord atrophy in NMOSD patients, likely due to the disease's propensity for severe spinal cord inflammation and demyelination (Liu et al., 2015; Mariano et al., 2021). In contrast, no significant differences in CSA were observed between MS patients and HC or between MS and AQP4-NMOSD patients. These findings suggest that while both diseases may involve spinal cord pathology, the extent and mechanisms of volume change differ substantially (Mariano et al., 2021).

Reduced FA in the cervical spinal cord NAWM was found in both MS and AQP4-NMOSD patients, compared with HC, although these differences did not reach statistical significance. This finding could be indicative of microstructural damage related to white matter integrity alterations, potentially reflecting axonal loss or demyelination, both of which are important features of MS and AQP4-NMOSD pathology (Carnero & Correale, 2021; Rodríguez et al., 2022). The trend-level reduction in FA may be explained by early or diffuse pathological changes that do not yet manifest as overt structural disruption detectable by diffusion metrics at a statistically significant level.

Additionally, the current study assessed MD in the cervical spinal cord grey matter. However, the analysis showed no significant differences between the studied groups. While this finding aligns with typical MS pathology, which generally spares the central grey matter (Ciccarelli et al., 2019), it was surprising given that spinal cord inflammation in AQP4-NMOSD tends to predominantly affect the central grey matter, a region rich in AQP4 (Kim et al., 2015). It is possible that while damage to spinal cord white matter spreads through axons transected by lesions, grey matter injury is more focal and localised, leading to microstructural alterations only within the lesioned sites.

5.2. Strengths and limitations

The strengths of this study lie in its novel and meticulous methodological approach and complex assessment of both the brain and cervical spinal cord. Previous studies investigating white matter damage in MS and NMOSD have focused on assessing NAWM as a whole region of interest. However, these approaches showed spurious results, and they did not account for possible lesion-dependent degeneration along the tract. To address this issue, the current study adopted a new methodology combining several advanced MRI-based tools to investigate white matter damage in greater detail. Specifically, white matter damage was evaluated using the biologically plausible NODDI model, with the NDI metric assessing white matter integrity. This approach was combined with a convolutional neural network-based method for white matter segmentation, allowing for the accurate identification and quantification of neurodegeneration along well-defined anatomical tracts. To refine the analysis, white matter tracts were segmented into fibres that either passed through white matter lesions (ensuring that lesion points were excluded from the affected tract segments) or remained lesion-free. This approach provided a more precise and detailed understanding of white matter damage patterns, which might have been obscured by the influence of white matter lesions. Moreover, the study employed state-of-the-art methodology to map T1 relaxation rates in the cerebral cortex. This advanced approach enabled a more precise detection and quantification of microstructural changes that were not evident through volumetric assessments. Unlike traditional volumetric measures, which primarily capture macroscopic atrophy, T1 relaxation mapping provides a more sensitive marker of cortical microstructural integrity, reflecting changes in myelination, water content, and cellular composition (Granziera et al., 2021). This novel application enhances the ability to detect early neurodegenerative processes that might otherwise go unnoticed, offering valuable insights into disease mechanisms.

Despite this study's strengths, several limitations should be considered when interpreting the findings. Due to the rarity of AQP4-NMOSD, the results are based on a relatively small cohort of patients. Additionally, MS patients were, on average, younger and less disabled than AQP4-NMOSD patients, reflecting the natural differences between the two conditions, with AQP4-NMOSD often presenting at an older age and being highly disabling early on (Wingerchuk et al., 2015). Despite these differences, MS was associated with greater white and grey matter damage when compared with AQP4-NMOSD and HC. This result,

combined with findings from Cox et al. (2016) and Giorgio et al. (2010), who demonstrated a gradual decrease in NDI and grey matter volume with age, suggests that the observed effects may be more pronounced in age-matched groups. Moreover, the tract segmentation approach, dividing fibres into those traversing and not traversing through white matter lesions, was based on visible hyperintensities from conventional FLAIR images and did not account for lesions that may have resolved over time. However, it is essential to highlight that in MS, white matter lesions typically accumulate over time rather than resolve (Todea et al., 2020). Another limitation is that the heterogeneity of both AQP4-NMOSD and MS patient groups when considering a history of TM may have hindered the detection of more pronounced changes in the cervical spinal cord. However, this issue is unlikely to significantly impact the overall findings, as most patients (18/20 in AQP4-NMOSD and 11/20 in MS) had documented TM. Moreover, in MS, spinal cord pathology, including atrophy and asymptomatic T2-hyperintense lesions, has been reported even in RRMS patients without clinical signs of spinal cord involvement. This suggests that the spinal cord is often affected by the disease, regardless of acute clinical episodes (Bischof et al., 2022; Bot et al., 2004). In this study, MRI-based spinal cord assessment may also have been hindered by substantial artifacts in MEDIC images, preventing grey matter mask extraction for one HC, three AQP4-NMOSD patients, and four MS patients. These artifacts, likely resulting from susceptibility effects or CSF pulsation, compromised image segmentation and led to data loss, potentially affecting the reliability of the grey matter analysis. Lastly, the lesion-free fibres assessed in the brain, particularly in the corticospinal tracts, may have been influenced by spinal cord lesions and could be undergoing neurodegenerative changes due to retrograde degeneration. However, no significant NDI differences were found in corticospinal lesion-free white matter fibers between AQP4-NMOSD patients and HC, suggesting that any potential retrograde effects may be subtle or regionally specific.

5.3. Future directions

Future studies should address several key aspects highlighted by the findings of this study. Firstly, NODDI measurements are practical for clinical application but require multi-shell diffusion-based protocols, which are accessible in most modern clinical MRI scanners. However, additional studies are necessary to confirm reproducibility and to establish reference cut-off values for healthy populations (Chung et al., 2016; Kamiya et al., 2020).

If validated in well-defined cohorts of MS and AQP4-NMOSD patients, non-conventional MRI metrics (e.g., NDI in lesion-free white matter fibres) could be incorporated to assist in diagnosing challenging cases with minimal brain lesions or ambiguous conventional MRI findings (Juryńczyk et al., 2022). It is also important to further investigate this effect in AQP4-IgG negative NMOSD patients, as they could benefit from potential clinical applications, given their frequent presentation of overlapping MS and NMOSD characteristics (Juryńczyk et al., 2016). This thesis also provides further evidence for the interdependence of cortical grey matter and diffuse white matter damage in MS (Androdias et al., 2010; Haider et al., 2016). Future studies should aim to clarify this relationship's directionality, which could provide valuable insights into the mechanisms underlying neurodegeneration. Furthermore, it would be worth investigating lesion heterogeneity in the MS and AQP4-NMOSD cohorts and assessing whether neurodegeneration in white matter fibers traversing through white matter lesions differs between certain lesion types. It would be especially interesting to compare non-chronic lesions with lesions exhibiting paramagnetic rims and slowly expanding lesions in MS, as there is substantial evidence for the more destructive role of these two lesion types (Calvi et al., 2023). Lastly, it would be valuable to assess the potential brain damage resulting from spinal cord attacks in AQP4-NMOSD patients. The effect of anterograde and trans-synaptic degeneration was previously reported in AQP4-NMOSD in patients with a history of ON and was demonstrated in the optic pathways at the level of the retina, thalamus, and visual cortex (Manogaran et al., 2016; Tian et al., 2018). Although TM in AQP4-NMOSD is locally destructive, little is understood about whether it is associated with neurodegenerative processes in the brain and, if so, how such processes might correlate with clinical outcomes.

5.4. Concluding remarks

This study underscores the distinct pathophysiological mechanisms of MS and AQP4-NMOSD, emphasizing the diverse and complex nature of neurodegeneration in these conditions. The results provide further evidence that MS is likely driven by complex inflammatory and neurodegenerative processes that extend beyond visible lesions, affecting deep grey matter, non-lesional white matter, and cerebral cortex, while relatively sparing cervical spinal cord, at least in the early stages of the disease. In contrast, AQP4-NMOSD is primarily characterised by a localised, antibody-mediated, complement-dependent immune

attack that leads to severe, focal damage, such as LETM and spinal cord atrophy. However, this study also provides new evidence that AQP4-NMOSD does not exhibit the widespread, non-attack-related neurodegenerative processes typically seen in MS, suggesting that the neurodegenerative mechanisms in AQP4-NMOSD are more selective and localized to areas directly affected by inflammation. Additionally, the findings, particularly the lower NODDI-derived NDI in lesion-free white matter fibres in MS compared to AQP4-NMOSD, suggest a potential diagnostic marker, with the increased damage to cerebellar tracts in MS further highlighting a key region that may help distinguish between the two conditions.

The non-conventional MRI techniques used in this thesis, including tract segmentation and lesion localisation, provide a robust framework for future research. These approaches not only improve the understanding of white matter damage but also hold promise for developing new diagnostic tools. Further validation will be essential to integrating these imaging metrics into clinical practice, potentially enhancing the diagnosis and management of MS and AQP4-NMOSD.

6. SUMMARY AND CONCLUSIONS

The results presented in this work focus on investigating cerebrospinal white and grey matter damage patterns through non-conventional imaging techniques in MS and AQP4-NMOSD patients, with comparisons made to HC as reference measures. This section offers a concise summary of the key findings of this thesis.

I. The results regarding white and grey matter damage in the brain in MS and AQP4-NMOSD patients indicate that:

A. MS patients exhibit significantly lower normalised white matter and subcortical grey matter volumes than HC, while no such volumetric changes are observed in AQP4-NMOSD patients. No significant volumetric differences are found between MS and AQP4-NMOSD patients.

B. Compared with AQP4-NMOSD, MS patients show significant NDI reductions in fibres traversing through white matter lesions in 1 tract and in lesion-free fibres in 6 tracts.

C. MS patients show significant reductions in NDI across most tracts, regardless of whether the fibres traverse through white matter lesions (40 out of 50) or are lesion-free (34 out of 50). In contrast, AQP4-NMOSD patients exhibit NDI reductions only in white matter fibres that traverse through white matter lesions (9 out of 48).

D. MS patients have significantly more cortical lesions than AQP4-NMOSD patients, in whom cortical lesions are uncommon.

E. Compared with AQP4-NMOSD, MS patients exhibit significantly lower T1 relaxation rates in 28 out of 150 cortical regions.

F. Compared with HC, cortical T1 relaxation rates are significantly lower in 103 out of 150 cortical regions in MS patients and 4 out of 150 in AQP4-NMOSD patients.

II. **The investigation of the association between damage to lesion-free white matter fibres in the brain and the presence of cortical lesions in MS patients demonstrates that:**

   A. In MS patients, the cortical lesion count exhibits a statistically significant negative correlation with NDI in white matter fibres that do not traverse through white matter lesions in 38 out of 50 tracts.

III. **The investigation of the association between damage to lesion-free white matter fibres in the brain of MS patients and chronic active lesions, evidenced by the presence of a paramagnetic rim, shows that:**

   A. In MS, no significant correlation is observed between PRL count and NDI in white matter fibres that do not traverse through white matter lesions.

IV. **The results regarding cervical spinal cord damage in MS and AQP4-NMOSD patients demonstrate that:**

   A. AQP4-NMOSD patients exhibit significantly lower CSA when compared with HC, while no significant CSA alterations are observed in MS patients. No significant CSA differences are found between MS and AQP4-NMOSD patients.

   B. AQP4-NMOSD and MS patients show lower NAWM FA in the cervical spinal cord, though the differences are not statistically significant.

   C. No significant MD alterations are observed in the cervical spinal cord grey matter in the studied groups.

This study reveals distinct patterns of cerebrospinal damage in MS and AQP4-NMOSD patients. MS is characterised by widespread neurodegeneration affecting both grey matter and white matter diffusely, whereas, in AQP4-NMOSD, damage appears to be focal and attack-related, without widespread changes. These differences can be detected and quantified using non-conventional imaging techniques, which may serve as valuable diagnostic tools for distinguishing between the two diseases.

7. REFERENCES

1. Aboul-Enein, F., Kršśák, M., Höftberger, R., Prayer, D., & Kristoferitsch, W. (2010). Diffuse White Matter Damage Is Absent in Neuromyelitis Optica. *AJNR. American Journal of Neuroradiology*, *31*(1), 76.
2. Alshehri, A., Al-Iedani, O., Arm, J., Gholizadeh, N., Billiet, T., Lea, R., Lechner-Scott, J., & Ramadan, S. (2022). Neural diffusion tensor imaging metrics correlate with clinical measures in people with relapsing-remitting MS. *The Neuroradiology Journal*, *35*(5). https://doi.org/10.1177/19714009211067400
3. Andravizou, A., Dardiotis, E., Artemiadis, A., Sokratous, M., Siokas, V., Tsouris, Z., Aloizou, A.-M., Nikolaidis, I., Bakirtzis, C., Tsivgoulis, G., Deretzi, G., Grigoriadis, N., Bogdanos, D. P., & Hadjigeorgiou, G. M. (2019). Brain atrophy in multiple sclerosis: mechanisms, clinical relevance and treatment options. *Autoimmunity Highlights*, *10*(1). https://doi.org/10.1186/s13317-019-0117-5
4. Androdias, G., Reynolds, R., Chanal, M., Ritleng, C., Confavreux, C., & Nataf, S. (2010). Meningeal T cells associate with diffuse axonal loss in multiple sclerosis spinal cords. *Annals of Neurology*, *68*(4). https://doi.org/10.1002/ana.22054
5. Balcer, L. J. (2006). Clinical practice. Optic neuritis. *The New England Journal of Medicine*, *354*(12). https://doi.org/10.1056/NEJMcp053247
6. Barnett, M. H., & Prineas, J. W. (2004). Relapsing and remitting multiple sclerosis: pathology of the newly forming lesion. *Annals of Neurology*, *55*(4). https://doi.org/10.1002/ana.20016
7. Barzegar, M., Najdaghi, S., Afshari-Safavi, A., Nehzat, N., Mirmosayyeb, O., & Shaygannejad, V. (2021). Early predictors of conversion to secondary progressive multiple sclerosis. *Multiple Sclerosis and Related Disorders*, *54*. https://doi.org/10.1016/j.msard.2021.103115
8. Bastiani, M., Cottaar, M., Fitzgibbon, S. P., Suri, S., Alfaro-Almagro, F., Sotiropoulos, S. N., Jbabdi, S., & Andersson, J. L. R. (2019). Automated quality control for within and between studies diffusion MRI data using a non-parametric framework for movement and distortion correction. *NeuroImage*, *184*. https://doi.org/10.1016/j.neuroimage.2018.09.073
9. Bennett, J. L., Lam, C., Kalluri, S. R., Saikali, P., Bautista, K., Dupree, C., Glogowska, M., Case, D., Antel, J. P., Owens, G. P., Gilden, D., Nessler, S., Stadelmann, C., & Hemmer, B. (2009). Intrathecal pathogenic anti-aquaporin-4 antibodies in early neuromyelitis optica. *Annals of Neurology*, *66*(5). https://doi.org/10.1002/ana.21802
10. Berkovich, R. R. (2016). Acute Multiple Sclerosis Relapse. *Continuum* , *22*(3). https://doi.org/10.1212/CON.0000000000000330
11. Bischof, A., Papinutto, N., Keshavan, A., Rajesh, A., Kirkish, G., Zhang, X., Mallott, J. M., Asteggiano, C., Sacco, S., Gundel, T. J., Zhao, C., Stern, W. A., Caverzasi, E., Zhou, Y., Gomez, R., Ragan, N. R., Santaniello, A., Zhu, A. H., Juwono, J., … Henry, R. G. (2022). Spinal Cord Atrophy Predicts Progressive Disease in Relapsing Multiple Sclerosis. *Annals of Neurology*, *91*(2). https://doi.org/10.1002/ana.26281
12. Boaventura, M., Fragoso, D. C., Avolio, I., Pereira, S. A., Callegaro, D., Sato, D. K., da Costa Leite, C., Rovira, À., Sastre-Garriga, J., Pareto, D., & de Medeiros Rimkus, C. (2025). Brain tissue integrity in neuromyelitis optica spectrum disorder through T1-w/T2-w ratio, MTR and DTI. *Journal of Neurology*, *272*(2). https://doi.org/10.1007/s00415-024-12869-1
13. Bonnan, M., Valentino, R., Debeugny, S., Merle, H., Fergé, J. L., Mehdaoui, H., & Cabre, P. (2018). Short delay to initiate plasma exchange is the strongest predictor of outcome in severe attacks of NMO spectrum disorders. *Journal of Neurology, Neurosurgery, and Psychiatry*, *89*(4). https://doi.org/10.1136/jnnp-2017-316286
14. Bonnier, G., Fischi-Gomez, E., Roche, A., Hilbert, T., Kober, T., Krueger, G., & Granziera, C. (2019). Personalized pathology maps to quantify diffuse and focal brain damage. *NeuroImage. Clinical*, *21*. https://doi.org/10.1016/j.nicl.2018.11.017
15. Bot, J. C., Barkhof, F., Polman, C. H., Gj, L. à. N., de Groot, V., Bergers, E., Ader, H. J., &

Castelijns, J. A. (2004). Spinal cord abnormalities in recently diagnosed MS patients: added value of spinal MRI examination. *Neurology*, *62*(2). https://doi.org/10.1212/wnl.62.2.226
16. Brück, W., Porada, P., Poser, S., Rieckmann, P., Hanefeld, F., Kretzschmar, H. A., & Lassmann, H. (1995). Monocyte/macrophage differentiation in early multiple sclerosis lesions. *Annals of Neurology*, *38*(5). https://doi.org/10.1002/ana.410380514
17. Burman, J., Raininko, R., & Fagius, J. (2011). Bilateral and recurrent optic neuritis in multiple sclerosis. *Acta Neurologica Scandinavica*, *123*(3). https://doi.org/10.1111/j.1600-0404.2010.01388.x
18. Cacciaguerra, L., & Flanagan, E. P. (2024). Updates in NMOSD and MOGAD Diagnosis and Treatment: A Tale of Two Central Nervous System Autoimmune Inflammatory Disorders. *Neurologic Clinics*, *42*(1). https://doi.org/10.1016/j.ncl.2023.06.009
19. Cacciaguerra, L., Meani, A., Mesaros, S., Radaelli, M., Palace, J., Dujmovic-Basuroski, I., Pagani, E., Martinelli, V., Matthews, L., Drulovic, J., Leite, M. I., Comi, G., Filippi, M., & Rocca, M. A. (2019). Brain and cord imaging features in neuromyelitis optica spectrum disorders. *Annals of Neurology*, *85*(3). https://doi.org/10.1002/ana.25411
20. Cacciaguerra, L., Rocca, M. A., Storelli, L., Radaelli, M., & Filippi, M. (2021). Mapping white matter damage distribution in neuromyelitis optica spectrum disorders with a multimodal MRI approach. *Multiple Sclerosis* , *27*(6). https://doi.org/10.1177/1352458520941493
21. Cadavid, D., Balcer, L., Galetta, S., Aktas, O., Ziemssen, T., Vanopdenbosch, L., Frederiksen, J., Skeen, M., Jaffe, G. J., Butzkueven, H., Ziemssen, F., Massacesi, L., Chai, Y., Xu, L., & Freeman, S. (2017). Safety and efficacy of opicinumab in acute optic neuritis (RENEW): a randomised, placebo-controlled, phase 2 trial. *The Lancet. Neurology*, *16*(3). https://doi.org/10.1016/S1474-4422(16)30377-5
22. Cagol, A., Cortese, R., Barakovic, M., Schaedelin, S., Ruberte, E., Absinta, M., Barkhof, F., Calabrese, M., Castellaro, M., Ciccarelli, O., Cocozza, S., De Stefano, N., Enzinger, C., Filippi, M., Jurynczyk, M., Maggi, P., Mahmoudi, N., Messina, S., Montalban, X., … Granziera, C. (2024). Diagnostic Performance of Cortical Lesions and the Central Vein Sign in Multiple Sclerosis. *JAMA Neurology*, *81*(2). https://doi.org/10.1001/jamaneurol.2023.4737
23. Cagol, A., Schaedelin, S., Barakovic, M., Benkert, P., Todea, R. A., Rahmanzadeh, R., Galbusera, R., Lu, P. J., Weigel, M., Melie-Garcia, L., Ruberte, E., Siebenborn, N., Battaglini, M., Radue, E. W., Yaldizli, Ö., Oechtering, J., Sinnecker, T., Lorscheider, J., Fischer-Barnicol, B., … Granziera, C. (2022). Association of Brain Atrophy With Disease Progression Independent of Relapse Activity in Patients With Relapsing Multiple Sclerosis. *JAMA Neurology*, *79*(7). https://doi.org/10.1001/jamaneurol.2022.1025
24. Calabrese, M., Filippi, M., & Gallo, P. (2010). Cortical lesions in multiple sclerosis. *Nature Reviews. Neurology*, *6*(8). https://doi.org/10.1038/nrneurol.2010.93
25. Calabrese, M., Magliozzi, R., Ciccarelli, O., Geurts, J. J., Reynolds, R., & Martin, R. (2015). Exploring the origins of grey matter damage in multiple sclerosis. *Nature Reviews. Neuroscience*, *16*(3). https://doi.org/10.1038/nrn3900
26. Calvi, A., Clarke, M. A., Prados, F., Chard, D., Ciccarelli, O., Alberich, M., Pareto, D., Rodríguez, B. M., Sastre-Garriga, J., Tur, C., Rovira, A., & Barkhof, F. (2023). Relationship between paramagnetic rim lesions and slowly expanding lesions in multiple sclerosis. *Multiple Sclerosis (Houndmills, Basingstoke, England)*, *29*(3). https://doi.org/10.1177/13524585221141964
27. Calvi, A., Haider, L., Prados, F., Tur, C., Chard, D., & Barkhof, F. (2022). In vivo imaging of chronic active lesions in multiple sclerosis. *Multiple Sclerosis (Houndmills, Basingstoke, England)*, *28*(5). https://doi.org/10.1177/1352458520958589
28. Carnero, C. E., & Correale, J. (2021). Neuromyelitis optica spectrum disorders: from pathophysiology to therapeutic strategies. *Journal of Neuroinflammation*, *18*(1). https://doi.org/10.1186/s12974-021-02249-1
29. Casserly, C., Seyman, E. E., Alcaide-Leon, P., Guenette, M., Lyons, C., Sankar, S., Svendrovski, A., Baral, S., & Oh, J. (2018). Spinal Cord Atrophy in Multiple Sclerosis: A

Systematic Review and Meta-Analysis. *Journal of Neuroimaging: Official Journal of the American Society of Neuroimaging*, *28*(6). https://doi.org/10.1111/jon.12553
30. Cercignani, M., Iannucci, G., Rocca, M. A., Comi, G., Horsfield, M. A., & Filippi, M. (2000). Pathologic damage in MS assessed by diffusion-weighted and magnetization transfer MRI. *Neurology*, *54*(5). https://doi.org/10.1212/wnl.54.5.1139
31. Chamberland, M., Winter, M., Brice, T. A. W., Jones., D. K., & Tallantyre, E. C. (2021). Beyond Lesion-Load: Tractometry-Based Metrics for Characterizing White Matter Lesions within Fibre Pathways. *Computational Diffusion MRI*, 227–237.
32. Chang, A., Tourtellotte, W. W., Rudick, R., & Trapp, B. D. (2002). Premyelinating oligodendrocytes in chronic lesions of multiple sclerosis. *The New England Journal of Medicine*, *346*(3). https://doi.org/10.1056/NEJMoa010994
33. Chanson, J. B., Lamy, J., Rousseau, F., Blanc, F., Collongues, N., Fleury, M., Armspach, J. P., Kremer, S., & de Seze, J. (2013). White matter volume is decreased in the brain of patients with neuromyelitis optica. *European Journal of Neurology: The Official Journal of the European Federation of Neurological Societies*, *20*(2). https://doi.org/10.1111/j.1468-1331.2012.03867.x
34. Charcot, & Oliver, T. (1876). Sclerosis in Scattered Patches. *Edinburgh Medical Journal*, *21*(11), 1010.
35. Chari, D. M. (2007). Remyelination in multiple sclerosis. *International Review of Neurobiology*, *79*. https://doi.org/10.1016/S0074-7742(07)79026-8
36. Chou, I.-J., Tanasescu, R., Mougin, O. E., Gowland, P. A., Tench, C. R., Whitehouse, W. P., Gran, B., Nikfekr, E., Sharrack, B., Mazibrada, G., & Constantinescu, C. S. (2019). Reduced Myelin Signal in Normal-appearing White Matter in Neuromyelitis Optica Measured by 7T Magnetic Resonance Imaging. *Scientific Reports*, *9*. https://doi.org/10.1038/s41598-019-50928-0
37. Chung, A. W., Seunarine, K. K., & Clark, C. A. (2016). NODDI reproducibility and variability with magnetic field strength: A comparison between 1.5 T and 3 T. *Human Brain Mapping*, *37*(12). https://doi.org/10.1002/hbm.23328
38. Ciccarelli, O., Cohen, J. A., Reingold, S. C., & Weinshenker, B. G. (2019). Spinal cord involvement in multiple sclerosis and neuromyelitis optica spectrum disorders. *Lancet Neurology*, *18*(2). https://doi.org/10.1016/S1474-4422(18)30460-5
39. Cohen, J. A., Coles, A. J., Arnold, D. L., Confavreux, C., Fox, E. J., Hartung, H. P., Havrdova, E., Selmaj, K. W., Weiner, H. L., Fisher, E., Brinar, V. V., Giovannoni, G., Stojanovic, M., Ertik, B. I., Lake, S. L., Margolin, D. H., Panzara, M. A., & Compston, D. A. (2012). Alemtuzumab versus interferon beta 1a as first-line treatment for patients with relapsing-remitting multiple sclerosis: a randomised controlled phase 3 trial. *Lancet*, *380*(9856). https://doi.org/10.1016/S0140-6736(12)61769-3
40. Coles, A. J., Twyman, C. L., Arnold, D. L., Cohen, J. A., Confavreux, C., Fox, E. J., Hartung, H. P., Havrdova, E., Selmaj, K. W., Weiner, H. L., Miller, T., Fisher, E., Sandbrink, R., Lake, S. L., Margolin, D. H., Oyuela, P., Panzara, M. A., & Compston, D. A. (2012). Alemtuzumab for patients with relapsing multiple sclerosis after disease-modifying therapy: a randomised controlled phase 3 trial. *Lancet*, *380*(9856). https://doi.org/10.1016/S0140-6736(12)61768-1
41. Collorone, S., Cawley, N., Grussu, F., Prados, F., Tona, F., Calvi, A., Kanber, B., Schneider, T., Kipp, L., Zhang, H., Alexander, D. C., Thompson, A. J., Toosy, A., Wheeler-Kingshott, C. A. G., & Ciccarelli, O. (2020a). Reduced neurite density in the brain and cervical spinal cord in relapsing-remitting multiple sclerosis: A NODDI study. *Multiple Sclerosis* , *26*(13). https://doi.org/10.1177/1352458519885107
42. Comi, G., Bar-Or, A., Lassmann, H., Uccelli, A., Hartung, H.-P., Montalban, X., Sørensen, P. S., Hohlfeld, R., & Hauser, S. L. (2020). The role of B cells in Multiple Sclerosis and related disorders. *Annals of Neurology*, *89*(1), 13.
43. Cortese, R., Battaglini, M., Prados, F., Gentile, G., Luchetti, L., Bianchi, A., Haider, L., Jacob, A., Palace, J., Messina, S., Paul, F., Marignier, R., Durand-Dubief, F., de Medeiros Rimkus, C., Sato, D. K., Filippi, M., Rocca, M. A., Cacciaguerra, L., Rovira, À., … De Stefano, N.

(2024). Grey Matter Atrophy and its Relationship with White Matter Lesions in Patients with Myelin Oligodendrocyte Glycoprotein Antibody-associated Disease, Aquaporin-4 Antibody-Positive Neuromyelitis Optica Spectrum Disorder, and Multiple Sclerosis. *Annals of Neurology*, *96*(2). https://doi.org/10.1002/ana.26951

44. Cox, S. R., Ritchie, S. J., Tucker-Drob, E. M., Liewald, D. C., Hagenaars, S. P., Davies, G., Wardlaw, J. M., Gale, C. R., Bastin, M. E., & Deary, I. J. (2016). Ageing and brain white matter structure in 3,513 UK Biobank participants. *Nature Communications*, *7*(1), 1–13.
45. Cree, B. A. C., Bennett, J. L., Kim, H. J., Weinshenker, B. G., Pittock, S. J., Wingerchuk, D. M., Fujihara, K., Paul, F., Cutter, G. R., Marignier, R., Green, A. J., Aktas, O., Hartung, H. P., Lublin, F. D., Drappa, J., Barron, G., Madani, S., Ratchford, J. N., She, D., … Katz, E. (2019). Inebilizumab for the treatment of neuromyelitis optica spectrum disorder (N-MOmentum): a double-blind, randomised placebo-controlled phase 2/3 trial. *Lancet*, *394*(10206). https://doi.org/10.1016/S0140-6736(19)31817-3
46. Dale, A. M., Fischl, B., & Sereno, M. I. (1999). Cortical surface-based analysis. I. Segmentation and surface reconstruction. *NeuroImage*, *9*(2). https://doi.org/10.1006/nimg.1998.0395
47. Dawson, J. W. (1916). The Histology of Disseminated Sclerosis. *Edinburgh Medical Journal*, *17*(5), 311.
48. De Leener, B., Fonov, V. S., Collins, D. L., Callot, V., Stikov, N., & Cohen-Adad, J. (2018). PAM50: Unbiased multimodal template of the brainstem and spinal cord aligned with the ICBM152 space. *NeuroImage*, *165*. https://doi.org/10.1016/j.neuroimage.2017.10.041
49. De Leener, B., Lévy, S., Dupont, S. M., Fonov, V. S., Stikov, N., Louis, C. D., Callot, V., & Cohen-Adad, J. (2017). SCT: Spinal Cord Toolbox, an open-source software for processing spinal cord MRI data. *NeuroImage*, *145*(Pt A). https://doi.org/10.1016/j.neuroimage.2016.10.009
50. Dendrou, C. A., Fugger, L., & Friese, M. A. (2015). Immunopathology of multiple sclerosis. *Nature Reviews. Immunology*, *15*(9). https://doi.org/10.1038/nri3871
51. Deppe, M., Tabelow, K., Krämer, J., Tenberge, J. G., Schiffler, P., Bittner, S., Schwindt, W., Zipp, F., Wiendl, H., & Meuth, S. G. (2016). Evidence for early, non-lesional cerebellar damage in patients with multiple sclerosis: DTI measures correlate with disability, atrophy, and disease duration. *Multiple Sclerosis* , *22*(1). https://doi.org/10.1177/1352458515579439
52. Destrieux, C., Fischl, B., Dale, A., & Halgren, E. (2010). Automatic parcellation of human cortical gyri and sulci using standard anatomical nomenclature. *NeuroImage*, *53*(1). https://doi.org/10.1016/j.neuroimage.2010.06.010
53. Dhollander, T., & Connelly, A. (2016). A novel iterative approach to reap the benefits of multi-tissue CSD from just single-shell (+b=0) diffusion MRI data. *24th International Society of Magnetic Resonance in Medicine*.
54. Dziedzic, T., Metz, I., Dallenga, T., König, F. B., Müller, S., Stadelmann, C., & Brück, W. (2010). Wallerian degeneration: a major component of early axonal pathology in multiple sclerosis. *Brain Pathology* , *20*(5). https://doi.org/10.1111/j.1750-3639.2010.00401.x
55. Eshaghi, A., Prados, F., Brownlee, W. J., Altmann, D. R., Tur, C., Cardoso, M. J., De Angelis, F., van de Pavert, S. H., Cawley, N., De Stefano, N., Stromillo, M. L., Battaglini, M., Ruggieri, S., Gasperini, C., Filippi, M., Rocca, M. A., Rovira, A., Sastre-Garriga, J., Vrenken, H., … Ciccarelli, O. (2018). Deep gray matter volume loss drives disability worsening in multiple sclerosis. *Annals of Neurology*, *83*(2). https://doi.org/10.1002/ana.25145
56. Fazekas, F., Offenbacher, H., Schmidt, R., & Strasser-Fuchs, S. (1994). MRI of neuromyelitis optica: evidence for a distinct entity. *Journal of Neurology, Neurosurgery, and Psychiatry*, *57*(9). https://doi.org/10.1136/jnnp.57.9.1140
57. Filippi, M., Brück, W., Chard, D., Fazekas, F., Geurts, J. J. G., Enzinger, C., Hametner, S., Kuhlmann, T., Preziosa, P., Rovira, À., Schmierer, K., Stadelmann, C., & Rocca, M. A. (2019). Association between pathological and MRI findings in multiple sclerosis. *Lancet Neurology*, *18*(2). https://doi.org/10.1016/S1474-4422(18)30451-4
58. Filippi, M., Iannucci, G., Cercignani, M., Assunta, R. M., Pratesi, A., & Comi, G. (2000). A

quantitative study of water diffusion in multiple sclerosis lesions and normal-appearing white matter using echo-planar imaging. *Archives of Neurology*, *57*(7). https://doi.org/10.1001/archneur.57.7.1017
59. Filippi, M., Preziosa, P., Banwell, B. L., Barkhof, F., Ciccarelli, O., De Stefano, N., Geurts, J. J. G., Paul, F., Reich, D. S., Toosy, A. T., Traboulsee, A., Wattjes, M. P., Yousry, T. A., Gass, A., Lubetzki, C., Weinshenker, B. G., & Rocca, M. A. (2019). Assessment of lesions on magnetic resonance imaging in multiple sclerosis: practical guidelines. *Brain: A Journal of Neurology*, *142*(7). https://doi.org/10.1093/brain/awz144
60. Filippi, M., Rocca, M. A., Ciccarelli, O., De Stefano, N., Evangelou, N., Kappos, L., Rovira, A., Sastre-Garriga, J., Tintorè, M., Frederiksen, J. L., Gasperini, C., Palace, J., Reich, D. S., Banwell, B., Montalban, X., & Barkhof, F. (2016). MRI criteria for the diagnosis of multiple sclerosis: MAGNIMS consensus guidelines. *Lancet Neurology*, *15*(3). https://doi.org/10.1016/S1474-4422(15)00393-2
61. Fischer, M. T., Wimmer, I., Höftberger, R., Gerlach, S., Haider, L., Zrzavy, T., Hametner, S., Mahad, D., Binder, C. J., Krumbholz, M., Bauer, J., Bradl, M., & Lassmann, H. (2013). Disease-specific molecular events in cortical multiple sclerosis lesions. *Brain : A Journal of Neurology*, *136*(Pt 6). https://doi.org/10.1093/brain/awt110
62. Franklin, R. J., & Ffrench-Constant, C. (2008). Remyelination in the CNS: from biology to therapy. *Nature Reviews. Neuroscience*, *9*(11). https://doi.org/10.1038/nrn2480
63. Galbusera, R., Bahn, E., Weigel, M., Schaedelin, S., Franz, J., Lu, P. J., Barakovic, M., Melie-Garcia, L., Dechent, P., Lutti, A., Sati, P., Reich, D. S., Nair, G., Brück, W., Kappos, L., Stadelmann, C., & Granziera, C. (2023). Postmortem quantitative MRI disentangles histological lesion types in multiple sclerosis. *Brain Pathology (Zurich, Switzerland)*, *33*(6). https://doi.org/10.1111/bpa.13136
64. Geraldes, R., Ciccarelli, O., Barkhof, F., De Stefano, N., Enzinger, C., Filippi, M., Hofer, M., Paul, F., Preziosa, P., Rovira, A., DeLuca, G. C., Kappos, L., Yousry, T., Fazekas, F., Frederiksen, J., Gasperini, C., Sastre-Garriga, J., Evangelou, N., & Palace, J. (2018). The current role of MRI in differentiating multiple sclerosis from its imaging mimics. *Nature Reviews. Neurology*, *14*(4). https://doi.org/10.1038/nrneurol.2018.14
65. Ghazanfari, H. M., Talebi, V., Abbasi, K. N., Abbasi, M., Asgari, N., & Sahraian, M. A. (2024). T1 hypointense brain lesions in NMOSD and its relevance with disability: a single institution cross-sectional study. BMC Neurology, 24(1). https://doi.org/10.1186/s12883-024-03550-1
66. Giorgio, A., Santelli, L., Tomassini, V., Bosnell, R., Smith, S., De Stefano, N., & Johansen-Berg, H. (2010). Age-related changes in grey and white matter structure throughout adulthood. Neuroimage, 51(3-2), 943.
67. Giorgio, A., & De Stefano, N. (2013). Clinical use of brain volumetry. *Journal of Magnetic Resonance Imaging: JMRI*, *37*(1). https://doi.org/10.1002/jmri.23671
68. Glasser, M. F., Sotiropoulos, S. N., Wilson, J. A., Coalson, T. S., Fischl, B., Andersson, J. L., Xu, J., Jbabdi, S., Webster, M., Polimeni, J. R., Van Essen, D. C., & Jenkinson, M. (2013). The minimal preprocessing pipelines for the Human Connectome Project. *NeuroImage*, *80*. https://doi.org/10.1016/j.neuroimage.2013.04.127
69. Gleiser, C., Wagner, A., Fallier-Becker, P., Wolburg, H., Hirt, B., & Mack, A. F. (2016). Aquaporin-4 in Astroglial Cells in the CNS and Supporting Cells of Sensory Organs—A Comparative Perspective. *International Journal of Molecular Sciences*, *17*(9). https://doi.org/10.3390/ijms17091411
70. Granberg, T., Fan, Q., Treaba, C. A., Ouellette, R., Herranz, E., Mangeat, G., Louapre, C., Cohen-Adad, J., Klawiter, E. C., Sloane, J. A., & Mainero, C. (2017). In vivo characterization of cortical and white matter neuroaxonal pathology in early multiple sclerosis. *Brain: A Journal of Neurology*, *140*(11), 2912.
71. Granziera, C., Wuerfel, J., Barkhof, F., Calabrese, M., De Stefano, N., Enzinger, C., Evangelou, N., Filippi, M., Geurts, J. J. G., Reich, D. S., Rocca, M. A., Ropele, S., Rovira, À., Sati, P., Toosy, A. T., Vrenken, H., Cam, G. W.-K., & Kappos, L. (2021). Quantitative

magnetic resonance imaging towards clinical application in multiple sclerosis. *Brain: A Journal of Neurology*, *144*(5). https://doi.org/10.1093/brain/awab029
72. Green, A. J., Gelfand, J. M., Cree, B. A., Bevan, C., Boscardin, W. J., Mei, F., Inman, J., Arnow, S., Devereux, M., Abounasr, A., Nobuta, H., Zhu, A., Friessen, M., Gerona, R., von Büdingen, H. C., Henry, R. G., Hauser, S. L., & Chan, J. R. (2017). Clemastine fumarate as a remyelinating therapy for multiple sclerosis (ReBUILD): a randomised, controlled, double-blind, crossover trial. *Lancet (London, England)*, *390*(10111). https://doi.org/10.1016/S0140-6736(17)32346-2
73. Gros, C., De Leener, B., Badji, A., Maranzano, J., Eden, D., Dupont, S. M., Talbott, J., Zhuoquiong, R., Liu, Y., Granberg, T., Ouellette, R., Tachibana, Y., Hori, M., Kamiya, K., Chougar, L., Stawiarz, L., Hillert, J., Bannier, E., Kerbrat, A., … Cohen-Adad, J. (2019). Automatic segmentation of the spinal cord and intramedullary multiple sclerosis lesions with convolutional neural networks. *NeuroImage*, *184*. https://doi.org/10.1016/j.neuroimage.2018.09.081
74. Grussu, F., Schneider, T., Tur, C., Yates, R. L., Tachrount, M., Ianuş, A., Yiannakas, M. C., Newcombe, J., Zhang, H., Alexander, D. C., DeLuca, G. C., & Cam, G. W.-K. (2017). Neurite dispersion: a new marker of multiple sclerosis spinal cord pathology? *Annals of Clinical and Translational Neurology*, *4*(9). https://doi.org/10.1002/acn3.445
75. Grussu, F., Schneider, T., Zhang, H., Alexander, D. C., & Wheeler-Kingshott, C. A. (2015). Neurite orientation dispersion and density imaging of the healthy cervical spinal cord in vivo. *NeuroImage*, *111*. https://doi.org/10.1016/j.neuroimage.2015.01.045
76. Hagiwara, A., Kamagata, K., Shimoji, K., Yokoyama, K., Andica, C., Hori, M., Fujita, S., Maekawa, T., Irie, R., Akashi, T., Wada, A., Suzuki, M., Abe, O., Hattori, N., & Aoki, S. (2019). White Matter Abnormalities in Multiple Sclerosis Evaluated by Quantitative Synthetic MRI, Diffusion Tensor Imaging, and Neurite Orientation Dispersion and Density Imaging. *AJNR. American Journal of Neuroradiology*, *40*(10). https://doi.org/10.3174/ajnr.A6209
77. Haider, L., Zrzavy, T., Hametner, S., Höftberger, R., Bagnato, F., Grabner, G., Trattnig, S., Pfeifenbring, S., Brück, W., & Lassmann, H. (2016). The topograpy of demyelination and neurodegeneration in the multiple sclerosis brain. *Brain: A Journal of Neurology*, *139*(Pt 3). https://doi.org/10.1093/brain/awv398
78. Hauser, S. L., Bar-Or, A., Comi, G., Giovannoni, G., Hartung, H. P., Hemmer, B., Lublin, F., Montalban, X., Rammohan, K. W., Selmaj, K., Traboulsee, A., Wolinsky, J. S., Arnold, D. L., Klingelschmitt, G., Masterman, D., Fontoura, P., Belachew, S., Chin, P., Mairon, N., … Kappos, L. (2017). Ocrelizumab versus Interferon Beta-1a in Relapsing Multiple Sclerosis. *The New England Journal of Medicine*, *376*(3). https://doi.org/10.1056/NEJMoa1601277
79. Hauser, S. L., & Cree, B. A. C. (2020). Treatment of Multiple Sclerosis: A Review. *The American Journal of Medicine*, *133*(12). https://doi.org/10.1016/j.amjmed.2020.05.049
80. Hinson, S. R., Pittock, S. J., Lucchinetti, C. F., Roemer, S. F., Fryer, J. P., Kryzer, T. J., & Lennon, V. A. (2007). Pathogenic potential of IgG binding to water channel extracellular domain in neuromyelitis optica. *Neurology*, *69*(24). https://doi.org/10.1212/01.WNL.0000289761.64862.ce
81. Hinson, S. R., Roemer, S. F., Lucchinetti, C. F., Fryer, J. P., Kryzer, T. J., Chamberlain, J. L., Howe, C. L., Pittock, S. J., & Lennon, V. A. (2008). Aquaporin-4-binding autoantibodies in patients with neuromyelitis optica impair glutamate transport by down-regulating EAAT2. *The Journal of Experimental Medicine*, *205*(11). https://doi.org/10.1084/jem.20081241
82. Hokari, M., Yokoseki, A., Arakawa, M., Saji, E., Yanagawa, K., Yanagimura, F., Toyoshima, Y., Okamoto, K., Ueki, S., Hatase, T., Ohashi, R., Fukuchi, T., Akazawa, K., Yamada, M., Kakita, A., Takahashi, H., Nishizawa, M., & Kawachi, I. (2016). Clinicopathological features in anterior visual pathway in neuromyelitis optica. *Annals of Neurology*, *79*(4). https://doi.org/10.1002/ana.24608
83. Holroyd, K., Vogel, A., Lynch, K., Gazdag, B., Voghel, M., Alakel, N., Patenaude, B. N., Chiong-Rivero, H., & Mateen, F. J. (2019). Neuromyelitis optica testing and treatment:

Availability and affordability in 60 countries. *Multiple Sclerosis and Related Disorders*, *33*. https://doi.org/10.1016/j.msard.2019.05.013
84. Hor, J. Y., Asgari, N., Nakashima, I., Broadley, S. A., Isabel Leite, M., Kissani, N., Jacob, A., Marignier, R., Weinshenker, B. G., Paul, F., Pittock, S. J., Palace, J., Wingerchuk, D. M., Behne, J. M., Yeaman, M. R., & Fujihara, K. (2020). Epidemiology of Neuromyelitis Optica Spectrum Disorder and Its Prevalence and Incidence Worldwide. *Frontiers in Neurology*, *11*. https://doi.org/10.3389/fneur.2020.00501
85. Howell, O. W., Reeves, C. A., Nicholas, R., Carassiti, D., Radotra, B., Gentleman, S. M., Serafini, B., Aloisi, F., Roncaroli, F., Magliozzi, R., & Reynolds, R. (2011). Meningeal inflammation is widespread and linked to cortical pathology in multiple sclerosis. *Brain : A Journal of Neurology*, *134*(Pt 9). https://doi.org/10.1093/brain/awr182
86. Huda, S., Whittam, D., Bhojak, M., Chamberlain, J., Noonan, C., & Jacob, A. (2019). Neuromyelitis optica spectrum disorders. *Clinical Medicine* , *19*(2). https://doi.org/10.7861/clinmedicine.19-2-169
87. Jarius, S., Aktas, O., Ayzenberg, I., Bellmann-Strobl, J., Berthele, A., Giglhuber, K., Häußler, V., Havla, J., Hellwig, K., Hümmert, M. W., Kleiter, I., Klotz, L., Krumbholz, M., Kümpfel, T., Paul, F., Ringelstein, M., Ruprecht, K., Senel, M., Stellmann, J. P., … Trebst, C. (2023). Update on the diagnosis and treatment of neuromyelits optica spectrum disorders (NMOSD) - revised recommendations of the Neuromyelitis Optica Study Group (NEMOS). Part I: Diagnosis and differential diagnosis. *Journal of Neurology*, *270*(7). https://doi.org/10.1007/s00415-023-11634-0
88. Jarius, S., Ruprecht, K., Wildemann, B., Kuempfel, T., Ringelstein, M., Geis, C., Kleiter, I., Kleinschnitz, C., Berthele, A., Brettschneider, J., Hellwig, K., Hemmer, B., Linker, R. A., Lauda, F., Mayer, C. A., Tumani, H., Melms, A., Trebst, C., Stangel, M., … Paul, F. (2012). Contrasting disease patterns in seropositive and seronegative neuromyelitis optica: A multicentre study of 175 patients. *Journal of Neuroinflammation*, *9*. https://doi.org/10.1186/1742-2094-9-14
89. Jarius, S., & Wildemann, B. (2013). The history of neuromyelitis optica. *Journal of Neuroinflammation*, *10*. https://doi.org/10.1186/1742-2094-10-8
90. Jarius, S., Wildemann, B., & Paul, F. (2014). Neuromyelitis optica: clinical features, immunopathogenesis and treatment. *Clinical and Experimental Immunology*, *176*(2). https://doi.org/10.1111/cei.12271
91. Jeyalatha, M. V., Therese, K. L., & Anand, A. R. (2022). An Update on the Laboratory Diagnosis of Neuromyelitis Optica Spectrum Disorders. *Journal of Clinical Neurology* , *18*(2). https://doi.org/10.3988/jcn.2022.18.2.152
92. Jiao, Y., Fryer, J. P., Lennon, V. A., Jenkins, S. M., Quek, A. M., Smith, C. Y., McKeon, A., Costanzi, C., Iorio, R., Weinshenker, B. G., Wingerchuk, D. M., Shuster, E. A., Lucchinetti, C. F., & Pittock, S. J. (2013). Updated estimate of AQP4-IgG serostatus and disability outcome in neuromyelitis optica. *Neurology*, *81*(14). https://doi.org/10.1212/WNL.0b013e3182a6cb5c
93. Juryńczyk, M., Craner, M., & Palace, J. (2015). Overlapping CNS inflammatory diseases: differentiating features of NMO and MS. *Journal of Neurology, Neurosurgery, and Psychiatry*, *86*(1). https://doi.org/10.1136/jnnp-2014-308984
94. Juryńczyk, M., Klimiec-Moskal, E., Kong, Y., Hurley, S., Messina, S., Yeo, T., Jenkinson, M., Leite, M. I., & Palace, J. (2022). Elucidating distinct clinico-radiologic signatures in the borderland between neuromyelitis optica and multiple sclerosis. *Journal of Neurology*, *269*(1). https://doi.org/10.1007/s00415-021-10619-1
95. Jurynczyk, M., Messina, S., Woodhall, M. R., Raza, N., Everett, R., Roca-Fernandez, A., Tackley, G., Hamid, S., Sheard, A., Reynolds, G., Chandratre, S., Hemingway, C., Jacob, A., Vincent, A., Leite, M. I., Waters, P., & Palace, J. (2017). Clinical presentation and prognosis in MOG-antibody disease: a UK study. *Brain: A Journal of Neurology*, *140*(12). https://doi.org/10.1093/brain/awx276
96. Juryńczyk, M., Weinshenker, B., Akman-Demir, G., Asgari, N., Barnes, D., Boggild, M.,

Chaudhuri, A., D'hooghe, M., Evangelou, N., Geraldes, R., Illes, Z., Jacob, A., Kim, H. J., Kleiter, I., Levy, M., Marignier, R., McGuigan, C., Murray, K., Nakashima, I., … Palace, J. (2016). Status of diagnostic approaches to AQP4-IgG seronegative NMO and NMO/MS overlap syndromes. *Journal of Neurology*, *263*(1). https://doi.org/10.1007/s00415-015-7952-8

97. Juryńczyk, M., Zaleski, K., & Selmaj, K. (2013). Natalizumab and the development of extensive brain lesions in neuromyelitis optica. *Journal of Neurology*, *260*(7). https://doi.org/10.1007/s00415-013-6965-4
98. Kamiya, K., Hori, M., & Aoki, S. (2020). NODDI in clinical research. *Journal of Neuroscience Methods*, *346*. https://doi.org/10.1016/j.jneumeth.2020.108908
99. Kappos, L., Bar-Or, A., Cree, B. A. C., Fox, R. J., Giovannoni, G., Gold, R., Vermersch, P., Arnold, D. L., Arnould, S., Scherz, T., Wolf, C., Wallström, E., & Dahlke, F. (2018). Siponimod versus placebo in secondary progressive multiple sclerosis (EXPAND): a double-blind, randomised, phase 3 study. *Lancet*, *391*(10127). https://doi.org/10.1016/S0140-6736(18)30475-6
100. Kato, S., Hagiwara, A., Yokoyama, K., Andica, C., Tomizawa, Y., Hoshino, Y., Uchida, W., Nishimura, Y., Fujita, S., Kamagata, K., Hori, M., Hattori, N., Abe, O., & Aoki, S. (2022). Microstructural white matter abnormalities in multiple sclerosis and neuromyelitis optica spectrum disorders: Evaluation by advanced diffusion imaging. *Journal of the Neurological Sciences*, *436*. https://doi.org/10.1016/j.jns.2022.120205
101. Kawachi, I., & Lassmann, H. (2017). Neurodegeneration in multiple sclerosis and neuromyelitis optica. *Journal of Neurology, Neurosurgery, and Psychiatry*, *88*(2). https://doi.org/10.1136/jnnp-2016-313300
102. Kermode, A. G. (2008). Aquaporin-4 IgG: overview and future perspectives. *Neurology Asia*, *13*, 179–183.
103. Khanna, S., Sharma, A., Huecker, J., Gordon, M., Naismith, R. T., & Van Stavern, G. P. (2012). Magnetic resonance imaging of optic neuritis in patients with neuromyelitis optica versus multiple sclerosis. *Journal of Neuro-Ophthalmology: The Official Journal of the North American Neuro-Ophthalmology Society*, *32*(3). https://doi.org/10.1097/WNO.0b013e318254c62d
104. Kimbrough, D. J., Fujihara, K., Jacob, A., Lana-Peixoto, M. A., Leite, M. I., Levy, M., Marignier, R., Nakashima, I., Palace, J., de Seze, J., Stuve, O., Tenembaum, S. N., Traboulsee, A., Waubant, E., Weinshenker, B. G., & Wingerchuk, D. M. (2012). Treatment of Neuromyelitis Optica: Review and Recommendations. *Multiple Sclerosis and Related Disorders*, *1*(4). https://doi.org/10.1016/j.msard.2012.06.002
105. Kim, H. J., Paul, F., Lana-Peixoto, M. A., Tenembaum, S., Asgari, N., Palace, J., Klawiter, E. C., Sato, D. K., de Seze, J., Wuerfel, J., Banwell, B. L., Villoslada, P., Saiz, A., Fujihara, K., Kim, S.-H., & With The Guthy-Jackson Charitable Foundation NMO International Clinical Consortium & Biorepository. (2015). MRI characteristics of neuromyelitis optica spectrum disorder: An international update. *Neurology*, *84*(11), 1165.
106. Kim, W., Kim, S. H., Huh, S. Y., & Kim, H. J. (2012). Brain abnormalities in neuromyelitis optica spectrum disorder. *Multiple Sclerosis International*, *2012*. https://doi.org/10.1155/2012/735486
107. Kim, W., Lee, J. E., Kim, S.-H., Huh, S.-Y., Hyun, J.-W., Jeong, I. H., Park, M.-S., Cho, J. Y., Lee, S.-H., Lee, K. S., & Kim, H. J. (2016). Cerebral Cortex Involvement in Neuromyelitis Optica Spectrum Disorder. *Journal of Clinical Neurology (Seoul, Korea)*, *12*(2), 188.
108. Kim, W., Park, M. S., Lee, S. H., Kim, S. H., Jung, I. J., Takahashi, T., Misu, T., Fujihara, K., & Kim, H. J. (2010). Characteristic brain magnetic resonance imaging abnormalities in central nervous system aquaporin-4 autoimmunity. *Multiple Sclerosis (Houndmills, Basingstoke, England)*, *16*(10). https://doi.org/10.1177/1352458510376640
109. Kim, W., Shin, H. G., Lee, H., Park, D., Kang, J., Nam, Y., Lee, J., & Jang, J. (2023). χ-Separation Imaging for Diagnosis of Multiple Sclerosis versus Neuromyelitis Optica Spectrum Disorder. *Radiology*, *307*(1). https://doi.org/10.1148/radiol.220941

110. Kitley, J., Leite, M. I., Nakashima, I., Waters, P., McNeillis, B., Brown, R., Takai, Y., Takahashi, T., Misu, T., Elsone, L., Woodhall, M., George, J., Boggild, M., Vincent, A., Jacob, A., Fujihara, K., & Palace, J. (2012a). Prognostic factors and disease course in aquaporin-4 antibody-positive patients with neuromyelitis optica spectrum disorder from the United Kingdom and Japan. *Brain: A Journal of Neurology*, *135*(Pt 6). https://doi.org/10.1093/brain/aws109
111. Kitley, J. L., Leite, M. I., George, J. S., & Palace, J. A. (2012b). The differential diagnosis of longitudinally extensive transverse myelitis. *Multiple Sclerosis* , *18*(3). https://doi.org/10.1177/1352458511406165
112. Klawiter, E. C., Xu, J., Naismith, R. T., Benzinger, T. L., Shimony, J. S., Lancia, S., Snyder, A. Z., Trinkaus, K., Song, S. K., & Cross, A. H. (2012). Increased radial diffusivity in spinal cord lesions in neuromyelitis optica compared with multiple sclerosis. *Multiple Sclerosis* , *18*(9). https://doi.org/10.1177/1352458512436593
113. Kolasinski, J., Stagg, C. J., Chance, S. A., Deluca, G. C., Esiri, M. M., Chang, E. H., Palace, J. A., McNab, J. A., Jenkinson, M., Miller, K. L., & Johansen-Berg, H. (2012). A combined post-mortem magnetic resonance imaging and quantitative histological study of multiple sclerosis pathology. *Brain: A Journal of Neurology*, *135*(Pt 10). https://doi.org/10.1093/brain/aws242
114. Krijnen, E. A., Broeders, T. A. A., Noteboom, S., van Dam, M., Bajrami, A., Bouman, P. M., Barkhof, F., Uitdehaag, B. M. J., Klawiter, E. C., Koubiyr, I., & Schoonheim, M. M. (2024). The cognitive relevance of non-lesional damage to cortical networks in people with multiple sclerosis. *Journal of Neurology*, *271*(6). https://doi.org/10.1007/s00415-024-12240-4
115. Kugler, A. V., & Deppe, M. (2018). Non-lesional cerebellar damage in patients with clinically isolated syndrome: DTI measures predict early conversion into clinically definite multiple sclerosis. *NeuroImage. Clinical*, *19*. https://doi.org/10.1016/j.nicl.2018.04.028
116. Kuhlmann, T., Miron, V., Cui, Q., Wegner, C., Antel, J., & Brück, W. (2008). Differentiation block of oligodendroglial progenitor cells as a cause for remyelination failure in chronic multiple sclerosis. *Brain : A Journal of Neurology*, *131*(Pt 7). https://doi.org/10.1093/brain/awn096
117. Kümpfel, T., Giglhuber, K., Aktas, O., Ayzenberg, I., Bellmann-Strobl, J., Häußler, V., Havla, J., Hellwig, K., Hümmert, M. W., Jarius, S., Kleiter, I., Klotz, L., Krumbholz, M., Paul, F., Ringelstein, M., Ruprecht, K., Senel, M., Stellmann, J. P., Bergh, F. T., … Berthele, A. (2024). Update on the diagnosis and treatment of neuromyelitis optica spectrum disorders (NMOSD) - revised recommendations of the Neuromyelitis Optica Study Group (NEMOS). Part II: Attack therapy and long-term management. *Journal of Neurology*, *271*(1). https://doi.org/10.1007/s00415-023-11910-z
118. Kurtzke, J. F. (1983). Rating neurologic impairment in multiple sclerosis: an expanded disability status scale (EDSS). *Neurology*, *33*(11). https://doi.org/10.1212/wnl.33.11.1444
119. Kutzelnigg, A., Lucchinetti, C. F., Stadelmann, C., Brück, W., Rauschka, H., Bergmann, M., Schmidbauer, M., Parisi, J. E., & Lassmann, H. (2005). Cortical demyelination and diffuse white matter injury in multiple sclerosis. *Brain: A Journal of Neurology*, *128*(Pt 11). https://doi.org/10.1093/brain/awh641
120. Kwong, K. C., Mollison, D., Meijboom, R., York, E. N., Kampaite, A., Thrippleton, M. J., Chandran, S., & Waldman, A. D. (2021). The prevalence of paramagnetic rim lesions in multiple sclerosis: A systematic review and meta-analysis. *PloS One*, *16*(9). https://doi.org/10.1371/journal.pone.0256845
121. Landman, B. A., Wan, H., Bogovic, J. A., Bazin, P.-L., & Prince, J. L. (2010). Resolution of Crossing Fibers with Constrained Compressed Sensing using Traditional Diffusion Tensor MRI. *Proceedings of SPIE--the International Society for Optical Engineering*, *7623*, 76231H.
122. Langkammer, C., Schweser, F., Shmueli, K., Kames, C., Li, X., Guo, L., Milovic, C., Kim, J., Wei, H., Bredies, K., Buch, S., Guo, Y., Liu, Z., Meineke, J., Rauscher, A., Marques, J. P., & Bilgic, B. (2018). Quantitative susceptibility mapping: Report from the 2016 reconstruction challenge. *Magnetic Resonance in Medicine: Official Journal of the Society of*

Magnetic Resonance in Medicine / Society of Magnetic Resonance in Medicine, *79*(3). https://doi.org/10.1002/mrm.26830
123. Lassmann, H. (2018). Multiple Sclerosis Pathology. *Cold Spring Harbor Perspectives in Medicine*, *8*(3). https://doi.org/10.1101/cshperspect.a028936
124. Laule, C., Vavasour, I. M., Kolind, S. H., Li, D. K., Traboulsee, T. L., Moore, G. R., & MacKay, A. L. (2007). Magnetic resonance imaging of myelin. *Neurotherapeutics : The Journal of the American Society for Experimental NeuroTherapeutics*, *4*(3). https://doi.org/10.1016/j.nurt.2007.05.004
125. Le Bihan, D., & Johansen-Berg, H. (2012). Diffusion MRI at 25: Exploring brain tissue structure and function. *NeuroImage*, *61*(2), 324.
126. Lennon, V. A., Wingerchuk, D. M., Kryzer, T. J., Pittock, S. J., Lucchinetti, C. F., Fujihara, K., Nakashima, I., & Weinshenker, B. G. (2004). A serum autoantibody marker of neuromyelitis optica: distinction from multiple sclerosis. *Lancet*, *364*(9451). https://doi.org/10.1016/S0140-6736(04)17551-X
127. Lersy, F., Noblet, V., Willaume, T., Collongues, N., Kremer, L., Fleury, M., de Seze, J., & Kremer, S. (2021). Identification and measurement of cervical spinal cord atrophy in neuromyelitis optica spectrum disorders (NMOSD) and correlation with clinical characteristics and cervical spinal cord MRI data. *Revue Neurologique*, *177*(1-2). https://doi.org/10.1016/j.neurol.2020.05.007
128. Levy, M., Haycox, A. R., Becker, U., Costantino, C., Damonte, E., Klingelschmitt, G., von Büdingen, H. C., Wallenstein, G., Maio, D. D., & Szczechowski, L. (2022). Quantifying the relationship between disability progression and quality of life in patients treated for NMOSD: Insights from the SAkura studies. *Multiple Sclerosis and Related Disorders*, *57*. https://doi.org/10.1016/j.msard.2021.103332
129. Lévy, S., Benhamou, M., Naaman, C., Rainville, P., Callot, V., & Cohen-Adad, J. (2015). White matter atlas of the human spinal cord with estimation of partial volume effect. *NeuroImage*, *119*. https://doi.org/10.1016/j.neuroimage.2015.06.040
130. Lie, I. A., Weeda, M. M., Mattiesing, R. M., Mol, M. A. E., Pouwels, P. J. W., Barkhof, F., Torkildsen, Ø., Bø, L., Myhr, K.-M., & Vrenken, H. (2022). Relationship Between White Matter Lesions and Gray Matter Atrophy in Multiple Sclerosis: A Systematic Review. *Neurology*, *98*(15), e1562.
131. Liu, C., Wei, H., Gong, N.-J., Cronin, M., Dibb, R., & Decker, K. (2015). Quantitative Susceptibility Mapping: Contrast Mechanisms and Clinical Applications. *Tomography*, *1*(1), 3.
132. Liu, T., Liu, J., de Rochefort, L., Spincemaille, P., Khalidov, I., Ledoux, J. R., & Wang, Y. (2011). Morphology enabled dipole inversion (MEDI) from a single-angle acquisition: comparison with COSMOS in human brain imaging. *Magnetic Resonance in Medicine: Official Journal of the Society of Magnetic Resonance in Medicine / Society of Magnetic Resonance in Medicine*, *66*(3), 777–783.
133. Liu, Y., Duan, Y., He, Y., Yu, C., Wang, J., Huang, J., Ye, J., Butzkueven, H., Li, K., & Shu, N. (2012). A tract-based diffusion study of cerebral white matter in neuromyelitis optica reveals widespread pathological alterations. *Multiple Sclerosis* , *18*(7). https://doi.org/10.1177/1352458511431731
134. Liu, Y., Wang, J., Daams, M., Weiler, F., Hahn, H. K., Duan, Y., Huang, J., Ren, Z., Ye, J., Dong, H., Vrenken, H., Wattjes, M. P., Shi, F. D., Li, K., & Barkhof, F. (2015). Differential patterns of spinal cord and brain atrophy in NMO and MS. *Neurology*, *84*(14). https://doi.org/10.1212/WNL.0000000000001441
135. Louis, E. D., Mayer, S. A., & Noble, J. M. (2021). *Merritt's Neurology*. Wolters Kluwer.
136. Lubetzki, C., Zalc, B., Williams, A., Stadelmann, C., & Stankoff, B. (2020). Remyelination in multiple sclerosis: from basic science to clinical translation. *The Lancet. Neurology*, *19*(8). https://doi.org/10.1016/S1474-4422(20)30140-X
137. Lublin, F. D., Reingold, S. C., Cohen, J. A., Cutter, G. R., Sørensen, P. S., Thompson, A. J., Wolinsky, J. S., Balcer, L. J., Banwell, B., Barkhof, F., Bebo, B., Jr, Calabresi, P. A.,

Clanet, M., Comi, G., Fox, R. J., Freedman, M. S., Goodman, A. D., Inglese, M., Kappos, L., … Polman, C. H. (2014). Defining the clinical course of multiple sclerosis: The 2013 revisions. *Neurology*, *83*(3), 278.

138. Lucchinetti, C., Brück, W., Parisi, J., Scheithauer, B., Rodriguez, M., & Lassmann, H. (2000). Heterogeneity of multiple sclerosis lesions: implications for the pathogenesis of demyelination. *Annals of Neurology*, *47*(6). https://doi.org/10.1002/1531-8249(200006)47:6<707::aid-ana3>3.0.co;2-q
139. Luo, W., Xu, H., Xu, L., Jiang, W., Chen, C., Chang, Y., Liu, C., Tian, Z., Qiu, X., Xie, C., Li, X., Chen, H., Lai, S., Wu, L., Cui, Y., Tang, C., & Qiu, W. (2023). Remyelination in neuromyelitis optica spectrum disorder is promoted by edaravone through mTORC1 signaling activation. *Glia*, *71*(2). https://doi.org/10.1002/glia.24271
140. Maggi, P., Sati, P., Nair, G., Cortese, I. C. M., Jacobson, S., Smith, B. R., Nath, A., Ohayon, J., van Pesch, V., Perrotta, G., Pot, C., Théaudin, M., Martinelli, V., Scotti, R., Wu, T., Du Pasquier, R., Calabresi, P. A., Filippi, M., Reich, D. S., & Absinta, M. (2020). Paramagnetic Rim Lesions are Specific to Multiple Sclerosis: An International Multicenter 3T MRI Study. *Annals of Neurology*, *88*(5). https://doi.org/10.1002/ana.25877
141. Mandler, R. N. (2006). Neuromyelitis optica - Devic's syndrome, update. *Autoimmunity Reviews*, *5*(8). https://doi.org/10.1016/j.autrev.2006.02.008
142. Manogaran, P., Hanson, J. V. M., Olbert, E. D., Egger, C., Wicki, C., Gerth-Kahlert, C., Landau, K., & Schippling, S. (2016). Optical Coherence Tomography and Magnetic Resonance Imaging in Multiple Sclerosis and Neuromyelitis Optica Spectrum Disorder. *International Journal of Molecular Sciences*, *17*(11), 1894.
143. Margoni, M., Villani, U., Silvestri, E., Franciotta, S., Anglani, M. G., Causin, F., Rinaldi, F., Perini, P., Bertoldo, A., & Gallo, P. (2022). Quantification of normal-appearing white matter damage in early relapse-onset multiple sclerosis through neurite orientation dispersion and density imaging. *Multiple Sclerosis and Related Disorders*, *58*. https://doi.org/10.1016/j.msard.2021.103396
144. Mariano, R., Messina, S., Roca-Fernandez, A., Leite, M. I., Kong, Y., & Palace, J. A. (2021). Quantitative spinal cord MRI in MOG-antibody disease, neuromyelitis optica and multiple sclerosis. *Brain: A Journal of Neurology*, *144*(1). https://doi.org/10.1093/brain/awaa347
145. Matthews, L., Kolind, S., Brazier, A., Leite, M. I., Brooks, J., Traboulsee, A., Jenkinson, M., Johansen-Berg, H., & Palace, J. (2015). Imaging Surrogates of Disease Activity in Neuromyelitis Optica Allow Distinction from Multiple Sclerosis. *PloS One*, *10*(9). https://doi.org/10.1371/journal.pone.0137715
146. Matthews, L., Marasco, R., Jenkinson, M., Küker, W., Luppe, S., Leite, M. I., Giorgio, A., De Stefano, N., Robertson, N., Johansen-Berg, H., Evangelou, N., & Palace, J. (2013). Distinction of seropositive NMO spectrum disorder and MS brain lesion distribution. *Neurology*, *80*(14). https://doi.org/10.1212/WNL.0b013e3182887957
147. Matthews, L., & Palace, J. (2014). The role of imaging in diagnosing neuromyelitis optica spectrum disorder. *Multiple Sclerosis and Related Disorders*, *3*(3). https://doi.org/10.1016/j.msard.2013.11.003
148. McCarthy, P. (2022). *FSLeyes*. https://doi.org/10.5281/zenodo.11047709
149. McNicholas, N., Lockhart, A., Yap, S. M., O'Connell, K., Tubridy, N., Hutchinson, M., & McGuigan, C. (2019). New versus old: Implications of evolving diagnostic criteria for relapsing-remitting multiple sclerosis. *Multiple Sclerosis* , *25*(6). https://doi.org/10.1177/1352458518770088
150. Mealy, M. A., Boscoe, A., Caro, J., & Levy, M. (2019). Assessment of Patients with Neuromyelitis Optica Spectrum Disorder Using the EQ-5D. *International Journal of MS Care*, *21*(3). https://doi.org/10.7224/1537-2073.2017-076
151. Mealy, M. A., Kessler, R. A., Rimler, Z., Reid, A., Totonis, L., Cutter, G., Kister, I., & Levy, M. (2018). Mortality in neuromyelitis optica is strongly associated with African ancestry. *Neurology® Neuroimmunology & Neuroinflammation*, *5*(4).

https://doi.org/10.1212/NXI.0000000000000468
152. Messina, S., Mariano, R., Roca-Fernandez, A., Cavey, A., Jurynczyk, M., Leite, M. I., Calabrese, M., Jenkinson, M., & Palace, J. (2022). Contrasting the brain imaging features of MOG-antibody disease, with AQP4-antibody NMOSD and multiple sclerosis. *Multiple Sclerosis* , *28*(2), 217.
153. Mina, Y., Azodi, S., Dubuche, T., Andrada, F., Osuorah, I., Ohayon, J., Cortese, I., Wu, T., Johnson, K. R., Reich, D. S., Nair, G., & Jacobson, S. (2021). Cervical and thoracic cord atrophy in multiple sclerosis phenotypes: Quantification and correlation with clinical disability. *NeuroImage. Clinical*, *30*. https://doi.org/10.1016/j.nicl.2021.102680
154. Misu, T., Fujihara, K., Kakita, A., Konno, H., Nakamura, M., Watanabe, S., Takahashi, T., Nakashima, I., Takahashi, H., & Itoyama, Y. (2007). Loss of aquaporin 4 in lesions of neuromyelitis optica: distinction from multiple sclerosis. *Brain : A Journal of Neurology*, *130*(Pt 5). https://doi.org/10.1093/brain/awm047
155. Misu, T., Höftberger, R., Fujihara, K., Wimmer, I., Takai, Y., Nishiyama, S., Nakashima, I., Konno, H., Bradl, M., Garzuly, F., Itoyama, Y., Aoki, M., & Lassmann, H. (2013). Presence of six different lesion types suggests diverse mechanisms of tissue injury in neuromyelitis optica. *Acta Neuropathologica*, *125*(6). https://doi.org/10.1007/s00401-013-1116-7
156. Mollink, J., Kleinnijenhuis, M., van Walsum AV, C., Sotiropoulos, S. N., Cottaar, M., Mirfin, C., Heinrich, M. P., Jenkinson, M., Pallebage-Gamarallage, M., Ansorge, O., Jbabdi, S., & Miller, K. L. (2017). Evaluating fibre orientation dispersion in white matter: Comparison of diffusion MRI, histology and polarized light imaging. *NeuroImage*, *157*. https://doi.org/10.1016/j.neuroimage.2017.06.001
157. Montalban, X., Hauser, S. L., Kappos, L., Arnold, D. L., Bar-Or, A., Comi, G., de Seze, J., Giovannoni, G., Hartung, H. P., Hemmer, B., Lublin, F., Rammohan, K. W., Selmaj, K., Traboulsee, A., Sauter, A., Masterman, D., Fontoura, P., Belachew, S., Garren, H., … Wolinsky, J. S. (2017). Ocrelizumab versus Placebo in Primary Progressive Multiple Sclerosis. *The New England Journal of Medicine*, *376*(3). https://doi.org/10.1056/NEJMoa1606468
158. Mottershead, J. P., Schmierer, K., Clemence, M., Thornton, J. S., Scaravilli, F., Barker, G. J., Tofts, P. S., Newcombe, J., Cuzner, M. L., Ordidge, R. J., McDonald, W. I., & Miller, D. H. (2003). High field MRI correlates of myelin content and axonal density in multiple sclerosis--a post-mortem study of the spinal cord. *Journal of Neurology*, *250*(11). https://doi.org/10.1007/s00415-003-0192-3
159. Murchison, A., Kitley, J., Leite, M. I., Küker, W., & Palace, J. (2015). Predictive value of MRI parameters in severity and recovery of first-episode myelitis in aquaporin-4 antibody disease. *Journal of the Neurological Sciences*, *355*(1-2). https://doi.org/10.1016/j.jns.2015.05.011
160. Naismith, R. T., Xu, J., Klawiter, E. C., Lancia, S., Tutlam, N. T., Wagner, J. M., Qian, P., Trinkaus, K., Song, S.-K., & Cross, A. H. (2013). Spinal cord tract diffusion tensor imaging reveals disability substrate in demyelinating disease. *Neurology*, *80*(24), 2201.
161. Nakaya, M., Sato, N., Suzuki, F., Maikusa, N., Matsuda, H., Kimura, Y., Shigemoto, Y., Chiba, E., Ota, M., Yamamura, T., Sato, W., Okamoto, T., & Abe, O. (2024). Multimodal imaging analyses in neuromyelitis optica spectrum disorder with or without visual disturbance. *Journal of the Neurological Sciences*, *462*. https://doi.org/10.1016/j.jns.2024.123090
162. O'Donnell, L. J., & Westin, C. F. (2011). An introduction to diffusion tensor image analysis. *Neurosurgery Clinics of North America*, *22*(2). https://doi.org/10.1016/j.nec.2010.12.004
163. Oertel, F. C., Kuchling, J., Zimmermann, H., Chien, C., Schmidt, F., Knier, B., Bellmann-Strobl, J., Korn, T., Scheel, M., Klistorner, A., Ruprecht, K., Paul, F., & Brandt, A. U. (2017). Microstructural visual system changes in AQP4-antibody-seropositive NMOSD. *Neurology(R) Neuroimmunology & Neuroinflammation*, *4*(3).

https://doi.org/10.1212/NXI.0000000000000334
164. Ontaneda, D., & Rae-Grant, A. D. (2009). Management of acute exacerbations in multiple sclerosis. *Annals of Indian Academy of Neurology*, *12*(4), 264.
165. Optic Neuritis Study Group. (2008). Visual function 15 years after optic neuritis: a final follow-up report from the Optic Neuritis Treatment Trial. *Ophthalmology*, *115*(6). https://doi.org/10.1016/j.ophtha.2007.08.004
166. Ota, M., Sato, N., Okamoto, T., Noda, T., Araki, M., Yamamura, T., & Kunugi, H. (2015). Neuromyelitis optica spectrum disorder and multiple sclerosis: Differentiation by a multimodal approach. *Multiple Sclerosis and Related Disorders*, *4*(6), 515–520.
167. Palace, J., Leite, M. I., Nairne, A., & Vincent, A. (2010). Interferon Beta treatment in neuromyelitis optica: increase in relapses and aquaporin 4 antibody titers. *Archives of Neurology*, *67*(8). https://doi.org/10.1001/archneurol.2010.188
168. Papadopoulos, M. C., & Verkman, A. S. (2012). Aquaporin 4 and neuromyelitis optica. *The Lancet. Neurology*, *11*(6). https://doi.org/10.1016/S1474-4422(12)70133-3
169. Papadopoulou, A., Oertel, F. C., Gaetano, L., Kuchling, J., Zimmermann, H., Chien, C., Siebert, N., Asseyer, S., Bellmann-Strobl, J., Ruprecht, K., Chakravarty, M. M., Scheel, M., Magon, S., Wuerfel, J., Paul, F., & Brandt, A. U. (2019). Attack-related damage of thalamic nuclei in neuromyelitis optica spectrum disorders. *Journal of Neurology, Neurosurgery, and Psychiatry*, *90*(10). https://doi.org/10.1136/jnnp-2018-320249
170. Pareto, D., Sastre-Garriga, J., Auger, C., Vives-Gilabert, Y., Delgado, J., Tintoré, M., Montalban, X., & Rovira, A. (2015). Juxtacortical Lesions and Cortical Thinning in Multiple Sclerosis. *AJNR. American Journal of Neuroradiology*, *36*(12). https://doi.org/10.3174/ajnr.A4485
171. Pasquier, B., Borisow, N., Rasche, L., Bellmann-Strobl, J., Ruprecht, K., Niendorf, T., Derfuss, T. J., Wuerfel, J., Paul, F., & Sinnecker, T. (2019). Quantitative 7T MRI does not detect occult brain damage in neuromyelitis optica. *Neurology® Neuroimmunology & Neuroinflammation*, *6*(3). https://doi.org/10.1212/NXI.0000000000000541
172. Peterson, J. W., Bö, L., Mörk, S., Chang, A., & Trapp, B. D. (2001). Transected neurites, apoptotic neurons, and reduced inflammation in cortical multiple sclerosis lesions. *Annals of Neurology*, *50*(3). https://doi.org/10.1002/ana.1123
173. Pichiecchio, A., Tavazzi, E., Poloni, G., Ponzio, M., Palesi, F., Pasin, M., Piccolo, L., Tosello, D., Romani, A., Bergamaschi, R., Piccolo, G., & Bastianello, S. (2012). Advanced magnetic resonance imaging of neuromyelitis optica: a multiparametric approach. *Multiple Sclerosis* , *18*(6). https://doi.org/10.1177/1352458511431072
174. Pittock, S. J., Berthele, A., Fujihara, K., Kim, H. J., Levy, M., Palace, J., Nakashima, I., Terzi, M., Totolyan, N., Viswanathan, S., Wang, K. C., Pace, A., Fujita, K. P., Armstrong, R., & Wingerchuk, D. M. (2019). Eculizumab in Aquaporin-4-Positive Neuromyelitis Optica Spectrum Disorder. *The New England Journal of Medicine*, *381*(7). https://doi.org/10.1056/NEJMoa1900866
175. Pittock, S. J., Weinshenker, B. G., Lucchinetti, C. F., Wingerchuk, D. M., Corboy, J. R., & Lennon, V. A. (2006). Neuromyelitis optica brain lesions localized at sites of high aquaporin 4 expression. *Archives of Neurology*, *63*(7). https://doi.org/10.1001/archneur.63.7.964
176. Polman, C. H., O'Connor, P. W., Havrdova, E., Hutchinson, M., Kappos, L., Miller, D. H., Phillips, J. T., Lublin, F. D., Giovannoni, G., Wajgt, A., Toal, M., Lynn, F., Panzara, M. A., & Sandrock, A. W. (2006). A randomized, placebo-controlled trial of natalizumab for relapsing multiple sclerosis. *The New England Journal of Medicine*, *354*(9). https://doi.org/10.1056/NEJMoa044397
177. Popescu, B. F., & Lucchinetti, C. F. (2012). Pathology of demyelinating diseases. *Annual Review of Pathology*, *7*. https://doi.org/10.1146/annurev-pathol-011811-132443
178. Popescu, B. F., Pirko, I., & Lucchinetti, C. F. (2013). Pathology of Multiple Sclerosis: Where Do We Stand? *Continuum : Lifelong Learning in Neurology*, *19*(4 Multiple Sclerosis), 901.
179. Qiu, W., Raven, S., Wu, J. S., Bundell, C., Hollingsworth, P., Carroll, W. M., Mastaglia, F.

L., & Kermode, A. G. (2011). Hypothalamic lesions in multiple sclerosis. *Journal of Neurology, Neurosurgery, and Psychiatry*, *82*(7). https://doi.org/10.1136/jnnp.2009.198192

180. Rahmanzadeh, R., Galbusera, R., Lu, P. J., Bahn, E., Weigel, M., Barakovic, M., Franz, J., Nguyen, T. D., Spincemaille, P., Schiavi, S., Daducci, A., La Rosa, F., Absinta, M., Sati, P., Bach, C. M., Radue, E. W., Leppert, D., Kuhle, J., Kappos, L., … Granziera, C. (2022a). A New Advanced MRI Biomarker for Remyelinated Lesions in Multiple Sclerosis. *Annals of Neurology*, *92*(3). https://doi.org/10.1002/ana.26441
181. Rahmanzadeh, R., Weigel, M., Lu, P. J., Melie-Garcia, L., Nguyen, T. D., Cagol, A., La Rosa, F., Barakovic, M., Lutti, A., Wang, Y., Bach, C. M., Radue, E. W., Gaetano, L., Kappos, L., Kuhle, J., Magon, S., & Granziera, C. (2022b). A comparative assessment of myelin-sensitive measures in multiple sclerosis patients and healthy subjects. *NeuroImage. Clinical*, *36*. https://doi.org/10.1016/j.nicl.2022.103177
182. Rivero, R. L., Oliveira, E. M., Bichuetti, D. B., Gabbai, A. A., Nogueira, R. G., & Abdala, N. (2014). Diffusion tensor imaging of the cervical spinal cord of patients with Neuromyelitis Optica. *Magnetic Resonance Imaging*, *32*(5). https://doi.org/10.1016/j.mri.2014.01.023
183. Robertson, D., & Moreo, N. (2016). Disease-Modifying Therapies in Multiple Sclerosis: Overview and Treatment Considerations. *Federal Practitioner: For the Health Care Professionals of the VA, DoD, and PHS*, *33*(6), 28.
184. Rocca, M. A., Agosta, F., Mezzapesa, D. M., Martinelli, V., Salvi, F., Ghezzi, A., Bergamaschi, R., Comi, G., & Filippi, M. (2004). Magnetization transfer and diffusion tensor MRI show gray matter damage in neuromyelitis optica. *Neurology*, *62*(3). https://doi.org/10.1212/01.wnl.0000106946.08741.41
185. Rocca, M. A., Battaglini, M., Benedict, R. H. B., De Stefano, N., Geurts, J. J. G., Henry, R. G., Horsfield, M. A., Jenkinson, M., Pagani, E., & Filippi, M. (2017). Brain MRI atrophy quantification in MS: From methods to clinical application. *Neurology*, *88*(4), 403.
186. Rodríguez, M. S., Farez, M. F., & Quintana, F. J. (2022). The Immune Response in Multiple Sclerosis. *Annual Review of Pathology*, *17*. https://doi.org/10.1146/annurev-pathol-052920-040318
187. Rudick, R. A., Stuart, W. H., Calabresi, P. A., Confavreux, C., Galetta, S. L., Radue, E. W., Lublin, F. D., Weinstock-Guttman, B., Wynn, D. R., Lynn, F., Panzara, M. A., & Sandrock, A. W. (2006). Natalizumab plus interferon beta-1a for relapsing multiple sclerosis. *The New England Journal of Medicine*, *354*(9). https://doi.org/10.1056/NEJMoa044396
188. Saji, E., Arakawa, M., Yanagawa, K., Toyoshima, Y., Yokoseki, A., Okamoto, K., Otsuki, M., Akazawa, K., Kakita, A., Takahashi, H., Nishizawa, M., & Kawachi, I. (2013). Cognitive impairment and cortical degeneration in neuromyelitis optica. *Annals of Neurology*, *73*(1). https://doi.org/10.1002/ana.23721
189. Salzer, J., Svenningsson, R., Alping, P., Novakova, L., Björck, A., Fink, K., Islam-Jakobsson, P., Malmeström, C., Axelsson, M., Vågberg, M., Sundström, P., Lycke, J., Piehl, F., & Svenningsson, A. (2016). Rituximab in multiple sclerosis: A retrospective observational study on safety and efficacy. *Neurology*, *87*(20), 2074.
190. Sanfilipo, M. P., Benedict, R. H., Weinstock-Guttman, B., & Bakshi, R. (2006). Gray and white matter brain atrophy and neuropsychological impairment in multiple sclerosis. *Neurology*, *66*(5). https://doi.org/10.1212/01.wnl.0000201238.93586.d9
191. Sastre-Garriga, J., Vidal-Jordana, A., Toosy, A. T., Enzinger, C., Granziera, C., Frederiksen, J., Ciccarelli, O., Filippi, M., Montalban, X., Tintore, M., Pareto, D., & Rovira, À. (2024). Value of Optic Nerve MRI in Multiple Sclerosis Clinical Management: A MAGNIMS Position Paper and Future Perspectives. *Neurology*, *103*(3). https://doi.org/10.1212/WNL.0000000000209677
192. Sati, P., Oh, J., Constable, R. T., Evangelou, N., Guttmann, C. R., Henry, R. G., Klawiter, E. C., Mainero, C., Massacesi, L., McFarland, H., Nelson, F., Ontaneda, D., Rauscher, A., Rooney, W. D., Samaraweera, A. P., Shinohara, R. T., Sobel, R. A., Solomon, A. J., Treaba, C. A., … Reich, D. S. (2016). The central vein sign and its clinical evaluation for the diagnosis

of multiple sclerosis: a consensus statement from the North American Imaging in Multiple Sclerosis Cooperative. *Nature Reviews. Neurology*, *12*(12). https://doi.org/10.1038/nrneurol.2016.166

193. Schilling, K., Gao, Y., Janve, V., Stepniewska, I., Landman, B. A., & Anderson, A. W. (2017). Can increased spatial resolution solve the crossing fiber problem for diffusion MRI? *NMR in Biomedicine*, *30*(12). https://doi.org/10.1002/nbm.3787
194. Schneider, T., Brownlee, W., Zhang, H., Ciccarelli, O., Miller, D. H., & Wheeler-Kingshott, C. G. (2017). Sensitivity of multi-shell NODDI to multiple sclerosis white matter changes: a pilot study. *Functional Neurology*, *32*(2). https://doi.org/10.11138/fneur/2017.32.2.097
195. Sethi, V., Yousry, T. A., Muhlert, N., Ron, M., Golay, X., Wheeler-Kingshott, C., Miller, D. H., & Chard, D. T. (2012). Improved detection of cortical MS lesions with phase-sensitive inversion recovery MRI. *Journal of Neurology, Neurosurgery, and Psychiatry*, *83*(9). https://doi.org/10.1136/jnnp-2012-303023
196. Sherman, E., & Han, M. H. (2015). Acute and Chronic Management of Neuromyelitis Optica Spectrum Disorder. *Current Treatment Options in Neurology*, *17*(11). https://doi.org/10.1007/s11940-015-0378-x
197. Shim, E., Lee, E., Lee, J. W., Kang, Y., Ahn, J. M., & Kang, H. S. (2020). Feasibility of postoperative 3-tesla diffusion tensor imaging in cervical spondylotic myelopathy: A comparison of single-shot EPI and multi-shot EPI. *European Journal of Radiology*, *122*. https://doi.org/10.1016/j.ejrad.2019.108751
198. Sinnecker, T., Dörr, J., Pfueller, C. F., Harms, L., Ruprecht, K., Jarius, S., Brück, W., Niendorf, T., Wuerfel, J., & Paul, F. (2012). Distinct lesion morphology at 7-T MRI differentiates neuromyelitis optica from multiple sclerosis. *Neurology*, *79*(7). https://doi.org/10.1212/WNL.0b013e3182648bc8
199. Sinnecker, T., Schumacher, S., Mueller, K., Pache, F., Dusek, P., Harms, L., Ruprecht, K., Nytrova, P., Chawla, S., Niendorf, T., Kister, I., Paul, F., Ge, Y., & Wuerfel, J. (2016). MRI phase changes in multiple sclerosis vs neuromyelitis optica lesions at 7T. *Neurology(R) Neuroimmunology & Neuroinflammation*, *3*(4). https://doi.org/10.1212/NXI.0000000000000259
200. Smith, A. D., Moog, T. M., Burgess, K. W., McCreary, M., & Okuda, D. T. (2023). Factors associated with the misdiagnosis of neuromyelitis optica spectrum disorder. *Multiple Sclerosis and Related Disorders*, *70*. https://doi.org/10.1016/j.msard.2023.104498
201. Spanò, B., Giulietti, G., Pisani, V., Morreale, M., Tuzzi, E., Nocentini, U., Francia, A., Caltagirone, C., Bozzali, M., & Cercignani, M. (2018). Disruption of neurite morphology parallels MS progression. *Neurology® Neuroimmunology & Neuroinflammation*, *5*(6). https://doi.org/10.1212/NXI.0000000000000502
202. Steenwijk, Vrenken, H., Jonkman, L. E., Daams, M., Geurts, J. J., Barkhof, F., & Pouwels, P. J. (2016). High-resolution T1-relaxation time mapping displays subtle, clinically relevant, gray matter damage in long-standing multiple sclerosis. *Multiple Sclerosis* , *22*(10). https://doi.org/10.1177/1352458515615953
203. Storelli, L., Pagani, E., Meani, A., Preziosa, P., Filippi, M., & Rocca, M. A. (2022). Advanced diffusion-weighted imaging models better characterize white matter neurodegeneration and clinical outcomes in multiple sclerosis. *Journal of Neurology*, *269*(9). https://doi.org/10.1007/s00415-022-11104-z
204. Sun, J., Xu, S., Tian, D., Duan, Y., Xu, X., Lv, S., Cao, G., Shi, F. D., Chard, D., Barkhof, F., Zhuo, Z., Zhang, X., & Liu, Y. (2023). Periventricular gradients in NAWM abnormalities differ in MS, NMOSD and MOGAD. *Multiple Sclerosis and Related Disorders*, *75*. https://doi.org/10.1016/j.msard.2023.104732
205. Tackley, G., O'Brien, F., Rocha, J., Woodhall, M., Waters, P., Chandratre, S., Halfpenny, C., Hemingway, C., Wassmer, E., Wasiewski, W., Leite, M. I., & Palace, J. (2016). Neuromyelitis optica relapses: Race and rate, immunosuppression and impairment. *Multiple Sclerosis and Related Disorders*, *7*. https://doi.org/10.1016/j.msard.2016.02.014

206. Tahedl, M., Levine, S. M., Greenlee, M. W., Weissert, R., & Schwarzbach, J. V. (2018). Functional Connectivity in Multiple Sclerosis: Recent Findings and Future Directions. *Frontiers in Neurology*, *9*, 828.
207. Tedone, N., Preziosa, P., Meani, A., Pagani, E., Vizzino, C., Filippi, M., & Rocca, M. A. (2023). Regional white matter and gray matter damage and cognitive performances in multiple sclerosis according to sex. *Molecular Psychiatry*, *28*(4). https://doi.org/10.1038/s41380-023-01996-2
208. Thompson, A. J., Banwell, B. L., Barkhof, F., Carroll, W. M., Coetzee, T., Comi, G., Correale, J., Fazekas, F., Filippi, M., Freedman, M. S., Fujihara, K., Galetta, S. L., Hartung, H. P., Kappos, L., Lublin, F. D., Marrie, R. A., Miller, A. E., Miller, D. H., Montalban, X., … Cohen, J. A. (2018). Diagnosis of multiple sclerosis: 2017 revisions of the McDonald criteria. *Lancet Neurology*, *17*(2). https://doi.org/10.1016/S1474-4422(17)30470-2
209. Tian, D. C., Su, L., Fan, M., Yang, J., Zhang, R., Wen, P., Han, Y., Yu, C., Zhang, C., Ren, H., Shi, K., Zhu, Z., Dong, Y., Liu, Y., & Shi, F. D. (2018). Bidirectional degeneration in the visual pathway in neuromyelitis optica spectrum disorder (NMOSD). *Multiple Sclerosis (Houndmills, Basingstoke, England)*, *24*(12). https://doi.org/10.1177/1352458517727604
210. Todea, R.-A., Lu, P.-J., Fartaria, M. J., Bonnier, G., Du Pasquier, R., Krueger, G., Bach Cuadra, M., Psychogios, M. N., Kappos, L., Kuhle, J., & Granziera, C. (2020). Evolution of Cortical and White Matter Lesion Load in Early-Stage Multiple Sclerosis: Correlation With Neuroaxonal Damage and Clinical Changes. *Frontiers in Neurology*, *11*, 554803.
211. Toosy, A. T., Mason, D. F., & Miller, D. H. (2014). Optic neuritis. *The Lancet. Neurology*, *13*(1). https://doi.org/10.1016/S1474-4422(13)70259-X
212. Tournier, J. D., Smith, R., Raffelt, D., Tabbara, R., Dhollander, T., Pietsch, M., Christiaens, D., Jeurissen, B., Yeh, C. H., & Connelly, A. (2019). MRtrix3: A fast, flexible and open software framework for medical image processing and visualisation. *NeuroImage*, *202*. https://doi.org/10.1016/j.neuroimage.2019.116137
213. Tsagkas, C., Magon, S., Gaetano, L., Pezold, S., Naegelin, Y., Amann, M., Stippich, C., Cattin, P., Wuerfel, J., Bieri, O., Sprenger, T., Kappos, L., & Parmar, K. (2018). Spinal cord volume loss: A marker of disease progression in multiple sclerosis. *Neurology*, *91*(4). https://doi.org/10.1212/WNL.0000000000005853
214. Tur, C., Carbonell-Mirabent, P., Cobo-Calvo, Á., Otero-Romero, S., Arrambide, G., Midaglia, L., Castilló, J., Vidal-Jordana, Á., Rodríguez-Acevedo, B., Zabalza, A., Galán, I., Nos, C., Salerno, A., Auger, C., Pareto, D., Comabella, M., Río, J., Sastre-Garriga, J., Rovira, À., … Montalban, X. (2023). Association of Early Progression Independent of Relapse Activity With Long-term Disability After a First Demyelinating Event in Multiple Sclerosis. *JAMA Neurology*, *80*(2). https://doi.org/10.1001/jamaneurol.2022.4655
215. Vandebroek, A., & Yasui, M. (2020). Regulation of AQP4 in the Central Nervous System. *International Journal of Molecular Sciences*, *21*(5), 1603.
216. Vedantam, A., Jirjis, M. B., Schmit, B. D., Wang, M. C., Ulmer, J. L., & Kurpad, S. N. (2014). Diffusion Tensor Imaging of the Spinal Cord: Insights From Animal and Human Studies. *Neurosurgery*, *74*(1), 1.
217. Voelker, M. N., Kraff, O., Brenner, D., Wollrab, A., Weinberger, O., Berger, M. C., Robinson, S., Bogner, W., Wiggins, C., Trampel, R., Stöcker, T., Niendorf, T., Quick, H. H., Norris, D. G., Ladd, M. E., & Speck, O. (2016). The traveling heads: multicenter brain imaging at 7 Tesla. *Magma* , *29*(3). https://doi.org/10.1007/s10334-016-0541-8
218. von Glehn, F., Jarius, S., Rp, C. L., Mc, A. F., von Glehn, F. H., Castro SM, C. E., Beltramini, G. C., Bergo, F. P., Farias, A. S., Brandão, C. O., Wildemann, B., Damasceno, B. P., Cendes, F., Santos, L. M., & Yasuda, C. L. (2014). Structural brain abnormalities are related to retinal nerve fiber layer thinning and disease duration in neuromyelitis optica spectrum disorders. *Multiple Sclerosis* , *20*(9). https://doi.org/10.1177/1352458513519838
219. Walton, C., King, R., Rechtman, L., Kaye, W., Leray, E., Marrie, R. A., Robertson, N., La Rocca, N., Uitdehaag, B., van der Mei, I., Wallin, M., Helme, A., Angood, N. C., Rijke, N., & Baneke, P. (2020). Rising prevalence of multiple sclerosis worldwide: Insights from the Atlas

of MS, third edition. *Multiple Sclerosis* , *26*(14). https://doi.org/10.1177/1352458520970841
220. Wasserthal, J., Maier-Hein, K. H., Neher, P. F., Northoff, G., Kubera, K. M., Fritze, S., Harneit, A., Geiger, L. S., Tost, H., Wolf, R. C., & Hirjak, D. (2020). Multiparametric mapping of white matter microstructure in catatonia. *Neuropsychopharmacology: Official Publication of the American College of Neuropsychopharmacology*, *45*(10). https://doi.org/10.1038/s41386-020-0691-2
221. Wasserthal, J., Neher, P., & Maier-Hein, K. H. (2018). TractSeg - Fast and accurate white matter tract segmentation. *NeuroImage*, *183*. https://doi.org/10.1016/j.neuroimage.2018.07.070
222. Waters, P. J., McKeon, A., Leite, M. I., Rajasekharan, S., Lennon, V. A., Villalobos, A., Palace, J., Mandrekar, J. N., Vincent, A., Bar-Or, A., & Pittock, S. J. (2012). Serologic diagnosis of NMO: a multicenter comparison of aquaporin-4-IgG assays. *Neurology*, *78*(9). https://doi.org/10.1212/WNL.0b013e318248dec1
223. Waters, P., Reindl, M., Saiz, A., Schanda, K., Tuller, F., Kral, V., Nytrova, P., Sobek, O., Nielsen, H. H., Barington, T., Lillevang, S. T., Illes, Z., Rentzsch, K., Berthele, A., Berki, T., Granieri, L., Bertolotto, A., Giometto, B., Zuliani, L., … Marignier, R. (2016). Multicentre comparison of a diagnostic assay: aquaporin-4 antibodies in neuromyelitis optica. *Journal of Neurology, Neurosurgery, and Psychiatry*, *87*(9). https://doi.org/10.1136/jnnp-2015-312601
224. Wheeler-Kingshott, C. A., Stroman, P. W., Schwab, J. M., Bacon, M., Bosma, R., Brooks, J., Cadotte, D. W., Carlstedt, T., Ciccarelli, O., Cohen-Adad, J., Curt, A., Evangelou, N., Fehlings, M. G., Filippi, M., Kelley, B. J., Kollias, S., Mackay, A., Porro, C. A., Smith, S., … Tracey, I. (2014). The current state-of-the-art of spinal cord imaging: applications. *NeuroImage*, *84*. https://doi.org/10.1016/j.neuroimage.2013.07.014
225. Wilkins, A. (2017). Cerebellar Dysfunction in Multiple Sclerosis. *Frontiers in Neurology*, *8*. https://doi.org/10.3389/fneur.2017.00312
226. Wingerchuk, D. M., Banwell, B., Bennett, J. L., Cabre, P., Carroll, W., Chitnis, T., de Seze, J., Fujihara, K., Greenberg, B., Jacob, A., Jarius, S., Lana-Peixoto, M., Levy, M., Simon, J. H., Tenembaum, S., Traboulsee, A. L., Waters, P., Wellik, K. E., & Weinshenker, B. G. (2015). International consensus diagnostic criteria for neuromyelitis optica spectrum disorders. *Neurology*, *85*(2). https://doi.org/10.1212/WNL.0000000000001729
227. Wingerchuk, D. M., Hogancamp, W. F., O'Brien, P. C., & Weinshenker, B. G. (1999). The clinical course of neuromyelitis optica (Devic's syndrome). *Neurology*, *53*(5). https://doi.org/10.1212/wnl.53.5.1107
228. Wingerchuk, D. M., Lennon, V. A., Lucchinetti, C. F., Pittock, S. J., & Weinshenker, B. G. (2007). The spectrum of neuromyelitis optica. *Lancet Neurology*, *6*(9). https://doi.org/10.1016/S1474-4422(07)70216-8
229. Wrzos, C., Winkler, A., Metz, I., Kayser, D. M., Thal, D. R., Wegner, C., Brück, W., Nessler, S., Bennett, J. L., & Stadelmann, C. (2014). Early loss of oligodendrocytes in human and experimental neuromyelitis optica lesions. *Acta Neuropathologica*, *127*(4). https://doi.org/10.1007/s00401-013-1220-8
230. Yamamura, T., Kleiter, I., Fujihara, K., Palace, J., Greenberg, B., Zakrzewska-Pniewska, B., Patti, F., Tsai, C. P., Saiz, A., Yamazaki, H., Kawata, Y., Wright, P., & De Seze, J. (2019). Trial of Satralizumab in Neuromyelitis Optica Spectrum Disorder. *The New England Journal of Medicine*, *381*(22). https://doi.org/10.1056/NEJMoa1901747
231. Yao, X., Su, T., & Verkman, A. S. (2016). Clobetasol promotes remyelination in a mouse model of neuromyelitis optica. *Acta Neuropathologica Communications*, *4*(1). https://doi.org/10.1186/s40478-016-0309-4
232. You, Y., Zhu, L., Zhang, T., Shen, T., Fontes, A., Yiannikas, C., Parratt, J., Barton, J., Schulz, A., Gupta, V., Barnett, M. H., Fraser, C. L., Gillies, M., Graham, S. L., & Klistorner, A. (2019). Evidence of Müller Glial Dysfunction in Patients with Aquaporin-4 Immunoglobulin G-Positive Neuromyelitis Optica Spectrum Disorder. *Ophthalmology*, *126*(6). https://doi.org/10.1016/j.ophtha.2019.01.016
233. Yu, F. F., Chiang, F. L., Stephens, N., Huang, S. Y., Bilgic, B., Tantiwongkosi, B., &

Romero, R. (2019). Characterization of normal-appearing white matter in multiple sclerosis using quantitative susceptibility mapping in conjunction with diffusion tensor imaging. *Neuroradiology*, *61*(1). https://doi.org/10.1007/s00234-018-2137-7

234. Zhang, H., Schneider, T., Wheeler-Kingshott, C. A., & Alexander, D. C. (2012). NODDI: practical in vivo neurite orientation dispersion and density imaging of the human brain. *NeuroImage*, *61*(4). https://doi.org/10.1016/j.neuroimage.2012.03.072

8. SUPPLEMENTARY MATERIAL

Supplementary Table 1. Comparison of NDI between MS and AQP4-NMOSD patients in unsegmented white matter tracts

Tract	MS			AQP4-NMOSD			T-value	Cohen's d	p-value (FDR corrected)
	M	*SD*	*n*	*M*	*SD*	*n*			
AF_left	0.58	0.06	20	0.62	0.06	20	-2.12	-0.67	0.08
AF_right	0.59	0.05	20	0.63	0.05	20	-1.95	-0.62	0.10
ATR_left	0.56	0.04	20	0.57	0.04	20	-1.18	-0.37	0.27
ATR_right	0.56	0.03	20	0.57	0.04	20	-0.95	-0.30	0.37
CC_1	0.53	0.06	20	0.55	0.05	20	-1.03	-0.32	0.33
CC_2	0.54	0.06	20	0.57	0.05	20	-1.94	-0.61	0.10
CC_3	0.58	0.06	20	0.62	0.05	20	-2.24	-0.71	0.07
CC_4	0.61	0.05	20	0.64	0.05	20	-2.22	-0.71	0.07
CC_5	0.60	0.04	20	0.63	0.04	20	-2.46	-0.78	**0.04***
CC_6	0.57	0.06	20	0.62	0.05	20	-2.92	-0.92	**0.02***
CC_7	0.57	0.06	20	0.63	0.04	20	-3.31	-1.05	**0.01****
CG_left	0.53	0.05	20	0.56	0.05	20	-2.02	-0.64	0.09
CG_right	0.55	0.04	20	0.57	0.05	20	-1.82	-0.57	0.12
CST_left	0.67	0.03	20	0.70	0.03	20	-3.26	-1.03	**0.01****
CST_right	0.68	0.03	20	0.70	0.03	20	-1.90	-0.60	0.11
FPT_left	0.64	0.03	20	0.66	0.04	20	-1.14	-0.36	0.28
FPT_right	0.65	0.03	20	0.66	0.04	20	-1.48	-0.47	0.18
ICP_left	0.68	0.04	20	0.71	0.03	20	-3.51	-1.11	**0.01****
ICP_right	0.69	0.03	20	0.70	0.04	20	-1.78	-0.56	0.12
IFO_left	0.48	0.06	20	0.54	0.05	20	-3.30	-1.04	**0.01****
IFO_right	0.47	0.08	20	0.53	0.04	20	-2.81	-0.89	**0.02***
ILF_left	0.47	0.07	20	0.54	0.05	20	-3.74	-1.18	**0.01***
ILF_right	0.46	0.09	20	0.52	0.05	20	-2.67	-0.84	**0.03***
MCP	0.72	0.04	20	0.75	0.03	20	-3.12	-0.99	**0.01***
OR_left	0.50	0.06	20	0.55	0.04	20	-3.14	-0.99	**0.01***
OR_right	0.50	0.07	20	0.55	0.04	20	-2.64	-0.83	**0.03***
POPT_left	0.62	0.04	20	0.66	0.03	20	-3.13	-0.99	**0.01***
POPT_right	0.62	0.04	20	0.65	0.03	20	-2.92	-0.92	**0.02***
SCP_left	0.67	0.02	20	0.68	0.03	20	-1.31	-0.41	0.22
SCP_right	0.67	0.02	20	0.69	0.03	20	-1.91	-0.60	0.11
SLF_III_left	0.60	0.05	20	0.63	0.05	20	-1.87	-0.59	0.11

SLF_III_right	0.60	0.05	20	0.63	0.05	20	-2.10	-0.66	0.08
SLF_II_left	0.61	0.06	20	0.64	0.05	20	-1.69	-0.53	0.14
SLF_II_right	0.61	0.05	20	0.64	0.05	20	-1.92	-0.61	0.11
SLF_I_left	0.60	0.05	20	0.63	0.04	20	-2.19	-0.69	0.07
SLF_I_right	0.61	0.05	20	0.63	0.04	20	-1.90	-0.60	0.11
STR_left	0.61	0.04	20	0.63	0.04	20	-2.03	-0.65	0.09
STR_right	0.61	0.04	20	0.63	0.04	20	-1.46	-0.46	0.19
ST_FO_left	0.51	0.04	20	0.52	0.05	20	-0.92	-0.29	0.38
ST_FO_right	0.50	0.05	20	0.52	0.05	20	-1.19	-0.38	0.27
ST_PREM_left	0.58	0.04	20	0.60	0.05	20	-1.61	-0.51	0.16
ST_PREM_right	0.59	0.04	20	0.62	0.04	20	-1.87	-0.59	0.11
T_OCC_left	0.50	0.07	20	0.55	0.04	20	-3.21	-1.01	**0.01***
T_OCC_right	0.49	0.07	20	0.55	0.04	20	-2.72	-0.86	**0.03***
T_PAR_left	0.56	0.05	20	0.59	0.04	20	-2.00	-0.63	0.10
T_PAR_right	0.55	0.05	20	0.58	0.04	20	-2.76	-0.87	**0.02***
T_PREM_left	0.60	0.03	20	0.61	0.04	20	-0.68	-0.21	0.51
T_PREM_right	0.61	0.03	20	0.62	0.04	20	-0.94	-0.30	0.37
UF_left	0.46	0.05	20	0.49	0.05	20	-2.25	-0.71	0.07
UF_right	0.45	0.04	20	0.48	0.04	20	-2.03	-0.64	0.09

*p < .05, **p < 0.01; AQP4 = aquaporin-4; NMOSD = neuromyelitis optica spectrum disorders; MS = multiple sclerosis; NDI = neurite density index; *n* = number of participants; AF = arcuate fascicle; ATR = anterior thalamic radiation; CC = corpus callosum; CC_1 = rostrum; CC_2 = genu; CC_3 = rostral body; CC_4 = anterior midbody; CC_5 = posterior midbody; CC_6 = isthmus; CC_7 = splenium; CG = cingulum; CST = corticospinal tract; FPT = fronto-pontine tract; ICP = inferior cerebellar peduncle; IFO = inferior occipito-frontal fascicle; ILF = inferior longitudinal fascicle; MCP = middle cerebellar peduncle; OR = optic radiation; POPT = parieto‑occipital pontine tract; SCP = superior cerebellar peduncle; SLF_I = superior longitudinal fascicle I; SLF_II = superior longitudinal fascicle II; SLF_III = superior longitudinal fascicle III; STR = superior thalamic radiation; ST_FO = striato-fronto-orbital; ST_PREM = striato-premotor; T_OCC = thalamo-occipital; T_PAR = thalamo-parietal; T_PREM = thalamo-premotor; UF = uncinate fascicle.

Supplementary Table 2. Comparison of NDI between MS and AQP4-NMOSD patients in white matter fibers traversing through white matter lesions

Tract	MS			AQP4-NMOSD			T-value	Cohen's d	p-value (FDR corrected)
	M	*SD*	*n*	*M*	*SD*	*n*			
AF_left	0.59	0.04	18	0.62	0.06	11	-1.69	-0.69	0.18
AF_right	0.59	0.03	16	0.61	0.05	2	-1.68	-0.67	0.12
ATR_left	0.55	0.03	17	0.56	0.04	16	-0.59	-0.22	0.64
ATR_right	0.56	0.03	17	0.56	0.04	17	-0.34	-0.13	0.78
CC_1	0.53	0.05	16	0.53	0.05	11	-0.06	-0.02	0.96
CC_2	0.55	0.04	19	0.57	0.05	13	-1.17	-0.42	0.34
CC_3	0.60	0.04	19	0.63	0.04	4	-1.63	-0.60	0.19
CC_4	0.62	0.04	19	0.64	0.04	14	-0.93	-0.36	0.45
CC_5	0.62	0.03	18	0.61	0.04	15	0.46	0.20	0.72
CC_6	0.59	0.05	19	0.63	0.05	11	-2.56	-0.87	**0.04***
CC_7	0.62	0.04	19	0.64	0.03	12	-1.16	-0.39	0.34
CG_left	0.54	0.04	16	0.58	0.06	2	-0.99	-0.30	0.16
CG_right	0.55	0.05	15	0.56	0.06	7	-0.35	-0.15	0.78
CST_left	0.67	0.03	18	0.69	0.02	9	-2.44	-0.82	0.06
CST_right	0.69	0.03	16	0.69	0.03	10	0.06	0.02	0.96
FPT_left	0.65	0.02	19	0.66	0.04	10	-0.50	-0.20	0.69
FPT_right	0.65	0.02	18	0.65	0.04	13	0.06	0.02	0.96
ICP_left	0.65	0.04	3	0.68	0.01	8	-1.20	-0.89	0.41
IFO_left	0.50	0.04	19	0.53	0.05	7	-1.85	-0.64	0.14
IFO_right	0.48	0.05	18	0.51	0.05	9	-1.96	-0.66	0.12
ILF_left	0.48	0.06	16	0.52	0.04	12	-2.01	-0.72	0.11
ILF_right	0.46	0.06	16	0.50	0.04	9	-1.79	-0.64	0.15
MCP	0.69	0.07	9	0.75	0.01	13	-2.60	-1.04	0.07
OR_left	0.55	0.04	19	0.55	0.03	12	0.33	0.11	0.79
OR_right	0.53	0.03	16	0.54	0.04	13	-0.60	-0.22	0.63
POPT_left	0.63	0.02	19	0.64	0.04	14	-0.70	-0.31	0.57
POPT_right	0.63	0.03	18	0.64	0.03	13	-0.61	-0.23	0.63
SCP_left	0.69	0.02	6	0.71	0.01	14	-1.65	-1.05	0.28
SLF_III_left	0.58	0.04	14	0.60	0.05	10	-0.76	-0.38	0.55
SLF_III_right	0.59	0.05	13	0.62	0.06	10	-1.34	-0.59	0.28
SLF_II_left	0.60	0.04	15	0.63	0.04	9	-2.03	-0.83	0.12
SLF_II_right	0.60	0.04	16	0.62	0.05	8	-1.05	-0.44	0.39

SLF_I_left	0.59	0.05	17	0.62	0.06	10	-1.49	-0.56	0.23
SLF_I_right	0.59	0.05	15	0.61	0.04	13	-1.08	-0.46	0.39
STR_left	0.61	0.03	17	0.60	0.02	8	0.84	0.34	0.50
STR_right	0.61	0.03	15	0.60	0.03	7	0.82	0.37	0.51
ST_FO_left	0.51	0.04	16	0.53	0.05	9	-0.79	-0.32	0.52
ST_FO_right	0.52	0.04	15	0.50	0.05	12	1.00	0.44	0.42
ST_PREM_left	0.56	0.03	18	0.59	0.05	9	-1.38	-0.55	0.27
ST_PREM_right	0.60	0.03	15	0.60	0.05	13	-0.40	-0.16	0.75
T_OCC_left	0.55	0.04	19	0.54	0.02	12	1.13	0.36	0.35
T_OCC_right	0.52	0.04	16	0.54	0.04	13	-1.23	-0.45	0.32
T_PAR_left	0.56	0.03	20	0.57	0.03	14	-0.48	-0.18	0.70
T_PAR_right	0.55	0.04	17	0.58	0.04	13	-1.71	-0.61	0.17
T_PREM_left	0.59	0.03	17	0.60	0.04	14	-0.71	-0.32	0.57
T_PREM_right	0.60	0.03	15	0.61	0.05	10	-0.19	-0.09	0.88
UF_left	0.48	0.05	16	0.51	0.06	10	-1.34	-0.60	0.28
UF_right	0.46	0.05	15	0.47	0.06	9	-0.07	-0.03	0.96

*p < .05, **p < 0.01; AQP4 = aquaporin-4; NMOSD = neuromyelitis optica spectrum disorders; MS = multiple sclerosis; NDI = neurite density index; *n* = number of participants; AF = arcuate fascicle; ATR = anterior thalamic radiation; CC = corpus callosum; CC_1 = rostrum; CC_2 = genu; CC_3 = rostral body; CC_4 = anterior midbody; CC_5 = posterior midbody; CC_6 = isthmus; CC_7 = splenium; CG = cingulum; CST = corticospinal tract; FPT = fronto-pontine tract; ICP = inferior cerebellar peduncle; IFO = inferior occipito-frontal fascicle; ILF = inferior longitudinal fascicle; MCP = middle cerebellar peduncle; OR = optic radiation; POPT = parieto‑occipital pontine tract; SCP = superior cerebellar peduncle; SLF_I = superior longitudinal fascicle I; SLF_II = superior longitudinal fascicle II; SLF_III = superior longitudinal fascicle III; STR = superior thalamic radiation; ST_FO = striato-fronto-orbital; ST_PREM = striato-premotor; T_OCC = thalamo-occipital; T_PAR = thalamo-parietal; T_PREM = thalamo-premotor; UF = uncinate fascicle.

Supplementary Table 3. Comparison of NDI between MS and AQP4-NMOSD patients in white matter fibers not traversing through white matter lesions

Tract	MS			AQP4-NMOSD			T-value	Cohen's d	p-value (FDR corrected)
	M	*SD*	*n*	*M*	*SD*	*n*			
AF_left	0.59	0.05	20	0.62	0.06	20	-1.73	-0.55	0.17
AF_right	0.60	0.05	20	0.63	0.05	20	-1.74	-0.55	0.17
ATR_left	0.57	0.03	20	0.58	0.04	20	-0.64	-0.20	0.56
ATR_right	0.58	0.03	20	0.58	0.04	20	-0.20	-0.06	0.85
CC_1	0.54	0.05	20	0.55	0.05	20	-0.92	-0.29	0.42
CC_2	0.55	0.05	20	0.58	0.05	20	-1.76	-0.56	0.17
CC_3	0.59	0.04	18	0.62	0.05	19	-2.09	-0.68	0.11
CC_4	0.63	0.03	15	0.65	0.04	18	-1.28	-0.43	0.28
CC_5	0.60	0.03	18	0.63	0.04	20	-2.33	-0.74	0.08
CC_6	0.59	0.04	20	0.62	0.05	20	-2.70	-0.85	**0.04***
CC_7	0.61	0.04	18	0.63	0.04	20	-1.99	-0.65	0.13
CG_left	0.54	0.04	20	0.56	0.05	20	-1.92	-0.61	0.13
CG_right	0.55	0.04	20	0.57	0.05	20	-1.82	-0.57	0.15
CST_left	0.68	0.03	20	0.70	0.03	20	-3.08	-0.97	**0.02***
CST_right	0.69	0.03	20	0.70	0.03	20	-2.06	-0.65	0.11
FPT_left	0.65	0.02	20	0.66	0.04	20	-0.96	-0.30	0.40
FPT_right	0.65	0.02	20	0.66	0.04	20	-1.19	-0.38	0.30
ICP_left	0.68	0.04	20	0.72	0.03	20	-3.40	-1.08	**0.01****
ICP_right	0.69	0.03	20	0.70	0.04	20	-1.62	-0.51	0.19
IFO_left	0.52	0.03	17	0.55	0.04	20	-2.41	-0.77	0.07
IFO_right	0.51	0.04	18	0.54	0.04	20	-2.29	-0.74	0.08
ILF_left	0.50	0.03	19	0.54	0.05	20	-2.99	-0.95	**0.02***
ILF_right	0.51	0.05	17	0.53	0.05	20	-1.04	-0.34	0.37
MCP	0.72	0.04	20	0.75	0.03	20	-3.11	-0.98	**0.02***
OR_left	0.54	0.03	15	0.56	0.04	20	-2.10	-0.68	0.11
OR_right	0.54	0.03	14	0.56	0.03	19	-1.75	-0.59	0.17
POPT_left	0.64	0.02	20	0.67	0.03	20	-2.73	-0.86	**0.04***
POPT_right	0.64	0.02	19	0.66	0.02	20	-1.93	-0.62	0.13
SCP_left	0.67	0.02	20	0.68	0.03	20	-1.33	-0.42	0.27
SCP_right	0.67	0.02	20	0.69	0.03	20	-1.93	-0.61	0.13
SLF_III_left	0.60	0.05	20	0.63	0.05	20	-1.75	-0.55	0.17
SLF_III_right	0.60	0.05	20	0.63	0.05	20	-1.97	-0.62	0.13

SLF_II_left	0.63	0.04	19	0.64	0.05	20	-1.21	-0.38	0.30
SLF_II_right	0.62	0.04	20	0.65	0.05	20	-2.00	-0.63	0.12
SLF_I_left	0.61	0.03	19	0.63	0.04	20	-2.07	-0.66	0.11
SLF_I_right	0.62	0.03	19	0.64	0.04	20	-1.53	-0.49	0.22
STR_left	0.63	0.03	18	0.64	0.04	19	-0.65	-0.21	0.56
STR_right	0.63	0.03	19	0.64	0.03	20	-0.61	-0.20	0.58
ST_FO_left	0.52	0.04	20	0.52	0.05	20	-0.47	-0.15	0.67
ST_FO_right	0.51	0.04	20	0.52	0.05	20	-0.97	-0.31	0.40
ST_PREM_left	0.59	0.03	20	0.61	0.04	20	-1.51	-0.48	0.22
ST_PREM_right	0.60	0.04	20	0.62	0.04	20	-1.88	-0.59	0.14
T_OCC_left	0.54	0.03	16	0.56	0.04	20	-1.91	-0.62	0.13
T_OCC_right	0.54	0.02	14	0.56	0.03	19	-1.67	-0.56	0.19
T_PAR_left	0.59	0.03	20	0.61	0.04	20	-1.40	-0.44	0.24
T_PAR_right	0.58	0.03	19	0.59	0.03	20	-1.25	-0.40	0.29
T_PREM_left	0.61	0.03	20	0.61	0.04	20	-0.07	-0.02	0.95
T_PREM_right	0.61	0.03	20	0.62	0.04	20	-0.67	-0.21	0.55
UF_left	0.46	0.05	20	0.49	0.05	20	-2.31	-0.73	0.08
UF_right	0.46	0.04	20	0.48	0.04	20	-1.94	-0.61	0.13

*p < .05, **p < 0.01; AQP4 = aquaporin-4; NMOSD = neuromyelitis optica spectrum disorders; MS = multiple sclerosis; NDI = neurite density index; *n* = number of participants; AF = arcuate fascicle; ATR = anterior thalamic radiation; CC = corpus callosum; CC_1 = rostrum; CC_2 = genu; CC_3 = rostral body; CC_4 = anterior midbody; CC_5 = posterior midbody; CC_6 = isthmus; CC_7 = splenium; CG = cingulum; CST = corticospinal tract; FPT = fronto-pontine tract; ICP = inferior cerebellar peduncle; IFO = inferior occipito-frontal fascicle; ILF = inferior longitudinal fascicle; MCP = middle cerebellar peduncle; OR = optic radiation; POPT = parieto‑occipital pontine tract; SCP = superior cerebellar peduncle; SLF_I = superior longitudinal fascicle I; SLF_II = superior longitudinal fascicle II; SLF_III = superior longitudinal fascicle III; STR = superior thalamic radiation; ST_FO = striato-fronto-orbital; ST_PREM = striato-premotor; T_OCC = thalamo-occipital; T_PAR = thalamo-parietal; T_PREM = thalamo-premotor; UF = uncinate fascicle.

Supplementary Table 4. Comparison of NDI in unsegmented white matter tracts between in MS patients and whole tracts in HC

Tract	MS			HC			T-value	Cohen's d	p-value (FDR corrected)
	M	*SD*	*n*	*M*	*SD*	*n*			
AF_left	0.58	0.06	20	0.64	0.04	20	-3.71	-1.17	**0.00****
AF_right	0.59	0.05	20	0.65	0.04	20	-3.71	-1.17	**0.00****
ATR_left	0.56	0.04	20	0.59	0.02	20	-3.01	-0.95	**0.01***
ATR_right	0.56	0.03	20	0.59	0.03	20	-2.77	-0.88	**0.02***
CC_1	0.53	0.06	20	0.56	0.04	20	-2.28	-0.72	0.06
CC_2	0.54	0.06	20	0.60	0.04	20	-3.84	-1.22	**0.00****
CC_3	0.58	0.06	20	0.64	0.04	20	-3.98	-1.26	**0.00****
CC_4	0.61	0.05	20	0.67	0.03	20	-4.74	-1.50	**0.00****
CC_5	0.59	0.04	20	0.65	0.03	20	-4.51	-1.43	**0.00****
CC_6	0.57	0.06	20	0.65	0.04	20	-4.66	-1.47	**0.00****
CC_7	0.57	0.06	20	0.65	0.03	20	-5.04	-1.59	**0.00****
CG_left	0.53	0.05	20	0.58	0.03	20	-3.91	-1.24	**0.00****
CG_right	0.55	0.04	20	0.59	0.03	20	-3.78	-1.19	**0.00****
CST_left	0.67	0.03	20	0.71	0.02	20	-4.67	-1.48	**0.00****
CST_right	0.68	0.03	20	0.72	0.02	20	-3.84	-1.21	**0.00****
FPT_left	0.64	0.03	20	0.67	0.02	20	-3.51	-1.11	**0.00****
FPT_right	0.65	0.03	20	0.68	0.02	20	-3.35	-1.06	**0.01***
ICP_left	0.68	0.04	20	0.72	0.03	20	-3.59	-1.14	**0.00****
ICP_right	0.69	0.02	20	0.71	0.03	20	-2.42	-0.77	**0.05***
IFO_left	0.48	0.06	20	0.56	0.03	20	-4.96	-1.57	**0.00****
IFO_right	0.47	0.08	20	0.55	0.03	20	-4.23	-1.34	**0.00****
ILF_left	0.47	0.07	20	0.56	0.03	20	-5.38	-1.70	**0.00****
ILF_right	0.46	0.09	20	0.55	0.03	20	-4.38	-1.38	**0.00****
MCP	0.72	0.04	20	0.75	0.02	20	-3.44	-1.09	0.01
OR_left	0.50	0.06	20	0.57	0.04	20	-4.50	-1.42	**0.00****
OR_right	0.50	0.07	20	0.57	0.03	20	-4.09	-1.29	**0.00****
POPT_left	0.62	0.04	20	0.67	0.03	20	-4.82	-1.52	**0.00****
POPT_right	0.62	0.04	20	0.66	0.02	20	-4.24	-1.34	**0.00****
SCP_left	0.67	0.02	20	0.69	0.02	20	-2.42	-0.76	**0.05***
SCP_right	0.67	0.02	20	0.69	0.02	20	-2.30	-0.73	0.06
SLF_III_left	0.59	0.05	20	0.65	0.04	20	-3.49	-1.11	**0.00****
SLF_III_right	0.60	0.05	20	0.65	0.04	20	-3.72	-1.18	**0.00****
SLF_II_left	0.61	0.06	20	0.67	0.03	20	-3.76	-1.19	**0.00****

SLF_II_right	0.61	0.05	20	0.67	0.03	20	-4.34	-1.37	**0.00****
SLF_I_left	0.60	0.05	20	0.65	0.03	20	-4.13	-1.31	**0.00****
SLF_I_right	0.61	0.05	20	0.66	0.03	20	-3.93	-1.24	**0.00****
STR_left	0.61	0.04	20	0.65	0.02	20	-4.46	-1.41	**0.00****
STR_right	0.61	0.04	20	0.65	0.02	20	-3.65	-1.15	**0.00****
ST_FO_left	0.51	0.04	20	0.54	0.03	20	-3.10	-0.98	**0.01***
ST_FO_right	0.50	0.05	20	0.54	0.03	20	-2.97	-0.94	**0.02***
ST_PREM_left	0.58	0.04	20	0.62	0.03	20	-3.77	-1.19	**0.00****
ST_PREM_right	0.59	0.04	20	0.63	0.03	20	-3.76	-1.19	**0.00****
T_OCC_left	0.50	0.07	20	0.57	0.04	20	-4.27	-1.35	**0.00****
T_OCC_right	0.49	0.07	20	0.57	0.03	20	-4.01	-1.27	**0.00****
T_PAR_left	0.56	0.05	20	0.62	0.03	20	-4.16	-1.32	**0.00****
T_PAR_right	0.55	0.05	20	0.60	0.03	20	-4.19	-1.33	**0.00****
T_PREM_left	0.60	0.03	20	0.63	0.02	20	-2.84	-0.90	**0.02***
T_PREM_right	0.61	0.03	20	0.63	0.02	20	-2.80	-0.89	**0.02***
UF_left	0.46	0.05	20	0.51	0.03	20	-4.36	-1.38	**0.00****
UF_right	0.45	0.04	20	0.49	0.02	20	-3.75	-1.19	**0.00****

*p < ,05, **p < 0,01, p*** < ,001; MS = multiple sclerosis; HC = healthy controls; NDI = neurite density index; *n* = number of participants; AF = arcuate fascicle; ATR = anterior thalamic radiation; CC = corpus callosum; CC_1 = rostrum; CC_2 = genu; CC_3 = rostral body; CC_4 = anterior midbody; CC_5 = posterior midbody; CC_6 = isthmus; CC_7 = splenium; CG = cingulum; CST = corticospinal tract; FPT = fronto-pontine tract; ICP = inferior cerebellar peduncle; IFO = inferior occipito-frontal fascicle; ILF = inferior longitudinal fascicle; MCP = middle cerebellar peduncle; OR = optic radiation; POPT = parieto‑occipital pontine tract; SCP = superior cerebellar peduncle; SLF_I = superior longitudinal fascicle I; SLF_II = superior longitudinal fascicle II; SLF_III = superior longitudinal fascicle III; STR = superior thalamic radiation; ST_FO = striato-fronto-orbital; ST_PREM = striato-premotor; T_OCC = thalamo-occipital; T_PAR = thalamo-parietal; T_PREM = thalamo-premotor; UF = uncinate fascicle.

Supplementary Table 5. Comparison of NDI in white matter fibers traversing through white matter lesions in MS patients and whole tracts in HC

Tract	MS			HC			T-value	Cohen's d	p-value (FDR corrected)
	M	*SD*	*n*	*M*	*SD*	*n*			
AF_left	0.57	0.04	18	0.64	0.04	20	-5.75	-1.87	**0.00*****
AF_right	0.59	0.04	16	0.65	0.04	20	-4.41	-1.51	**0.01****
ATR_left	0.55	0.03	17	0.59	0.02	20	-4.28	-1.44	**0.01****
ATR_right	0.56	0.03	17	0.59	0.03	20	-3.47	-1.14	**0.01****
CC_1	0.52	0.05	16	0.56	0.04	20	-2.53	-0.88	0.05
CC_2	0.55	0.04	19	0.60	0.04	20	-3.69	-1.19	**0.01****
CC_3	0.60	0.04	19	0.64	0.04	20	-3.01	-0.97	**0.02***
CC_4	0.62	0.04	19	0.67	0.03	20	-4.15	-1.34	**0.01****
CC_5	0.61	0.03	18	0.65	0.03	20	-2.95	-0.97	**0.02***
CC_6	0.59	0.05	19	0.65	0.04	20	-4.01	-1.30	**0.01****
CC_7	0.62	0.04	19	0.65	0.03	20	-2.56	-0.83	0.05
CG_left	0.54	0.04	16	0.58	0.03	20	-3.58	-1.27	**0.01****
CG_right	0.55	0.05	15	0.59	0.03	20	-2.82	-1.04	**0.03***
CST_left	0.67	0.03	18	0.71	0.02	20	-4.70	-1.55	**0.00*****
CST_right	0.69	0.03	16	0.72	0.02	20	-3.63	-1.25	**0.01****
FPT_left	0.65	0.02	19	0.67	0.02	20	-2.76	-0.88	**0.03***
FPT_right	0.65	0.02	18	0.68	0.02	20	-2.86	-0.93	**0.02***
ICP_left	0.65	0.04	3	0.72	0.03	20	-2.72	-1.92	0.16
ICP_right	0.67	0.05	5	0.71	0.03	20	-1.55	-0.99	0.27
IFO_left	0.50	0.04	19	0.56	0.03	20	-4.88	-1.56	**0.00*****
IFO_right	0.48	0.05	18	0.55	0.03	20	-4.78	-1.59	**0.00*****
ILF_left	0.48	0.06	16	0.56	0.03	20	-5.05	-1.79	**0.00*****
ILF_right	0.46	0.06	16	0.55	0.03	20	-5.46	-1.94	**0.00*****
MCP	0.69	0.07	9	0.75	0.02	20	-2.77	-1.59	0.06
OR_left	0.55	0.04	19	0.57	0.04	20	-1.72	-0.55	0.16
OR_right	0.53	0.03	16	0.57	0.03	20	-3.65	-1.22	0.00
POPT_left	0.63	0.02	19	0.67	0.03	20	-5.16	-1.65	**0.00*****
POPT_right	0.63	0.03	18	0.66	0.02	20	-3.23	-1.07	**0.01***
SCP_left	0.69	0.02	6	0.69	0.02	20	-0.01	0.00	0.99
SCP_right	0.68	0.03	6	0.69	0.02	20	-0.55	-0.30	0.67
SLF_III_left	0.58	0.04	14	0.65	0.04	20	-4.77	-1.67	**0.00*****
SLF_III_right	0.59	0.05	13	0.65	0.04	20	-3.28	-1.26	0.02
SLF_II_left	0.60	0.04	15	0.67	0.03	20	-5.55	-1.98	**0.00*****

SLF_II_right	0.60	0.04	16	0.67	0.03	20	-5.12	-1.79	**0.00*** **
SLF_I_left	0.59	0.05	17	0.65	0.03	20	-4.37	-1.49	**0.01** **
SLF_I_right	0.59	0.05	15	0.66	0.03	20	-4.56	-1.63	**0.01** **
STR_left	0.61	0.03	17	0.65	0.02	20	-4.43	-1.50	**0.01** **
STR_right	0.61	0.03	15	0.65	0.02	20	-3.89	-1.35	**0.01** **
ST_FO_left	0.51	0.04	16	0.54	0.03	20	-2.66	-0.90	**0.04***
ST_FO_right	0.52	0.04	15	0.54	0.03	20	-1.32	-0.46	0.28
ST_PREM_left	0.56	0.03	18	0.62	0.03	20	-5.98	-1.95	**0.00*** **
ST_PREM_right	0.60	0.03	15	0.63	0.03	20	-3.48	-1.21	**0.01** **
T_OCC_left	0.55	0.04	19	0.57	0.04	20	-1.53	-0.49	0.21
T_OCC_right	0.52	0.04	16	0.57	0.03	20	-3.68	-1.26	0.00
T_PAR_left	0.56	0.03	20	0.62	0.03	20	-6.14	-1.94	**0.00*** **
T_PAR_right	0.55	0.04	17	0.60	0.03	20	-3.68	-1.25	**0.01** **
T_PREM_left	0.59	0.03	17	0.63	0.02	20	-4.33	-1.46	**0.01** **
T_PREM_right	0.60	0.03	15	0.63	0.02	20	-2.95	-1.04	**0.02***
UF_left	0.48	0.05	16	0.51	0.03	20	-2.75	-0.98	**0.04***
UF_right	0.46	0.05	15	0.49	0.02	20	-2.28	-0.85	0.08

*p < ,05, **p < 0,01, p*** < ,001; MS = multiple sclerosis; HC = healthy controls; NDI = neurite density index; *n* = number of participants; AF = arcuate fascicle; ATR = anterior thalamic radiation; CC = corpus callosum; CC_1 = rostrum; CC_2 = genu; CC_3 = rostral body; CC_4 = anterior midbody; CC_5 = posterior midbody; CC_6 = isthmus; CC_7 = splenium; CG = cingulum; CST = corticospinal tract; FPT = fronto-pontine tract; ICP = inferior cerebellar peduncle; IFO = inferior occipito-frontal fascicle; ILF = inferior longitudinal fascicle; MCP = middle cerebellar peduncle; OR = optic radiation; POPT = parieto‑occipital pontine tract; SCP = superior cerebellar peduncle; SLF_I = superior longitudinal fascicle I; SLF_II = superior longitudinal fascicle II; SLF_III = superior longitudinal fascicle III; STR = superior thalamic radiation; ST_FO = striato-fronto-orbital; ST_PREM = striato-premotor; T_OCC = thalamo-occipital; T_PAR = thalamo-parietal; T_PREM = thalamo-premotor; UF = uncinate fascicle.

Supplementary Table 6. Comparison of NDI in white matter fibers not traversing through white matter lesions in MS patients and whole tracts in HC

Tract	MS			HC			T-value	Cohen's d	p-value (FDR corrected)
	M	*SD*	*n*	*M*	*SD*	*n*			
AF_left	0.59	0.05	20	0.64	0.04	20	-3.62	-1.14	**0.01****
AF_right	0.60	0.05	20	0.65	0.04	20	-3.52	-1.11	**0.01****
ATR_left	0.57	0.03	20	0.59	0.02	20	-2.05	-0.65	0.11
ATR_right	0.58	0.03	20	0.59	0.03	20	-1.34	-0.42	0.26
CC_1	0.53	0.05	20	0.56	0.04	20	-2.11	-0.67	0.11
CC_2	0.55	0.05	20	0.60	0.04	20	-3.59	-1.14	**0.01****
CC_3	0.59	0.04	18	0.64	0.04	20	-3.76	-1.22	**0.01****
CC_4	0.63	0.03	15	0.67	0.03	20	-3.67	-1.25	**0.01****
CC_5	0.60	0.03	18	0.65	0.03	20	-4.73	-1.54	**0.01****
CC_6	0.59	0.04	20	0.65	0.04	20	-4.75	-1.50	**0.01****
CC_7	0.61	0.04	18	0.65	0.03	20	-3.75	-1.24	**0.01****
CG_left	0.54	0.04	20	0.58	0.03	20	-4.19	-1.33	**0.01****
CG_right	0.55	0.04	20	0.59	0.03	20	-3.86	-1.22	**0.01****
CST_left	0.67	0.03	20	0.71	0.02	20	-4.41	-1.40	**0.01****
CST_right	0.69	0.03	20	0.72	0.02	20	-3.80	-1.20	**0.01****
FPT_left	0.65	0.02	20	0.67	0.02	20	-3.12	-0.99	**0.02***
FPT_right	0.65	0.02	20	0.68	0.02	20	-3.08	-0.97	**0.02***
ICP_left	0.68	0.04	20	0.72	0.03	20	-3.48	-1.10	**0.01****
ICP_right	0.69	0.03	20	0.71	0.03	20	-2.23	-0.71	0.09
IFO_left	0.52	0.03	17	0.56	0.03	20	-4.13	-1.34	**0.01****
IFO_right	0.51	0.04	18	0.55	0.03	20	-3.67	-1.20	**0.01****
ILF_left	0.50	0.03	19	0.56	0.03	20	-5.64	-1.81	**0.00*****
ILF_right	0.51	0.05	17	0.55	0.03	20	-3.06	-1.04	**0.02***
MCP	0.72	0.04	20	0.75	0.02	20	-3.46	-1.09	**0.01****
OR_left	0.54	0.03	15	0.57	0.04	20	-2.95	-0.95	**0.02***
OR_right	0.54	0.02	14	0.57	0.03	20	-2.54	-0.84	0.06
POPT_left	0.64	0.02	20	0.67	0.03	20	-3.69	-1.17	**0.01****
POPT_right	0.64	0.02	19	0.66	0.02	20	-2.94	-0.94	**0.02***
SCP_left	0.67	0.02	20	0.69	0.02	20	-2.46	-0.78	0.06
SCP_right	0.67	0.02	20	0.69	0.02	20	-2.29	-0.72	0.08
SLF_III_left	0.60	0.05	20	0.65	0.04	20	-3.44	-1.09	**0.01****
SLF_III_right	0.60	0.05	20	0.65	0.04	20	-3.63	-1.15	**0.01****
SLF_II_left	0.63	0.04	19	0.67	0.03	20	-3.74	-1.20	**0.01****

SLF_II_right	0.62	0.04	20	0.67	0.03	20	-4.25	-1.35	**0.01****
SLF_I_left	0.61	0.03	19	0.65	0.03	20	-4.21	-1.35	**0.01****
SLF_I_right	0.62	0.03	19	0.66	0.03	20	-3.77	-1.21	**0.01****
STR_left	0.63	0.03	18	0.65	0.02	20	-2.31	-0.77	0.08
STR_right	0.63	0.03	19	0.65	0.02	20	-2.20	-0.71	0.09
ST_FO_left	0.52	0.03	20	0.54	0.03	20	-2.52	-0.80	0.06
ST_FO_right	0.51	0.04	20	0.54	0.03	20	-2.59	-0.82	0.05
ST_PREM_left	0.59	0.03	20	0.62	0.03	20	-3.34	-1.06	**0.01****
ST_PREM_right	0.60	0.04	20	0.63	0.03	20	-3.59	-1.13	**0.01****
T_OCC_left	0.54	0.03	16	0.57	0.04	20	-2.43	-0.78	0.07
T_OCC_right	0.54	0.02	14	0.57	0.03	20	-2.37	-0.77	0.08
T_PAR_left	0.59	0.03	20	0.62	0.03	20	-2.62	-0.83	**0.05***
T_PAR_right	0.58	0.03	19	0.60	0.03	20	-2.07	-0.66	0.11
T_PREM_left	0.61	0.03	20	0.63	0.02	20	-2.08	-0.66	0.11
T_PREM_right	0.61	0.02	20	0.63	0.02	20	-2.33	-0.74	0.08
UF_left	0.46	0.05	20	0.51	0.03	20	-4.37	-1.38	**0.01****
UF_right	0.45	0.04	20	0.49	0.02	20	-3.93	-1.24	**0.01****

*p < ,05, **p < 0,01, p*** < ,001; MS = multiple sclerosis; HC = healthy controls; NDI = neurite density index; *n* = number of participants; AF = arcuate fascicle; ATR = anterior thalamic radiation; CC = corpus callosum; CC_1 = rostrum; CC_2 = genu; CC_3 = rostral body; CC_4 = anterior midbody; CC_5 = posterior midbody; CC_6 = isthmus; CC_7 = splenium; CG = cingulum; CST = corticospinal tract; FPT = fronto-pontine tract; ICP = inferior cerebellar peduncle; IFO = inferior occipito-frontal fascicle; ILF = inferior longitudinal fascicle; MCP = middle cerebellar peduncle; OR = optic radiation; POPT = parieto‑occipital pontine tract; SCP = superior cerebellar peduncle; SLF_I = superior longitudinal fascicle I; SLF_II = superior longitudinal fascicle II; SLF_III = superior longitudinal fascicle III; STR = superior thalamic radiation; ST_FO = striato-fronto-orbital; ST_PREM = striato-premotor; T_OCC = thalamo-occipital; T_PAR = thalamo-parietal; T_PREM = thalamo-premotor; UF = uncinate fascicle.

Supplementary Table 7. Comparison of NDI in unsegmented white matter tracts between AQP4-NMOSD patients and HC

Tract	AQP4-NMOSD			HC			T-value	Cohen's d	p-value (FDR corrected)
	M	*SD*	*n*	*M*	*SD*	*n*			
AF_left	0.62	0.06	20	0.64	0.04	20	1.48	0.47	0.18
AF_right	0.63	0.05	20	0.65	0.04	20	1.48	0.47	0.18
ATR_left	0.57	0.04	20	0.59	0.02	20	1.45	0.46	0.19
ATR_right	0.57	0.04	20	0.59	0.03	20	1.24	0.39	0.25
CC_1	0.55	0.05	20	0.56	0.04	20	1.16	0.37	0.27
CC_2	0.57	0.05	20	0.60	0.04	20	1.64	0.52	0.15
CC_3	0.62	0.05	20	0.64	0.04	20	1.60	0.51	0.16
CC_4	0.64	0.05	20	0.67	0.03	20	2.26	0.73	0.07
CC_5	0.63	0.04	20	0.65	0.03	20	1.62	0.51	0.16
CC_6	0.62	0.05	20	0.65	0.04	20	1.77	0.56	0.12
CC_7	0.63	0.04	20	0.65	0.03	20	2.14	0.68	0.08
CG_left	0.56	0.05	20	0.58	0.03	20	1.42	0.45	0.19
CG_right	0.57	0.05	20	0.59	0.03	20	1.43	0.45	0.19
CST_left	0.70	0.03	20	0.71	0.02	20	1.22	0.39	0.25
CST_right	0.70	0.03	20	0.72	0.02	20	1.84	0.58	0.11
FPT_left	0.66	0.04	20	0.67	0.02	20	1.55	0.49	0.17
FPT_right	0.66	0.04	20	0.68	0.02	20	1.35	0.43	0.21
ICP_left	0.71	0.03	20	0.72	0.03	20	0.23	0.07	0.82
ICP_right	0.70	0.04	20	0.71	0.03	20	0.32	0.10	0.76
IFO_left	0.54	0.05	20	0.56	0.03	20	1.73	0.55	0.13
IFO_right	0.53	0.04	20	0.55	0.03	20	1.86	0.59	0.11
ILF_left	0.54	0.05	20	0.56	0.03	20	1.87	0.59	0.11
ILF_right	0.52	0.05	20	0.55	0.03	20	2.24	0.71	0.07
MCP	0.75	0.02	20	0.75	0.02	20	0.24	0.08	0.82
OR_left	0.55	0.04	20	0.57	0.04	20	1.70	0.54	0.14
OR_right	0.54	0.04	20	0.57	0.03	20	1.84	0.58	0.11
POPT_left	0.66	0.03	20	0.67	0.03	20	1.56	0.49	0.17
POPT_right	0.65	0.03	20	0.66	0.02	20	1.39	0.44	0.20
SCP_left	0.68	0.03	20	0.69	0.02	20	0.84	0.26	0.42
SCP_right	0.69	0.03	20	0.69	0.02	20	0.02	0.01	0.98
SLF_III_left	0.63	0.05	20	0.65	0.04	20	1.44	0.45	0.19
SLF_III_right	0.63	0.05	20	0.65	0.04	20	1.29	0.41	0.23

SLF_II_left	0.64	0.05	20	0.67	0.03	20	2.13	0.67	0.08
SLF_II_right	0.64	0.05	20	0.67	0.03	20	1.91	0.60	0.11
SLF_I_left	0.63	0.04	20	0.65	0.03	20	1.75	0.55	0.13
SLF_I_right	0.63	0.04	20	0.66	0.03	20	2.02	0.64	0.09
STR_left	0.63	0.04	20	0.65	0.02	20	1.80	0.58	0.12
STR_right	0.63	0.03	20	0.65	0.02	20	1.96	0.62	0.10
ST_FO_left	0.52	0.05	20	0.54	0.03	20	1.92	0.61	0.11
ST_FO_right	0.52	0.05	20	0.54	0.03	20	1.51	0.48	0.18
ST_PREM_left	0.60	0.05	20	0.62	0.03	20	1.44	0.46	0.19
ST_PREM_right	0.62	0.04	20	0.63	0.03	20	1.48	0.47	0.18
T_OCC_left	0.55	0.04	20	0.57	0.04	20	1.50	0.48	0.18
T_OCC_right	0.55	0.04	20	0.57	0.03	20	1.77	0.56	0.12
T_PAR_left	0.59	0.04	20	0.62	0.03	20	2.30	0.73	0.06
T_PAR_right	0.58	0.04	20	0.60	0.03	20	1.43	0.45	0.19
T_PREM_left	0.61	0.04	20	0.63	0.02	20	1.58	0.50	0.17
T_PREM_right	0.62	0.04	20	0.63	0.02	20	1.37	0.43	0.21
UF_left	0.49	0.05	20	0.51	0.03	20	1.56	0.49	0.17
UF_right	0.48	0.04	20	0.49	0.02	20	1.45	0.46	0.19

p < ,05, **p < 0,01, ***p < ,001; AQP4 = aquaporin-4; NMOSD = neuromyelitis optica spectrum disorders; HC = healthy controls; NDI = neurite density index; *n* = number of participants; AF = arcuate fascicle; ATR = anterior thalamic radiation; CC = corpus callosum; CC_1 = rostrum; CC_2 = genu; CC_3 = rostral body; CC_4 = anterior midbody; CC_5 = posterior midbody; CC_6 = isthmus; CC_7 = splenium; CG = cingulum; CST = corticospinal tract; FPT = fronto-pontine tract; ICP = inferior cerebellar peduncle; IFO = inferior occipito-frontal fascicle; ILF = inferior longitudinal fascicle; MCP = middle cerebellar peduncle; OR = optic radiation; POPT = parieto‑occipital pontine tract; SCP = superior cerebellar peduncle; SLF_I = superior longitudinal fascicle I; SLF_II = superior longitudinal fascicle II; SLF_III = superior longitudinal fascicle III; STR = superior thalamic radiation; ST_FO = striato-fronto-orbital; ST_PREM = striato-premotor; T_OCC = thalamo-occipital; T_PAR = thalamo-parietal; T_PREM = thalamo-premotor; UF = uncinate fascicle.

Supplementary Table 8. Comparison of NDI in white matter fibers traversing through white matter lesions in AQP4-NMOSD patients and whole tracts in HC

Tract	AQP4-NMOSD			HC			T-value	Cohen's d	p-value (FDR corrected)
	M	*SD*	*n*	*M*	*SD*	*n*			
AF_left	0.61	0.06	12	0.64	0.04	20	1.48	0.61	0.24
AF_right	0.62	0.06	11	0.65	0.04	20	1.35	0.58	0.28
ATR_left	0.56	0.04	13	0.59	0.02	20	2.59	1.02	0.05
ATR_right	0.56	0.04	13	0.59	0.03	20	1.97	0.77	0.12
CC_1	0.53	0.05	10	0.56	0.04	20	2.03	0.88	0.12
CC_2	0.57	0.05	14	0.60	0.04	20	1.76	0.65	0.16
CC_3	0.62	0.04	12	0.64	0.04	20	0.91	0.34	0.45
CC_4	0.64	0.04	11	0.67	0.03	20	2.09	0.89	0.11
CC_5	0.61	0.04	8	0.65	0.03	20	2.61	1.20	0.06
CC_6	0.63	0.05	15	0.65	0.04	20	1.06	0.37	0.39
CC_7	0.64	0.03	16	0.65	0.03	20	1.40	0.48	0.26
CG_left	0.57	0.06	11	0.58	0.03	20	0.24	0.11	0.85
CG_right	0.56	0.06	9	0.59	0.03	20	1.60	0.83	0.22
CST_left	0.69	0.01	11	0.71	0.02	20	2.73	0.93	**0.04***
CST_right	0.68	0.03	9	0.72	0.02	20	3.12	1.36	**0.03***
FPT_left	0.66	0.04	14	0.67	0.02	20	1.04	0.40	0.39
FPT_right	0.65	0.04	11	0.68	0.02	20	1.87	0.80	0.15
ICP_left	0.68	0.01	2	0.72	0.03	20	2.88	1.09	0.15
IFO_left	0.53	0.05	16	0.56	0.03	20	2.71	0.92	0.09
IFO_right	0.51	0.05	17	0.55	0.03	20	3.51	1.33	**0.04***
ILF_left	0.52	0.04	11	0.56	0.03	20	4.16	1.55	**0.01****
ILF_right	0.49	0.04	13	0.55	0.03	20	0.44	0.17	**0.00****
MCP	0.75	0.01	4	0.75	0.02	20	2.18	0.73	0.74
OR_left	0.55	0.03	14	0.57	0.04	20	2.48	0.87	0.09
OR_right	0.54	0.04	15	0.57	0.03	20	2.22	0.96	0.05
POPT_left	0.64	0.04	11	0.67	0.03	20	2.16	0.85	0.10
POPT_right	0.64	0.03	12	0.66	0.02	20	-2.05	-1.22	0.10
SCP_left	0.71	0.01	2	0.69	0.02	20	2.30	1.16	0.32
SLF_III_left	0.60	0.05	7	0.65	0.04	20	2.43	1.04	0.11
SLF_III_right	0.62	0.06	9	0.65	0.04	20	2.48	1.15	0.39
SLF_II_left	0.63	0.04	10	0.67	0.03	20	1.68	0.68	0.07
SLF_II_right	0.62	0.05	10	0.67	0.03	20	2.70	1.23	0.07

SLF_I_left	0.62	0.06	13	0.65	0.03	20	4.89	2.13	0.18
SLF_I_right	0.61	0.04	8	0.66	0.03	20	3.60	1.65	0.06
STR_left	0.60	0.02	7	0.65	0.02	20	1.05	0.43	**0.00****
STR_right	0.60	0.03	9	0.65	0.02	20	2.00	0.92	**0.02***
ST_FO_left	0.53	0.05	12	0.54	0.03	20	2.02	0.82	0.39
ST_FO_right	0.50	0.05	9	0.54	0.03	20	1.87	0.78	0.13
ST_PREM_left	0.59	0.05	13	0.62	0.03	20	3.14	0.97	0.12
ST_PREM_right	0.60	0.05	12	0.63	0.03	20	2.15	0.77	0.15
T_OCC_left	0.54	0.02	13	0.57	0.04	20	4.94	1.69	**0.02***
T_OCC_right	0.54	0.04	14	0.57	0.03	20	1.62	0.59	0.09
T_PAR_left	0.57	0.03	13	0.62	0.03	20	1.73	0.83	**0.00*****
T_PAR_right	0.58	0.04	14	0.60	0.03	20	1.46	0.70	0.19
T_PREM_left	0.60	0.04	10	0.63	0.02	20	0.23	0.12	0.18
T_PREM_right	0.61	0.05	10	0.63	0.02	20	1.36	0.80	0.26
UF_left	0.51	0.06	9	0.51	0.03	20	1.54	0.49	0.86
UF_right	0.47	0.06	8	0.49	0.02	20	1.51	0.48	0.30

p < ,05, **p < 0,01, ***p < ,001; AQP4 = aquaporin-4; NMOSD = neuromyelitis optica spectrum disorders; HC = healthy controls; NDI = neurite density index; *n* = number of participants; AF = arcuate fascicle; ATR = anterior thalamic radiation; CC = corpus callosum; CC_1 = rostrum; CC_2 = genu; CC_3 = rostral body; CC_4 = anterior midbody; CC_5 = posterior midbody; CC_6 = isthmus; CC_7 = splenium; CG = cingulum; CST = corticospinal tract; FPT = fronto-pontine tract; ICP = inferior cerebellar peduncle; IFO = inferior occipito-frontal fascicle; ILF = inferior longitudinal fascicle; MCP = middle cerebellar peduncle; OR = optic radiation; POPT = parieto‑occipital pontine tract; SCP = superior cerebellar peduncle; SLF_I = superior longitudinal fascicle I; SLF_II = superior longitudinal fascicle II; SLF_III = superior longitudinal fascicle III; STR = superior thalamic radiation; ST_FO = striato-fronto-orbital; ST_PREM = striato-premotor; T_OCC = thalamo-occipital; T_PAR = thalamo-parietal; T_PREM = thalamo-premotor; UF = uncinate fascicle.

Supplementary Table 9. Comparison of NDI in white matter fibers not traversing through white matter lesions in AQP4-NMOSD patients and whole tracts in HC

Tract	AQP4-NMOSD			HC			T-value	Cohen's d	p-value (FDR corrected)
	M	*SD*	*n*	*M*	*SD*	*n*			
AF_left	0.62	0.06	20	0.64	0.04	20	1.29	0.41	0.28
AF_right	0.63	0.05	20	0.65	0.04	20	1.40	0.44	0.24
ATR_left	0.58	0.04	20	0.59	0.02	20	1.09	0.35	0.35
ATR_right	0.58	0.04	20	0.59	0.03	20	0.84	0.27	0.45
CC_1	0.55	0.05	20	0.56	0.04	20	1.07	0.34	0.36
CC_2	0.58	0.05	20	0.60	0.04	20	1.40	0.44	0.24
CC_3	0.62	0.05	19	0.64	0.04	20	1.25	0.40	0.29
CC_4	0.65	0.04	18	0.67	0.03	20	1.74	0.58	0.17
CC_5	0.63	0.04	20	0.65	0.03	20	1.61	0.51	0.19
CC_6	0.62	0.05	20	0.65	0.04	20	1.63	0.52	0.19
CC_7	0.63	0.04	20	0.65	0.03	20	1.64	0.52	0.19
CG_left	0.56	0.05	20	0.58	0.03	20	1.43	0.45	0.24
CG_right	0.57	0.05	20	0.59	0.03	20	1.47	0.47	0.23
CST_left	0.70	0.03	20	0.71	0.02	20	1.00	0.32	0.38
CST_right	0.70	0.03	20	0.72	0.02	20	1.55	0.49	0.21
FPT_left	0.66	0.04	20	0.67	0.02	20	1.40	0.44	0.24
FPT_right	0.66	0.03	20	0.68	0.02	20	1.23	0.39	0.29
ICP_left	0.71	0.03	20	0.72	0.03	20	0.22	0.07	0.84
ICP_right	0.70	0.04	20	0.71	0.03	20	0.32	0.10	0.78
IFO_left	0.54	0.04	20	0.56	0.03	20	1.23	0.39	0.29
IFO_right	0.54	0.04	20	0.55	0.03	20	1.26	0.40	0.29
ILF_left	0.54	0.05	20	0.56	0.03	20	1.78	0.56	0.16
ILF_right	0.53	0.05	20	0.55	0.03	20	1.94	0.61	0.13
MCP	0.75	0.02	20	0.75	0.02	20	0.26	0.08	0.81
OR_left	0.56	0.04	20	0.57	0.04	20	0.90	0.28	0.43
OR_right	0.56	0.03	19	0.57	0.03	20	0.67	0.22	0.55
POPT_left	0.67	0.03	20	0.67	0.03	20	0.58	0.18	0.59
POPT_right	0.66	0.02	20	0.66	0.02	20	0.86	0.27	0.45
SCP_left	0.68	0.03	20	0.69	0.02	20	0.85	0.27	0.45
SCP_right	0.69	0.03	20	0.69	0.02	20	0.02	0.01	0.98
SLF_III_left	0.63	0.05	20	0.65	0.04	20	1.41	0.45	0.24
SLF_III_right	0.63	0.05	20	0.65	0.04	20	1.22	0.39	0.29
SLF_II_left	0.64	0.05	20	0.67	0.03	20	1.96	0.62	0.13

SLF_II_right	0.65	0.04	20	0.67	0.03	20	1.61	0.51	0.19
SLF_I_left	0.63	0.04	20	0.65	0.03	20	1.56	0.49	0.21
SLF_I_right	0.64	0.04	20	0.66	0.03	20	1.85	0.58	0.15
STR_left	0.64	0.04	19	0.65	0.02	20	1.41	0.46	0.24
STR_right	0.63	0.03	20	0.65	0.02	20	1.42	0.45	0.24
ST_FO_left	0.52	0.05	20	0.54	0.03	20	1.67	0.53	0.19
ST_FO_right	0.52	0.05	20	0.54	0.03	20	1.34	0.42	0.26
ST_PREM_left	0.61	0.04	20	0.62	0.03	20	1.00	0.32	0.38
ST_PREM_right	0.62	0.04	20	0.63	0.03	20	1.22	0.39	0.29
T_OCC_left	0.56	0.04	20	0.57	0.04	20	0.69	0.22	0.55
T_OCC_right	0.56	0.03	19	0.57	0.03	20	0.63	0.20	0.57
T_PAR_left	0.61	0.04	20	0.62	0.03	20	1.07	0.34	0.36
T_PAR_right	0.59	0.03	20	0.60	0.03	20	0.72	0.23	0.53
T_PREM_left	0.61	0.04	20	0.63	0.02	20	1.46	0.46	0.24
T_PREM_right	0.62	0.04	20	0.63	0.02	20	1.13	0.36	0.33
UF_left	0.49	0.05	20	0.51	0.03	20	1.54	0.49	0.22
UF_right	0.48	0.04	20	0.49	0.02	20	1.51	0.48	0.22

p < ,05, **p < 0,01, ***p < ,001; AQP4 = aquaporin-4; NMOSD = neuromyelitis optica spectrum disorders; HC = healthy controls; NDI = neurite density index; *n* = number of participants; AF = arcuate fascicle; ATR = anterior thalamic radiation; CC = corpus callosum; CC_1 = rostrum; CC_2 = genu; CC_3 = rostral body; CC_4 = anterior midbody; CC_5 = posterior midbody; CC_6 = isthmus; CC_7 = splenium; CG = cingulum; CST = corticospinal tract; FPT = fronto-pontine tract; ICP = inferior cerebellar peduncle; IFO = inferior occipito-frontal fascicle; ILF = inferior longitudinal fascicle; MCP = middle cerebellar peduncle; OR = optic radiation; POPT = parieto‑occipital pontine tract; SCP = superior cerebellar peduncle; SLF_I = superior longitudinal fascicle I; SLF_II = superior longitudinal fascicle II; SLF_III = superior longitudinal fascicle III; STR = superior thalamic radiation; ST_FO = striato-fronto-orbital; ST_PREM = striato-premotor; T_OCC = thalamo-occipital; T_PAR = thalamo-parietal; T_PREM = thalamo-premotor; UF = uncinate fascicle.

Supplementary Table 10. Comparison of T1 relaxation rates in cerebral cortex between MS patients and HC

Parcellation	MS (*n* = 17)		HC (*n* = 20)		T-value	Cohen's d	p-value (FDR corrected)
	M	*SD*	*M*	*SD*			
lh_unknown	0.18	0.02	0.18	0.02	-0.35	-0.12	0.80
lh_Fronto-marginal gyrus (of Wernicke) and sulcus	0.67	0.01	0.69	0.02	-3.21	-1.02	**0.02***
lh_Inferior occipital gyrus (o3) and sulcus	0.73	0.02	0.74	0.02	-1.95	-0.64	0.14
lh_paracentral lobule and sulcus	0.74	0.02	0.76	0.02	-2.52	-0.81	0.05
lh_subcentral gyrus (central operculum) and sulci	0.70	0.01	0.72	0.01	-5.62	-1.90	**0.00****
lh_transverse frontopolar gyri and sulci	0.66	0.01	0.67	0.02	-3.10	-1.00	**0.02***
lh_anterior part of the cingulate gyrus and sulcus (aCC)	0.68	0.01	0.69	0.02	-3.38	-1.05	**0.01***
lh_middle-anterior part of the cingulate gyrus and sulcus (amCC)	0.69	0.01	0.71	0.02	-3.30	-1.06	**0.01***
lh_middle-posterior part of the cingulate gyrus and sulcus (pmCC)	0.71	0.02	0.72	0.02	-3.06	-1.02	**0.02***
lh_posterior-dorsal part of the cingulate gyrus (dpCC)	0.72	0.01	0.74	0.02	-3.38	-1.08	**0.01***
lh_posterior-ventral part of the cingulate gyrus (vpCC, isthmus of the cingulate gyrus)	0.75	0.01	0.76	0.02	-2.88	-0.92	**0.03***
lh_Cuneus (o6)	0.73	0.02	0.75	0.01	-2.98	-1.00	**0.02***
lh_opercular part of the inferior frontal gyrus	0.69	0.01	0.70	0.01	-5.04	-1.63	**0.00****
lh_orbital part of the inferior frontal gyrus	0.68	0.02	0.70	0.01	-3.39	-1.12	**0.01***
lh_triangular part of the inferior frontal gyrus	0.68	0.01	0.69	0.01	-2.88	-0.95	**0.03***
lh_middle frontal gyrus (F2)	0.67	0.01	0.68	0.01	-2.79	-0.90	**0.03***
lh_superior frontal gyrus (F1)	0.68	0.01	0.69	0.01	-2.98	-0.97	**0.02***
lh_long insular gyrus and central sulcus of the insula	0.68	0.01	0.70	0.01	-4.08	-1.34	**0.00****
lh_short insular gyri	0.66	0.01	0.68	0.01	-4.20	-1.34	**0.00****
lh_middle occipital gyrus (o2, lateral occipital gyrus)	0.71	0.01	0.73	0.01	-2.90	-0.97	**0.03***
lh_superior occipital gyrus (o1)	0.72	0.02	0.74	0.01	-3.61	-1.24	**0.01***
lh_lateral occipito-temporal gyrus (fusiform gyrus, o4-t4)	0.72	0.02	0.73	0.01	-3.09	-1.05	**0.02***

lh_lingual gyrus, lingual part of the medial occipito-temporal gyrus, (o5)	0.73	0.02	0.75	0.02	-2.09	-0.69	0.11
lh_parahippocampal gyrus, parahippocampal part of the medial occipito-temporal gyrus, (t5)	0.70	0.02	0.72	0.02	-4.39	-1.41	**0.00****
lh_orbital gyri	0.70	0.01	0.72	0.02	-3.84	-1.24	**0.01****
lh_angular gyrus	0.68	0.01	0.70	0.01	-4.72	-1.57	**0.00****
lh_supramarginal gyrus	0.69	0.01	0.71	0.01	-5.36	-1.83	**0.00****
lh_superior parietal lobule (lateral part of p1)	0.69	0.01	0.71	0.02	-3.82	-1.25	**0.01****
lh_postcentral gyrus	0.71	0.02	0.73	0.01	-3.91	-1.32	**0.01****
lh_precentral gyrus	0.73	0.02	0.74	0.02	-2.07	-0.67	0.11
lh_precuneus (medial part of p1)	0.71	0.01	0.72	0.01	-4.46	-1.43	**0.00****
lh_straight gyrus, gyrus rectus	0.69	0.01	0.70	0.02	-2.76	-0.87	**0.04***
lh_subcallosal area, subcallosal gyrus	0.64	0.07	0.69	0.03	-2.49	-0.87	0.06
lh_anterior transverse temporal gyrus (of heschl)	0.74	0.02	0.76	0.02	-1.59	-0.52	0.22
lh_lateral aspect of the superior temporal gyrus	0.69	0.01	0.71	0.01	-3.40	-1.14	**0.01***
lh_planum polare of the superior temporal gyrus	0.67	0.01	0.68	0.02	-1.95	-0.62	0.14
lh_planum temporale or temporal plane of the superior temporal gyrus	0.70	0.02	0.71	0.02	-2.17	-0.71	0.10
lh_Inferior temporal gyrus (t3)	0.69	0.02	0.71	0.01	-3.94	-1.32	**0.00****
lh_middle temporal gyrus (t2)	0.68	0.01	0.70	0.01	-4.68	-1.55	**0.00****
lh_horizontal ramus of the anterior segment of the lateral sulcus (or fissure)	0.70	0.01	0.73	0.02	-4.37	-1.38	**0.00****
lh_vertical ramus of the anterior segment of the lateral sulcus (or fissure)	0.71	0.02	0.73	0.02	-4.04	-1.32	**0.00****
lh_posterior ramus (or segment) of the lateral sulcus (or fissure)	0.73	0.02	0.74	0.02	-1.99	-0.65	0.12
lh_occipital pole	0.74	0.02	0.75	0.02	-2.67	-0.87	**0.04***
lh_temporal pole	0.67	0.01	0.69	0.03	-3.04	-0.95	**0.02***
lh_Calcarine sulcus	0.74	0.02	0.75	0.02	-2.91	-0.96	**0.03***
lh_Central sulcus (Rolando's fissure)	0.74	0.01	0.76	0.01	-3.85	-1.27	**0.01****
lh_marginal sulcus of cingulate gyrus	0.70	0.02	0.72	0.01	-3.64	-1.24	**0.01****
lh_anterior circular sulcus of the insula	0.68	0.01	0.70	0.02	-4.04	-1.30	**0.00****
lh_Inferior circular sulcus of the insula	0.69	0.01	0.70	0.02	-2.99	-0.96	**0.02***
lh_superior circular sulcus of the insula	0.70	0.01	0.72	0.01	-4.86	-1.56	**0.00****

lh_anterior transverse collateral sulcus	0.68	0.02	0.71	0.02	-4.50	-1.47	**0.00****
lh_posterior transverse collateral sulcus	0.75	0.02	0.76	0.03	-1.42	-0.46	0.27
lh_Inferior frontal sulcus	0.70	0.01	0.72	0.01	-3.03	-1.01	**0.02***
lh_middle frontal sulcus	0.68	0.01	0.69	0.01	-4.48	-1.46	**0.00****
lh_superior frontal sulcus	0.69	0.01	0.70	0.01	-4.97	-1.61	**0.00****
lh_Intermediate sulcus of Jensen	0.69	0.01	0.70	0.02	-1.75	-0.56	0.18
lh_Intraparietal sulcus and posterior transverse parietal sulcus	0.71	0.01	0.73	0.01	-4.46	-1.46	**0.00****
lh_middle occipital sulcus and sulcus lunatus (secondary intermediate sulcus)	0.72	0.01	0.74	0.03	-2.24	-0.70	0.09
lh_superior occipital sulcus and transverse occipital sulcus (superior intermediate sulcus)	0.72	0.02	0.74	0.02	-2.78	-0.90	**0.03***
lh_anterior occipital sulcus	0.72	0.02	0.74	0.03	-2.48	-0.79	0.06
lh_lateral occipito-temporal sulcus	0.71	0.02	0.72	0.02	-2.42	-0.79	0.06
lh_medial occipito-temporal sulcus and lingual sulcus	0.72	0.02	0.74	0.02	-4.60	-1.52	**0.00****
lh_lateral orbital sulcus	0.68	0.01	0.69	0.02	-2.03	-0.67	0.12
lh_medial orbital sulcus, olfactory sulcus	0.71	0.01	0.74	0.02	-4.41	-1.38	**0.00****
lh_h-shaped orbital sulcus	0.71	0.02	0.73	0.02	-3.92	-1.27	**0.00****
lh_parieto-occipital sulcus	0.74	0.01	0.75	0.02	-3.24	-1.03	**0.02***
lh_pericallosal sulcus	0.74	0.04	0.78	0.03	-3.14	-1.07	**0.02***
lh_postcentral sulcus	0.71	0.01	0.73	0.02	-3.55	-1.15	**0.01****
lh_Inferior part of the precentral sulcus	0.70	0.01	0.72	0.01	-4.09	-1.30	**0.01****
lh_superior part of the precentral sulcus	0.71	0.01	0.73	0.02	-3.11	-1.00	**0.02***
lh_suborbital sulcus	0.68	0.01	0.70	0.02	-3.27	-1.03	**0.02***
lh_subparietal sulcus	0.72	0.01	0.73	0.01	-3.65	-1.18	**0.01****
lh_Inferior temporal sulcus	0.69	0.01	0.71	0.01	-3.81	-1.26	**0.01****
lh_superior temporal sulcus	0.70	0.01	0.72	0.01	-3.33	-1.13	**0.01***
lh_transverse temporal sulcus (heschl's gyrus)	0.74	0.02	0.75	0.02	-1.82	-0.60	0.16
rh_unknown	0.17	0.01	0.17	0.02	-0.65	-0.21	0.62
rh_Fronto-marginal gyrus (of Wernicke) and sulcus	0.67	0.01	0.68	0.02	-2.00	-0.64	0.12
rh_Inferior occipital gyrus (o3) and sulcus	0.74	0.02	0.75	0.02	-1.41	-0.47	0.28
rh_paracentral lobule and sulcus	0.74	0.01	0.76	0.02	-4.88	-1.57	**0.00****
rh_subcentral gyrus (central operculum) and sulci	0.72	0.02	0.73	0.02	-2.86	-0.94	**0.03***

rh_transverse frontopolar gyri and sulci	0.65	0.01	0.67	0.02	-2.30	-0.73	0.08
rh_anterior part of the cingulate gyrus and sulcus (aCC)	0.67	0.01	0.69	0.01	-4.71	-1.51	**0.00****
rh_middle-anterior part of the cingulate gyrus and sulcus (amCC)	0.69	0.01	0.71	0.02	-3.88	-1.24	**0.01****
rh_middle-posterior part of the cingulate gyrus and sulcus (pmCC)	0.72	0.01	0.74	0.01	-4.35	-1.38	**0.00****
rh_posterior-dorsal part of the cingulate gyrus (dpCC)	0.73	0.01	0.75	0.01	-3.94	-1.26	**0.00****
rh_posterior-ventral part of the cingulate gyrus (vpCC, isthmus of the cingulate gyrus)	0.76	0.03	0.78	0.02	-2.23	-0.76	0.09
rh_Cuneus (o6)	0.74	0.02	0.76	0.01	-2.26	-0.76	0.08
rh_opercular part of the inferior frontal gyrus	0.69	0.01	0.71	0.02	-3.62	-1.15	**0.01****
rh_orbital part of the inferior frontal gyrus	0.68	0.02	0.70	0.02	-2.50	-0.81	0.06
rh_triangular part of the inferior frontal gyrus	0.69	0.01	0.70	0.02	-2.22	-0.72	0.09
rh_middle frontal gyrus (F2)	0.67	0.01	0.68	0.01	-3.25	-1.05	**0.01***
rh_superior frontal gyrus (F1)	0.68	0.01	0.69	0.01	-4.70	-1.51	**0.00****
rh_long insular gyrus and central sulcus of the insula	0.67	0.01	0.68	0.01	-2.62	-0.85	**0.05***
rh_short insular gyri	0.67	0.01	0.68	0.02	-1.85	-0.60	0.16
rh_middle occipital gyrus (o2, lateral occipital gyrus)	0.71	0.01	0.73	0.01	-3.82	-1.25	**0.01****
rh_superior occipital gyrus (o1)	0.73	0.01	0.75	0.01	-4.77	-1.60	**0.00****
rh_lateral occipito-temporal gyrus (fusiform gyrus, o4-t4)	0.76	0.01	0.77	0.02	-1.83	-0.59	0.16
rh_lingual gyrus, lingual part of the medial occipito-temporal gyrus, (o5)	0.75	0.02	0.76	0.02	-1.56	-0.51	0.23
rh_parahippocampal gyrus, parahippocampal part of the medial occipito-temporal gyrus, (t5)	0.72	0.01	0.74	0.02	-3.39	-1.07	**0.01***
rh_orbital gyri	0.69	0.01	0.71	0.02	-3.79	-1.20	**0.01****
rh_angular gyrus	0.70	0.01	0.71	0.01	-3.29	-1.08	**0.01***
rh_supramarginal gyrus	0.70	0.01	0.71	0.01	-2.47	-0.82	0.06
rh_superior parietal lobule (lateral part of p1)	0.70	0.01	0.72	0.01	-4.30	-1.38	0.00
rh_postcentral gyrus	0.72	0.02	0.74	0.02	-2.63	-0.88	0.05
rh_precentral gyrus	0.74	0.01	0.75	0.02	-2.85	-0.91	**0.03***

rh_precuneus (medial part of p1)	0.72	0.01	0.73	0.01	-3.33	-1.08	**0.01***
rh_straight gyrus, gyrus rectus	0.69	0.01	0.70	0.02	-2.40	-0.76	0.07
rh_subcallosal area, subcallosal gyrus	0.58	0.11	0.63	0.10	-1.45	-0.48	0.27
rh_anterior transverse temporal gyrus (of heschl)	0.76	0.02	0.77	0.02	-1.02	-0.33	0.43
rh_lateral aspect of the superior temporal gyrus	0.71	0.01	0.72	0.02	-2.32	-0.76	0.08
rh_planum polare of the superior temporal gyrus	0.68	0.02	0.69	0.02	-2.72	-0.87	**0.04***
rh_planum temporale or temporal plane of the superior temporal gyrus	0.72	0.02	0.73	0.02	-2.03	-0.68	0.12
rh_Inferior temporal gyrus (t3)	0.72	0.01	0.73	0.02	-2.65	-0.86	**0.04***
rh_middle temporal gyrus (t2)	0.69	0.01	0.70	0.01	-3.26	-1.09	**0.01***
rh_horizontal ramus of the anterior segment of the lateral sulcus (or fissure)	0.72	0.01	0.74	0.03	-4.02	-1.27	**0.00****
rh_vertical ramus of the anterior segment of the lateral sulcus (or fissure)	0.71	0.02	0.72	0.02	-1.46	-0.48	0.26
rh_posterior ramus (or segment) of the lateral sulcus (or fissure)	0.74	0.01	0.74	0.02	-1.65	-0.53	0.20
rh_occipital pole	0.75	0.02	0.76	0.02	-2.41	-0.79	0.06
rh_temporal pole	0.69	0.01	0.70	0.02	-2.60	-0.84	**0.05***
rh_Calcarine sulcus	0.75	0.02	0.77	0.02	-2.67	-0.87	**0.04***
rh_Central sulcus (Rolando's fissure)	0.75	0.01	0.77	0.01	-4.70	-1.57	**0.00****
rh_marginal sulcus of cingulate gyrus	0.72	0.01	0.74	0.01	-3.98	-1.30	**0.00****
rh_anterior circular sulcus of the insula	0.69	0.01	0.70	0.02	-2.80	-0.89	**0.03***
rh_Inferior circular sulcus of the insula	0.70	0.01	0.70	0.02	-1.46	-0.47	0.26
rh_superior circular sulcus of the insula	0.70	0.01	0.71	0.02	-2.99	-0.96	**0.02***
rh_anterior transverse collateral sulcus	0.73	0.02	0.75	0.02	-2.63	-0.86	**0.05***
rh_posterior transverse collateral sulcus	0.78	0.03	0.78	0.04	-0.23	-0.07	0.86
rh_Inferior frontal sulcus	0.71	0.02	0.72	0.02	-2.28	-0.75	0.08
rh_middle frontal sulcus	0.68	0.01	0.69	0.01	-3.39	-1.10	**0.01***
rh_superior frontal sulcus	0.69	0.01	0.71	0.02	-3.72	-1.19	**0.01****
rh_Intermediate sulcus of Jensen	0.70	0.02	0.72	0.03	-2.78	-0.90	**0.03***
rh_Intraparietal sulcus and posterior transverse parietal sulcus	0.73	0.01	0.74	0.01	-4.22	-1.38	**0.00****
rh_middle occipital sulcus and sulcus lunatus (secondary intermediate sulcus)	0.73	0.02	0.74	0.02	-1.84	-0.60	0.16

rh_superior occipital sulcus and transverse occipital sulcus (superior intermediate sulcus)	0.74	0.01	0.75	0.01	-3.06	-1.02	**0.02***
rh_anterior occipital sulcus	0.74	0.02	0.75	0.02	-1.67	-0.54	0.20
rh_lateral occipito-temporal sulcus	0.75	0.02	0.76	0.02	-1.31	-0.43	0.31
rh_medial occipito-temporal sulcus and lingual sulcus	0.74	0.02	0.76	0.02	-3.29	-1.07	**0.01***
rh_lateral orbital sulcus	0.68	0.02	0.69	0.02	-2.67	-0.88	**0.04***
rh_medial orbital sulcus, olfactory sulcus	0.69	0.02	0.72	0.03	-3.57	-1.12	**0.01****
rh_h-shaped orbital sulcus	0.69	0.01	0.72	0.02	-4.38	-1.38	**0.00****
rh_parieto-occipital sulcus	0.76	0.01	0.76	0.02	-1.72	-0.56	0.18
rh_pericallosal sulcus	0.72	0.07	0.78	0.03	-3.33	-1.16	**0.02***
rh_postcentral sulcus	0.73	0.02	0.74	0.02	-2.32	-0.77	0.08
rh_Inferior part of the precentral sulcus	0.70	0.01	0.72	0.01	-3.34	-1.09	**0.01***
rh_superior part of the precentral sulcus	0.72	0.01	0.74	0.02	-3.72	-1.18	**0.01****
rh_suborbital sulcus	0.67	0.01	0.69	0.02	-2.85	-0.90	**0.03***
rh_subparietal sulcus	0.72	0.01	0.74	0.01	-3.94	-1.25	**0.00****
rh_Inferior temporal sulcus	0.71	0.02	0.72	0.02	-2.18	-0.71	0.09
rh_superior temporal sulcus	0.72	0.01	0.73	0.01	-3.20	-1.05	**0.02***
rh_transverse temporal sulcus (heschl's gyrus)	0.75	0.01	0.76	0.02	-1.97	-0.63	0.13

p < ,05, **p < 0,01, ***p < ,001; MS = multiple sclerosis HC = healthy controls; lh = left hemisphere; rh = right hemisphere; *n* = number of participants.

Supplementary Table 11. Comparison of T1 relaxation rates in cerebral cortex between AQP4-NMOSD patients and HC

Parcellation	AQP4-NMOSD (*n* = 20)		HC (*n* = 20)		T-value	Cohen's d	p-value (FDR corrected)
	M	*SD*	*M*	*SD*			
lh_unknown	0.17	0.02	0.18	0.02	-1.43	-0.45	0.27
lh_Fronto-marginal gyrus (of Wernicke) and sulcus	0.68	0.03	0.69	0.02	-0.90	-0.28	0.49
lh_Inferior occipital gyrus (o3) and sulcus	0.75	0.03	0.74	0.02	0.69	0.22	0.60
lh_paracentral lobule and sulcus	0.75	0.02	0.76	0.02	-1.23	-0.39	0.34
lh_subcentral gyrus (central operculum) and sulci	0.72	0.02	0.72	0.01	0.35	0.11	0.80
lh_transverse frontopolar gyri and sulci	0.66	0.03	0.67	0.02	-1.00	-0.32	0.44
lh_anterior part of the cingulate gyrus and sulcus (aCC)	0.68	0.02	0.69	0.02	-1.21	-0.38	0.35
lh_middle-anterior part of the cingulate gyrus and sulcus (amCC)	0.70	0.02	0.71	0.02	-1.62	-0.51	0.21
lh_middle-posterior part of the cingulate gyrus and sulcus (pmCC)	0.71	0.02	0.72	0.02	-1.60	-0.51	0.21
lh_posterior-dorsal part of the cingulate gyrus (dpCC)	0.73	0.02	0.74	0.02	-0.82	-0.26	0.53
lh_posterior-ventral part of the cingulate gyrus (vpCC, isthmus of the cingulate gyrus)	0.77	0.03	0.76	0.02	0.91	0.29	0.49
lh_Cuneus (o6)	0.74	0.03	0.75	0.01	-1.47	-0.47	0.26
lh_opercular part of the inferior frontal gyrus	0.70	0.02	0.70	0.01	-1.30	-0.41	0.31
lh_orbital part of the inferior frontal gyrus	0.69	0.02	0.70	0.01	-0.43	-0.13	0.76
lh_triangular part of the inferior frontal gyrus	0.69	0.02	0.69	0.01	-0.23	-0.07	0.85
lh_middle frontal gyrus (F2)	0.68	0.02	0.68	0.01	-0.29	-0.09	0.83
lh_superior frontal gyrus (F1)	0.69	0.02	0.69	0.01	-0.96	-0.30	0.46
lh_long insular gyrus and central sulcus of the insula	0.69	0.02	0.70	0.01	-1.68	-0.53	0.20
lh_short insular gyri	0.67	0.01	0.68	0.01	-0.97	-0.31	0.46
lh_middle occipital gyrus (o2, lateral occipital gyrus)	0.72	0.02	0.73	0.01	-0.97	-0.31	0.46
lh_superior occipital gyrus (o1)	0.73	0.02	0.74	0.01	-1.57	-0.50	0.23
lh_lateral occipito-temporal gyrus (fusiform gyrus, o4-t4)	0.74	0.03	0.73	0.01	1.43	0.45	0.27

lh_lingual gyrus, lingual part of the medial occipito-temporal gyrus, (o5)	0.75	0.02	0.75	0.02	0.85	0.27	0.51
lh_parahippocampal gyrus, parahippocampal part of the medial occipito-temporal gyrus, (t5)	0.72	0.02	0.72	0.02	-1.07	-0.34	0.41
lh_orbital gyri	0.72	0.06	0.72	0.02	0.26	0.08	0.85
lh_angular gyrus	0.69	0.02	0.70	0.01	-1.70	-0.54	0.19
lh_supramarginal gyrus	0.70	0.02	0.71	0.01	-1.16	-0.37	0.38
lh_superior parietal lobule (lateral part of p1)	0.70	0.02	0.71	0.02	-1.93	-0.61	0.14
lh_postcentral gyrus	0.72	0.04	0.73	0.01	-1.19	-0.38	0.37
lh_precentral gyrus	0.74	0.02	0.74	0.02	-0.30	-0.09	0.83
lh_precuneus (medial part of p1)	0.71	0.02	0.72	0.01	-1.66	-0.52	0.20
lh_straight gyrus, gyrus rectus	0.72	0.09	0.70	0.02	0.89	0.28	0.49
lh_subcallosal area, subcallosal gyrus	0.66	0.06	0.69	0.03	-1.80	-0.57	0.17
lh_anterior transverse temporal gyrus (of heschl)	0.75	0.04	0.76	0.02	-1.02	-0.32	0.44
lh_lateral aspect of the superior temporal gyrus	0.70	0.02	0.71	0.01	-0.46	-0.15	0.74
lh_planum polare of the superior temporal gyrus	0.67	0.02	0.68	0.02	-1.42	-0.45	0.27
lh_planum temporale or temporal plane of the superior temporal gyrus	0.70	0.04	0.71	0.02	-1.86	-0.59	0.16
lh_Inferior temporal gyrus (t3)	0.71	0.02	0.71	0.01	0.30	0.09	0.83
lh_middle temporal gyrus (t2)	0.69	0.02	0.70	0.01	-1.29	-0.41	0.32
lh_horizontal ramus of the anterior segment of the lateral sulcus (or fissure)	0.74	0.02	0.73	0.02	0.70	0.22	0.59
lh_vertical ramus of the anterior segment of the lateral sulcus (or fissure)	0.72	0.02	0.73	0.02	-1.50	-0.47	0.25
lh_posterior ramus (or segment) of the lateral sulcus (or fissure)	0.74	0.02	0.74	0.02	-0.38	-0.12	0.78
lh_occipital pole	0.76	0.03	0.75	0.02	0.19	0.06	0.88
lh_temporal pole	0.69	0.02	0.69	0.03	-0.37	-0.12	0.79
lh_Calcarine sulcus	0.75	0.03	0.75	0.02	0.34	0.11	0.80
lh_Central sulcus (Rolando's fissure)	0.74	0.03	0.76	0.01	-2.84	-0.90	**0.03***
lh_marginal sulcus of cingulate gyrus	0.71	0.02	0.72	0.01	-1.81	-0.57	0.17
lh_anterior circular sulcus of the insula	0.70	0.02	0.70	0.02	-0.14	-0.04	0.91
lh_Inferior circular sulcus of the insula	0.69	0.02	0.70	0.02	-2.31	-0.73	0.08
lh_superior circular sulcus of the insula	0.72	0.02	0.72	0.01	-0.21	-0.07	0.87

lh_anterior transverse collateral sulcus	0.71	0.03	0.71	0.02	0.22	0.07	0.86
lh_posterior transverse collateral sulcus	0.78	0.04	0.76	0.03	1.66	0.53	0.20
lh_Inferior frontal sulcus	0.71	0.02	0.72	0.01	-0.24	-0.08	0.85
lh_middle frontal sulcus	0.68	0.02	0.69	0.01	-2.12	-0.67	0.10
lh_superior frontal sulcus	0.70	0.02	0.70	0.01	-0.91	-0.29	0.49
lh_Intermediate sulcus of Jensen	0.70	0.04	0.70	0.02	0.25	0.08	0.85
lh_Intraparietal sulcus and posterior transverse parietal sulcus	0.72	0.02	0.73	0.01	-1.46	-0.46	0.26
lh_middle occipital sulcus and sulcus lunatus (secondary intermediate sulcus)	0.73	0.03	0.74	0.03	-1.02	-0.32	0.43
lh_superior occipital sulcus and transverse occipital sulcus (superior intermediate sulcus)	0.72	0.02	0.74	0.02	-2.35	-0.74	0.07
lh_anterior occipital sulcus	0.73	0.03	0.74	0.03	-0.89	-0.28	0.49
lh_lateral occipito-temporal sulcus	0.73	0.04	0.72	0.02	0.94	0.30	0.47
lh_medial occipito-temporal sulcus and lingual sulcus	0.75	0.03	0.74	0.02	0.94	0.30	0.47
lh_lateral orbital sulcus	0.69	0.02	0.69	0.02	0.57	0.18	0.67
lh_medial orbital sulcus, olfactory sulcus	0.73	0.04	0.74	0.02	-0.72	-0.23	0.58
lh_h-shaped orbital sulcus	0.73	0.03	0.73	0.02	-0.61	-0.19	0.64
lh_parieto-occipital sulcus	0.75	0.02	0.75	0.02	-0.35	-0.11	0.80
lh_pericallosal sulcus	0.77	0.03	0.78	0.03	-0.64	-0.20	0.63
lh_postcentral sulcus	0.73	0.03	0.73	0.02	-0.19	-0.06	0.88
lh_Inferior part of the precentral sulcus	0.71	0.02	0.72	0.01	-1.77	-0.56	0.17
lh_superior part of the precentral sulcus	0.72	0.02	0.73	0.02	-1.35	-0.43	0.29
lh_suborbital sulcus	0.69	0.03	0.70	0.02	-0.47	-0.15	0.73
lh_subparietal sulcus	0.73	0.02	0.73	0.01	-0.80	-0.25	0.54
lh_Inferior temporal sulcus	0.72	0.03	0.71	0.01	1.52	0.48	0.25
lh_superior temporal sulcus	0.72	0.02	0.72	0.01	0.25	0.08	0.85
lh_transverse temporal sulcus (heschl's gyrus)	0.74	0.03	0.75	0.02	-1.36	-0.43	0.29
rh_unknown	0.16	0.02	0.17	0.02	-1.73	-0.55	0.18
rh_Fronto-marginal gyrus (of Wernicke) and sulcus	0.69	0.10	0.68	0.02	0.42	0.13	0.77
rh_Inferior occipital gyrus (o3) and sulcus	0.75	0.03	0.75	0.02	0.19	0.06	0.88
rh_paracentral lobule and sulcus	0.76	0.02	0.76	0.02	-1.13	-0.36	0.39
rh_subcentral gyrus (central operculum) and sulci	0.73	0.02	0.73	0.02	-1.14	-0.36	0.38
rh_transverse frontopolar gyri and sulci	0.66	0.03	0.67	0.02	-0.99	-0.31	0.45

rh_anterior part of the cingulate gyrus and sulcus (aCC)	0.69	0.02	0.69	0.01	0.06	0.02	0.96
rh_middle-anterior part of the cingulate gyrus and sulcus (amCC)	0.71	0.02	0.71	0.02	-0.18	-0.06	0.88
rh_middle-posterior part of the cingulate gyrus and sulcus (pmCC)	0.73	0.02	0.74	0.01	-0.65	-0.21	0.62
rh_posterior-dorsal part of the cingulate gyrus (dpCC)	0.74	0.02	0.75	0.01	-0.74	-0.23	0.57
rh_posterior-ventral part of the cingulate gyrus (vpCC, isthmus of the cingulate gyrus)	0.78	0.03	0.78	0.02	0.27	0.08	0.84
rh_Cuneus (o6)	0.75	0.02	0.76	0.01	-1.63	-0.52	0.21
rh_opercular part of the inferior frontal gyrus	0.70	0.02	0.71	0.02	-1.50	-0.47	0.25
rh_orbital part of the inferior frontal gyrus	0.69	0.02	0.70	0.02	-0.50	-0.16	0.72
rh_triangular part of the inferior frontal gyrus	0.69	0.02	0.70	0.02	-1.63	-0.52	0.21
rh_middle frontal gyrus (F2)	0.68	0.02	0.68	0.01	-0.89	-0.28	0.49
rh_superior frontal gyrus (F1)	0.69	0.02	0.69	0.01	-0.53	-0.17	0.70
rh_long insular gyrus and central sulcus of the insula	0.68	0.01	0.68	0.01	-1.42	-0.45	0.27
rh_short insular gyri	0.68	0.01	0.68	0.02	-0.34	-0.11	0.81
rh_middle occipital gyrus (o2, lateral occipital gyrus)	0.72	0.02	0.73	0.01	-0.39	-0.12	0.78
rh_superior occipital gyrus (o1)	0.73	0.02	0.75	0.01	-2.73	-0.86	**0.04***
rh_lateral occipito-temporal gyrus (fusiform gyrus, o4-t4)	0.77	0.02	0.77	0.02	0.12	0.04	0.92
rh_lingual gyrus, lingual part of the medial occipito-temporal gyrus, (o5)	0.76	0.02	0.76	0.02	-0.36	-0.11	0.80
rh_parahippocampal gyrus, parahippocampal part of the medial occipito-temporal gyrus, (t5)	0.73	0.02	0.74	0.02	-1.41	-0.44	0.28
rh_orbital gyri	0.71	0.09	0.71	0.02	0.16	0.05	0.90
rh_angular gyrus	0.70	0.02	0.71	0.01	-1.84	-0.58	0.16
rh_supramarginal gyrus	0.70	0.02	0.71	0.01	-1.52	-0.48	0.24
rh_superior parietal lobule (lateral part of p1)	0.70	0.03	0.72	0.01	-2.53	-0.80	0.05
rh_postcentral gyrus	0.73	0.02	0.74	0.02	-2.03	-0.64	0.12
rh_precentral gyrus	0.75	0.02	0.75	0.02	-0.38	-0.12	0.78
rh_precuneus (medial part of p1)	0.73	0.02	0.73	0.01	-0.74	-0.23	0.57
rh_straight gyrus, gyrus rectus	0.73	0.13	0.70	0.02	0.84	0.26	0.52

rh_subcallosal area, subcallosal gyrus	0.60	0.08	0.63	0.10	-1.01	-0.32	0.44
rh_anterior transverse temporal gyrus (of heschl)	0.77	0.03	0.77	0.02	0.76	0.24	0.56
rh_lateral aspect of the superior temporal gyrus	0.72	0.02	0.72	0.02	-0.50	-0.16	0.72
rh_planum polare of the superior temporal gyrus	0.69	0.02	0.69	0.02	-0.27	-0.08	0.84
rh_planum temporale or temporal plane of the superior temporal gyrus	0.73	0.02	0.73	0.02	-0.90	-0.28	0.49
rh_Inferior temporal gyrus (t3)	0.72	0.02	0.73	0.02	-1.06	-0.34	0.42
rh_middle temporal gyrus (t2)	0.70	0.02	0.70	0.01	-0.26	-0.08	0.85
rh_horizontal ramus of the anterior segment of the lateral sulcus (or fissure)	0.73	0.02	0.74	0.03	-1.84	-0.58	0.16
rh_vertical ramus of the anterior segment of the lateral sulcus (or fissure)	0.71	0.03	0.72	0.02	-1.66	-0.53	0.20
rh_posterior ramus (or segment) of the lateral sulcus (or fissure)	0.74	0.02	0.74	0.02	-0.48	-0.15	0.73
rh_occipital pole	0.76	0.02	0.76	0.02	-0.69	-0.22	0.60
rh_temporal pole	0.70	0.02	0.70	0.02	-0.32	-0.10	0.81
rh_Calcarine sulcus	0.76	0.02	0.77	0.02	-0.74	-0.23	0.57
rh_Central sulcus (Rolando's fissure)	0.75	0.02	0.77	0.01	-3.26	-1.03	**0.01***
rh_marginal sulcus of cingulate gyrus	0.73	0.02	0.74	0.01	-2.21	-0.70	0.09
rh_anterior circular sulcus of the insula	0.69	0.02	0.70	0.02	-1.05	-0.33	0.42
rh_Inferior circular sulcus of the insula	0.71	0.02	0.70	0.02	0.39	0.12	0.78
rh_superior circular sulcus of the insula	0.71	0.02	0.71	0.02	-1.39	-0.44	0.28
rh_anterior transverse collateral sulcus	0.74	0.02	0.75	0.02	-0.85	-0.27	0.51
rh_posterior transverse collateral sulcus	0.79	0.03	0.78	0.04	0.86	0.27	0.50
rh_Inferior frontal sulcus	0.71	0.02	0.72	0.02	-1.37	-0.43	0.29
rh_middle frontal sulcus	0.68	0.02	0.69	0.01	-2.26	-0.72	0.08
rh_superior frontal sulcus	0.70	0.02	0.71	0.02	-0.90	-0.28	0.49
rh_Intermediate sulcus of Jensen	0.71	0.03	0.72	0.03	-2.02	-0.64	0.12
rh_Intraparietal sulcus and posterior transverse parietal sulcus	0.73	0.02	0.74	0.01	-2.35	-0.74	0.08
rh_middle occipital sulcus and sulcus lunatus (secondary intermediate sulcus)	0.74	0.02	0.74	0.02	-0.56	-0.18	0.68
rh_superior occipital sulcus and transverse occipital sulcus (superior intermediate sulcus)	0.73	0.02	0.75	0.01	-2.60	-0.82	**0.05***
rh_anterior occipital sulcus	0.74	0.03	0.75	0.02	-0.32	-0.10	0.81

rh_lateral occipito-temporal sulcus	0.76	0.03	0.76	0.02	0.14	0.04	0.91
rh_medial occipito-temporal sulcus and lingual sulcus	0.76	0.03	0.76	0.02	-0.06	-0.02	0.96
rh_lateral orbital sulcus	0.68	0.02	0.69	0.02	-1.71	-0.54	0.19
rh_medial orbital sulcus, olfactory sulcus	0.71	0.07	0.72	0.03	-0.65	-0.21	0.62
rh_h-shaped orbital sulcus	0.71	0.04	0.72	0.02	-1.17	-0.37	0.37
rh_parieto-occipital sulcus	0.76	0.02	0.76	0.02	-0.50	-0.16	0.72
rh_pericallosal sulcus	0.78	0.03	0.78	0.03	-0.29	-0.09	0.83
rh_postcentral sulcus	0.74	0.02	0.74	0.02	-0.81	-0.26	0.53
rh_Inferior part of the precentral sulcus	0.71	0.02	0.72	0.01	-0.81	-0.26	0.53
rh_superior part of the precentral sulcus	0.72	0.02	0.74	0.02	-2.36	-0.74	0.07
rh_suborbital sulcus	0.70	0.05	0.69	0.02	0.87	0.28	0.50
rh_subparietal sulcus	0.74	0.02	0.74	0.01	-0.72	-0.23	0.59
rh_Inferior temporal sulcus	0.72	0.02	0.72	0.02	0.27	0.08	0.84
rh_superior temporal sulcus	0.73	0.02	0.73	0.01	-0.88	-0.28	0.49
rh_transverse temporal sulcus (heschl's gyrus)	0.76	0.02	0.76	0.02	0.03	0.01	0.97

p < ,05, **p < 0,01, ***p < ,001;AQP4 = aquaporin-4; HC = healthy controls; NMOSD = neuromyelitis optica spectrum disorders; lh = left hemisphere; rh = right hemisphere; *n* = number of participants.

Supplementary Table 12. Comparison of T1 relaxation rates in cerebral cortex between MS and AQP4-NMOSD patients

Parcellation	MS (*n* = 17)		AQP4-NMOSD (*n* = 20)		T-value	Cohen's d	p-value (FDR corrected)
	M	*SD*	*M*	*SD*			
lh_unknown	0,18	0,02	0,17	0,02	-0.90	-0.30	0.49
lh_Fronto-marginal gyrus (of Wernicke) and sulcus	0,67	0,01	0,68	0,03	1.08	0.33	0.41
lh_Inferior occipital gyrus (o3) and sulcus	0,73	0,02	0,75	0,03	2.17	0.69	0.10
lh_paracentral lobule and sulcus	0,74	0,02	0,75	0,02	1.35	0.44	0.29
lh_subcentral gyrus (central operculum) and sulci	0,70	0,01	0,72	0,02	4.29	1.37	**0.00****
lh_transverse frontopolar gyri and sulci	0,66	0,01	0,66	0,03	1.13	0.35	0.39
lh_anterior part of the cingulate gyrus and sulcus (aCC)	0,68	0,01	0,68	0,02	1.77	0.55	0.18
lh_middle-anterior part of the cingulate gyrus and sulcus (amCC)	0,69	0,01	0,70	0,02	1.35	0.43	0.29
lh_middle-posterior part of the cingulate gyrus and sulcus (pmCC)	0,71	0,02	0,71	0,02	1.50	0.50	0.25
lh_posterior-dorsal part of the cingulate gyrus (dpCC)	0,72	0,01	0,73	0,02	1.91	0.60	0.14
lh_posterior-ventral part of the cingulate gyrus (vpCC, isthmus of the cingulate gyrus)	0,75	0,01	0,77	0,03	3.05	0.95	**0.02***
lh_Cuneus (o6)	0,73	0,02	0,74	0,03	0.63	0.20	0.63
lh_opercular part of the inferior frontal gyrus	0,69	0,01	0,70	0,02	2.99	0.95	**0.02***
lh_orbital part of the inferior frontal gyrus	0,68	0,02	0,69	0,02	2.47	0.80	0.06
lh_triangular part of the inferior frontal gyrus	0,68	0,01	0,69	0,02	2.22	0.71	0.09
lh_middle frontal gyrus (F2)	0,67	0,01	0,68	0,02	1.90	0.60	0.14
lh_superior frontal gyrus (F1)	0,68	0,01	0,69	0,02	1.42	0.45	0.27
lh_long insular gyrus and central sulcus of the insula	0,68	0,01	0,69	0,02	1.84	0.59	0.16
lh_short insular gyri	0,66	0,01	0,67	0,01	3.33	1.07	**0.01***
lh_middle occipital gyrus (o2, lateral occipital gyrus)	0,71	0,01	0,72	0,02	1.39	0.45	0.28
lh_superior occipital gyrus (o1)	0,72	0,02	0,73	0,02	1.19	0.38	0.36
lh_lateral occipito-temporal gyrus (fusiform gyrus, o4-t4)	0,72	0,02	0,74	0,03	3.27	1.03	**0.01***

lh_lingual gyrus, lingual part of the medial occipito-temporal gyrus, (o5)	0,73	0,02	0,75	0,02	2.53	0.81	0.05
lh_parahippocampal gyrus, parahippocampal part of the medial occipito-temporal gyrus, (t5)	0,70	0,02	0,72	0,02	3.44	1.12	**0.01***
lh_orbital gyri	0,70	0,01	0,72	0,06	1.65	0.51	0.21
lh_angular gyrus	0,68	0,01	0,69	0,02	1.34	0.42	0.30
lh_supramarginal gyrus	0,69	0,01	0,70	0,02	2.32	0.73	0.08
lh_superior parietal lobule (lateral part of p1)	0,69	0,01	0,70	0,02	1.01	0.32	0.44
lh_postcentral gyrus	0,71	0,02	0,72	0,04	1.05	0.33	0.42
lh_precentral gyrus	0,73	0,02	0,74	0,02	1.67	0.53	0.20
lh_precuneus (medial part of p1)	0,71	0,01	0,71	0,02	1.20	0.37	0.36
lh_straight gyrus, gyrus rectus	0,69	0,01	0,72	0,09	1.61	0.49	0.22
lh_subcallosal area, subcallosal gyrus	0,64	0,07	0,66	0,06	0.91	0.31	0.49
lh_anterior transverse temporal gyrus (of heschl)	0,74	0,02	0,75	0,04	0.15	0.05	0.90
lh_lateral aspect of the superior temporal gyrus	0,69	0,01	0,70	0,02	2.31	0.74	0.08
lh_planum polare of the superior temporal gyrus	0,67	0,01	0,67	0,02	0.45	0.14	0.75
lh_planum temporale or temporal plane of the superior temporal gyrus	0,70	0,02	0,70	0,04	-0.47	-0.15	0.73
lh_Inferior temporal gyrus (t3)	0,69	0,02	0,71	0,02	3.42	1.10	**0.01***
lh_middle temporal gyrus (t2)	0,68	0,01	0,69	0,02	1.94	0.61	0.14
lh_horizontal ramus of the anterior segment of the lateral sulcus (or fissure)	0,70	0,01	0,74	0,02	4.98	1.57	**0.00****
lh_vertical ramus of the anterior segment of the lateral sulcus (or fissure)	0,71	0,02	0,72	0,02	2.56	0.84	**0.05***
lh_posterior ramus (or segment) of the lateral sulcus (or fissure)	0,73	0,02	0,74	0,02	1.38	0.44	0.29
lh_occipital pole	0,74	0,02	0,76	0,03	2.43	0.77	0.06
lh_temporal pole	0,67	0,01	0,69	0,02	2.64	0.82	**0.05***
lh_Calcarine sulcus	0,74	0,02	0,75	0,03	2.45	0.78	0.06
lh_Central sulcus (Rolando's fissure)	0,74	0,01	0,74	0,03	-0.01	0.00	0.99
lh_marginal sulcus of cingulate gyrus	0,70	0,02	0,71	0,02	1.35	0.44	0.29
lh_anterior circular sulcus of the insula	0,68	0,01	0,70	0,02	3.43	1.09	**0.01***
lh_Inferior circular sulcus of the insula	0,69	0,01	0,69	0,02	0.07	0.02	0.96
lh_superior circular sulcus of the insula	0,70	0,01	0,72	0,02	4.02	1.28	**0.00****

lh_anterior transverse collateral sulcus	0,68	0,02	0,71	0,03	3.60	1.14	**0.01****
lh_posterior transverse collateral sulcus	0,75	0,02	0,78	0,04	2.95	0.93	**0.03***
lh_Inferior frontal sulcus	0,70	0,01	0,71	0,02	2.10	0.67	0.11
lh_middle frontal sulcus	0,68	0,01	0,68	0,02	1.44	0.46	0.27
lh_superior frontal sulcus	0,69	0,01	0,70	0,02	2.64	0.83	**0.05***
lh_Intermediate sulcus of Jensen	0,69	0,01	0,70	0,04	1.43	0.44	0.27
lh_Intraparietal sulcus and posterior transverse parietal sulcus	0,71	0,01	0,72	0,02	1.88	0.60	0.15
lh_middle occipital sulcus and sulcus lunatus (secondary intermediate sulcus)	0,72	0,01	0,73	0,03	1.10	0.35	0.40
lh_superior occipital sulcus and transverse occipital sulcus (superior intermediate sulcus)	0,72	0,02	0,72	0,02	-0.05	-0.02	0.96
lh_anterior occipital sulcus	0,72	0,02	0,73	0,03	1.35	0.43	0.29
lh_lateral occipito-temporal sulcus	0,71	0,02	0,73	0,04	2.51	0.78	0.06
lh_medial occipito-temporal sulcus and lingual sulcus	0,72	0,02	0,75	0,03	4.02	1.26	**0.00****
lh_lateral orbital sulcus	0,68	0,01	0,69	0,02	2.30	0.74	0.08
lh_medial orbital sulcus, olfactory sulcus	0,71	0,01	0,73	0,04	1.74	0.53	0.19
lh_h-shaped orbital sulcus	0,71	0,02	0,73	0,03	2.59	0.82	**0.05***
lh_parieto-occipital sulcus	0,74	0,01	0,75	0,02	2.02	0.63	0.12
lh_pericallosal sulcus	0,74	0,04	0,77	0,03	2.53	0.85	0.05
lh_postcentral sulcus	0,71	0,01	0,73	0,03	2.27	0.71	0.08
lh_Inferior part of the precentral sulcus	0,70	0,01	0,71	0,02	0.96	0.30	0.47
lh_superior part of the precentral sulcus	0,71	0,01	0,72	0,02	1.05	0.33	0.43
lh_suborbital sulcus	0,68	0,01	0,69	0,03	1.93	0.60	0.14
lh_subparietal sulcus	0,72	0,01	0,73	0,02	1.80	0.57	0.17
lh_Inferior temporal sulcus	0,69	0,01	0,72	0,03	3.81	1.19	**0.01***
lh_superior temporal sulcus	0,70	0,01	0,72	0,02	2.60	0.83	**0.05***
lh_transverse temporal sulcus (heschl's gyrus)	0,74	0,02	0,74	0,03	0.17	0.05	0.89
rh_unknown	0,17	0,01	0,16	0,02	-1.24	-0.40	0.34
rh_Fronto-marginal gyrus (of Wernicke) and sulcus	0,67	0,01	0,69	0,10	0.93	0.28	0.49
rh_Inferior occipital gyrus (o3) and sulcus	0,74	0,02	0,75	0,03	1.36	0.44	0.29
rh_paracentral lobule and sulcus	0,74	0,01	0,76	0,02	2.85	0.90	**0.03***
rh_subcentral gyrus (central operculum) and sulci	0,72	0,02	0,73	0,02	1.52	0.49	0.24
rh_transverse frontopolar gyri and sulci	0,65	0,01	0,66	0,03	0.41	0.13	0.77

rh_anterior part of the cingulate gyrus and sulcus (aCC)	0,67	0,01	0,69	0,02	4.12	1.30	**0.00****
rh_middle-anterior part of the cingulate gyrus and sulcus (amCC)	0,69	0,01	0,71	0,02	3.78	1.21	**0.01****
rh_middle-posterior part of the cingulate gyrus and sulcus (pmCC)	0,72	0,01	0,73	0,02	3.15	0.99	**0.02***
rh_posterior-dorsal part of the cingulate gyrus (dpCC)	0,73	0,01	0,74	0,02	2.74	0.87	**0.04***
rh_posterior-ventral part of the cingulate gyrus (vpCC, isthmus of the cingulate gyrus)	0,76	0,03	0,78	0,03	2.16	0.71	0.10
rh_Cuneus (o6)	0,74	0,02	0,75	0,02	0.32	0.10	0.81
rh_opercular part of the inferior frontal gyrus	0,69	0,01	0,70	0,02	1.93	0.61	0.14
rh_orbital part of the inferior frontal gyrus	0,68	0,02	0,69	0,02	1.89	0.61	0.14
rh_triangular part of the inferior frontal gyrus	0,69	0,01	0,69	0,02	0.44	0.14	0.75
rh_middle frontal gyrus (F2)	0,67	0,01	0,68	0,02	1.83	0.58	0.16
rh_superior frontal gyrus (F1)	0,68	0,01	0,69	0,02	3.31	1.04	**0.01***
rh_long insular gyrus and central sulcus of the insula	0,67	0,01	0,68	0,01	1.36	0.45	0.29
rh_short insular gyri	0,67	0,01	0,68	0,01	1.64	0.53	0.20
rh_middle occipital gyrus (o2, lateral occipital gyrus)	0,71	0,01	0,72	0,02	2.09	0.65	0.11
rh_superior occipital gyrus (o1)	0,73	0,01	0,73	0,02	1.03	0.33	0.43
rh_lateral occipito-temporal gyrus (fusiform gyrus, o4-t4)	0,76	0,01	0,77	0,02	1.74	0.55	0.18
rh_lingual gyrus, lingual part of the medial occipito-temporal gyrus, (o5)	0,75	0,02	0,76	0,02	0.94	0.30	0.47
rh_parahippocampal gyrus, parahippocampal part of the medial occipito-temporal gyrus, (t5)	0,72	0,01	0,73	0,02	2.03	0.65	0.12
rh_orbital gyri	0,69	0,01	0,71	0,09	1.06	0.32	0.42
rh_angular gyrus	0,70	0,01	0,70	0,02	0.78	0.25	0.55
rh_supramarginal gyrus	0,70	0,01	0,70	0,02	0.59	0.19	0.66
rh_superior parietal lobule (lateral part of p1)	0,70	0,01	0,70	0,03	0.10	0.03	0.94
rh_postcentral gyrus	0,72	0,02	0,73	0,02	0.52	0.17	0.71
rh_precentral gyrus	0,74	0,01	0,75	0,02	2.23	0.71	0.09
rh_precuneus (medial part of p1)	0,72	0,01	0,73	0,02	1.85	0.58	0.16
rh_straight gyrus, gyrus rectus	0,69	0,01	0,73	0,13	1.27	0.38	0.34

rh_subcallosal area, subcallosal gyrus	0,58	0,11	0,60	0,08	0.66	0.22	0.62
rh_anterior transverse temporal gyrus (of heschl)	0,76	0,02	0,77	0,03	1.77	0.58	0.17
rh_lateral aspect of the superior temporal gyrus	0,71	0,01	0,72	0,02	1.66	0.54	0.20
rh_planum polare of the superior temporal gyrus	0,68	0,02	0,69	0,02	2.79	0.91	**0.03***
rh_planum temporale or temporal plane of the superior temporal gyrus	0,72	0,02	0,73	0,02	1.17	0.39	0.37
rh_Inferior temporal gyrus (t3)	0,72	0,01	0,72	0,02	1.08	0.34	0.41
rh_middle temporal gyrus (t2)	0,69	0,01	0,70	0,02	2.33	0.75	0.08
rh_horizontal ramus of the anterior segment of the lateral sulcus (or fissure)	0,72	0,01	0,73	0,02	2.21	0.71	0.09
rh_vertical ramus of the anterior segment of the lateral sulcus (or fissure)	0,71	0,02	0,71	0,03	-0.36	-0.11	0.80
rh_posterior ramus (or segment) of the lateral sulcus (or fissure)	0,74	0,01	0,74	0,02	0.86	0.27	0.51
rh_occipital pole	0,75	0,02	0,76	0,02	1.31	0.42	0.31
rh_temporal pole	0,69	0,01	0,70	0,02	2.33	0.75	0.08
rh_Calcarine sulcus	0,75	0,02	0,76	0,02	1.60	0.51	0.22
rh_Central sulcus (Rolando's fissure)	0,75	0,01	0,75	0,02	0.65	0.21	0.62
rh_marginal sulcus of cingulate gyrus	0,72	0,01	0,73	0,02	1.28	0.41	0.32
rh_anterior circular sulcus of the insula	0,69	0,01	0,69	0,02	1.98	0.64	0.13
rh_Inferior circular sulcus of the insula	0,70	0,01	0,71	0,02	1.94	0.62	0.14
rh_superior circular sulcus of the insula	0,70	0,01	0,71	0,02	1.41	0.45	0.27
rh_anterior transverse collateral sulcus	0,73	0,02	0,74	0,02	1.51	0.49	0.25
rh_posterior transverse collateral sulcus	0,78	0,03	0,79	0,03	1.19	0.38	0.36
rh_Inferior frontal sulcus	0,71	0,02	0,71	0,02	0.64	0.21	0.63
rh_middle frontal sulcus	0,68	0,01	0,68	0,02	0.33	0.10	0.81
rh_superior frontal sulcus	0,69	0,01	0,70	0,02	2.01	0.63	0.12
rh_Intermediate sulcus of Jensen	0,70	0,02	0,71	0,03	0.56	0.18	0.68
rh_Intraparietal sulcus and posterior transverse parietal sulcus	0,73	0,01	0,73	0,02	0.44	0.14	0.75
rh_middle occipital sulcus and sulcus lunatus (secondary intermediate sulcus)	0,73	0,02	0,74	0,02	1.07	0.35	0.41
rh_superior occipital sulcus and transverse occipital sulcus (superior intermediate sulcus)	0,74	0,01	0,73	0,02	-0.24	-0.08	0.85
rh_anterior occipital sulcus	0,74	0,02	0,74	0,03	1.17	0.37	0.37

rh_lateral occipito-temporal sulcus	0,75	0,02	0,76	0,03	1.13	0.36	0.39
rh_medial occipito-temporal sulcus and lingual sulcus	0,74	0,02	0,76	0,03	2.67	0.85	**0.04***
rh_lateral orbital sulcus	0,68	0,02	0,68	0,02	0.78	0.25	0.55
rh_medial orbital sulcus, olfactory sulcus	0,69	0,02	0,71	0,07	1.18	0.36	0.37
rh_h-shaped orbital sulcus	0,69	0,01	0,71	0,04	1.32	0.41	0.31
rh_parieto-occipital sulcus	0,76	0,01	0,76	0,02	0.95	0.30	0.47
rh_pericallosal sulcus	0,72	0,07	0,78	0,03	3.24	1.14	**0.02***
rh_postcentral sulcus	0,73	0,02	0,74	0,02	1.35	0.44	0.29
rh_Inferior part of the precentral sulcus	0,70	0,01	0,71	0,02	2.03	0.65	0.12
rh_superior part of the precentral sulcus	0,72	0,01	0,72	0,02	0.67	0.21	0.62
rh_suborbital sulcus	0,67	0,01	0,70	0,05	2.09	0.64	0.12
rh_subparietal sulcus	0,72	0,01	0,74	0,02	2.35	0.73	0.08
rh_Inferior temporal sulcus	0,71	0,02	0,72	0,02	2.05	0.65	0.12
rh_superior temporal sulcus	0,72	0,01	0,73	0,02	1.69	0.54	0.19
rh_transverse temporal sulcus (heschl's gyrus)	0,75	0,01	0,76	0,02	2.11	0.67	0.11

p < ,05, **p < 0,01, ***p < ,001;AQP4 = aquaporin-4; MS = multiple sclerosis HC = healthy controls; NMOSD = neuromyelitis optica spectrum disorders; lh = left hemisphere; rh = right hemisphere; *n* = number of participants.

Supplementary Table 13. Pairwise correlations between NDI in white matter fibres not traversing through white matter lesions and the number of cortical lesions in MS patients

Variable1	Variable 2	Rho	*n*	p-value (FDR corrected)
CL	LIT_AF_left	-0.68	20	**0.00****
CL	LIT_AF_right	-0.80	20	**0.00*****
CL	LIT_ATR_left	-0.55	20	**0.02***
CL	LIT_ATR_right	-0.57	20	**0.01***
CL	LIT_CC_1	-0.81	20	**0.00*****
CL	LIT_CC_2	-0.84	20	**0.00*****
CL	LIT_CC_3	-0.84	18	**0.00*****
CL	LIT_CC_4	-0.55	15	**0.04***
CL	LIT_CC_5	-0.56	18	**0.02***
CL	LIT_CC_6	-0.73	20	**0.00*****
CL	LIT_CC_7	-0.70	18	**0.00****
CL	LIT_CG_left	-0.84	20	**0.00*****
CL	LIT_CG_right	-0.78	20	**0.00*****
CL	LIT_CST_left	-0.58	20	**0.01***
CL	LIT_CST_right	-0.50	20	**0.04***
CL	LIT_FPT_left	-0.74	20	**0.00*****
CL	LIT_FPT_right	-0.67	20	**0.00****
CL	LIT_ICP_left	-0.33	20	0.18
CL	LIT_ICP_right	-0.09	20	0.72
CL	LIT_IFO_left	-0.28	17	0.30
CL	LIT_IFO_right	-0.56	18	**0.02***
CL	LIT_ILF_left	-0.57	19	**0.02***
CL	LIT_ILF_right	-0.52	17	**0.04***
CL	LIT_MCP_BI	-0.21	20	0.38
CL	LIT_OR_left	-0.35	15	0.23
CL	LIT_OR_right	-0.57	14	**0.04***
CL	LIT_POPT_left	-0.44	20	0.07
CL	LIT_POPT_right	-0.24	19	0.33
CL	LIT_SCP_left	-0.28	20	0.25
CL	LIT_SCP_right	0.16	20	0.51
CL	LIT_SLF_III_left	-0.68	20	**0.00****
CL	LIT_SLF_III_right	-0.80	20	**0.00*****
CL	LIT_SLF_II_left	-0.65	19	**0.01***
CL	LIT_SLF_II_right	-0.77	20	**0.00*****

CL	LIT_SLF_I_left	-0.83	19	**0.00*** **
CL	LIT_SLF_I_right	-0.72	19	**0.00** **
CL	LIT_STR_left	-0.67	18	**0.01** **
CL	LIT_STR_right	-0.63	19	**0.01** **
CL	LIT_ST_FO_left	-0.68	20	**0.00** **
CL	LIT_ST_FO_right	-0.63	20	**0.01** **
CL	LIT_ST_PREM_left	-0.76	20	**0.00*** **
CL	LIT_ST_PREM_right	-0.74	20	**0.00*** **
CL	LIT_T_OCC_left	-0.35	16	0.21
CL	LIT_T_OCC_right	-0.61	14	**0.03** *
CL	LIT_T_PAR_left	-0.54	20	**0.02** *
CL	LIT_T_PAR_right	-0.34	19	0.18
CL	LIT_T_PREM_left	-0.66	20	**0.00** **
CL	LIT_T_PREM_right	-0.71	20	**0.00** **
CL	LIT_UF_left	-0.59	20	**0.01** *
CL	LIT_UF_right	-0.65	20	**0.00** **

*p < ,05, **p < 0,01, ***p < 0,001; MS,= multiple sclerosis; NDI = neurite density index; CL= cortical lesions count; *n* = number of observations; AF = arcuate fascicle; ATR = anterior thalamic radiation; CC = corpus callosum; CC_1 = rostrum; CC_2 = genu; CC_3 = rostral body; CC_4 = anterior midbody; CC_5 = posterior midbody; CC_6 = isthmus; CC_7 = splenium; CG = cingulum; CST = corticospinal tract; FPT = fronto-pontine tract; ICP = inferior cerebellar peduncle; IFO = inferior occipito-frontal fascicle; ILF = inferior longitudinal fascicle; MCP = middle cerebellar peduncle; OR = optic radiation; POPT = parieto‑occipital pontine tract; SCP = superior cerebellar peduncle; SLF_I = superior longitudinal fascicle I; SLF_II = superior longitudinal fascicle II; SLF_III = superior longitudinal fascicle III; STR = superior thalamic radiation; ST_FO = striato-fronto-orbital; ST_PREM = striato-premotor; T_OCC = thalamo-occipital; T_PAR = thalamo-parietal; T_PREM = thalamo-premotor; UF = uncinate fascicle.

LIST OF FIGURES AND TABLES

Figure 1. Graphical representation of different pathophysiological mechanisms in MS and NMOSD..... 19
Figure 2. Examples of conventional MRI findings in MS..... 28
Figure 3. Examples of conventional MRI findings in NMOSD.....28
Table 1. Key features of MS and NMOSD facilitating differential diagnosis.....30
Figure 4. Graphical overview of non-conventional MRI methods.....39
Figure 5. Examples of PRL visible on FLAIR and corresponding QSM images..... 45
Figure 6. Flowchart of the brain-related dataset analysis process.....48
Table 2. Demographics and clinical/MRI characteristics of patients and controls.....52
Figure 7. Mean bundle load in MS and AQP4-NMOSD..... 53
Figure 8. Significant differences in mean NDI between MS and AQP4-NMOSD.....55
Figure 9. Significant differences in mean T1 relaxation rates observed between the studied groups.....57
Figure 10. Between-group differences in mean CSA of the cervical spinal cord..... 58
Supplementary Table 1. Comparison of NDI between MS and AQP4-NMOSD patients in unsegmented white matter tracts..... 88
Supplementary Table 2. Comparison of NDI between MS and AQP4-NMOSD patients in white matter fibers traversing through white matter lesions..... 90
Supplementary Table 3. Comparison of NDI between MS and AQP4-NMOSD patients in white matter fibers not traversing through white matter lesions.....92
Supplementary Table 4. Comparison of NDI in unsegmented white matter tracts between in MS patients and whole tracts in HC.....94
Supplementary Table 5. Comparison of NDI in white matter fibers traversing through white matter lesions in MS patients and whole tracts in HC..... 96
Supplementary Table 6. Comparison of NDI in white matter fibers not traversing through white matter lesions in MS patients and whole tracts in HC..... 98
Supplementary Table 7. Comparison of NDI in unsegmented white matter tracts between AQP4-NMOSD patients and HC..... 100
Supplementary Table 8. Comparison of NDI in white matter fibers traversing through white matter lesions in AQP4-NMOSD patients and whole tracts in HC..... 102
Supplementary Table 9. Comparison of NDI in white matter fibers not traversing through white matter lesions in AQP4-NMOSD patients and whole tracts in HC..... 104
Supplementary Table 10. Comparison of T1 relaxation rates in cerebral cortex between MS patients and HC..... 106
Supplementary Table 11. Comparison of T1 relaxation rates in cerebral cortex between AQP4-NMOSD patients and HC.....112
Supplementary Table 12. Comparison of T1 relaxation rates in cerebral cortex between MS and AQP4-NMOSD patients..... 118
Supplementary Table 13. Pairwise correlations between NDI in white matter fibres not traversing through white matter lesions and the number of cortical lesions in MS patients..124

PUBLICATIONS OF THE PhD CANDIDATE

Authors who equally contributed to a publication are marked with *

1. **Paweł Jakuszyk***, Aleksandra Podlecka-Piętowska*, Bartosz Kossowski, Monika Nojszewska, Beata Zakrzewska-Pniewska, Maciej Juryńczyk “Patterns of cerebral damage in multiple sclerosis and aquaporin-4 antibody-positive neuromyelitis optica spectrum disorders—major differences revealed by non-conventional imaging”, *Brain Communications*, Volume 6, Issue 5, 2024, https://doi.org/10.1093/braincomms/fcae295.

2. **Paweł Jakuszyk**, Piotr Szukało, Bartosz Kossowski, Maciej Juryńczyk “Anterograde and trans-synaptic neurodegeneration in aquaporin-4-antibody NMOSD patients with a history of transverse myelitis”, In review, *Brain Communications.*

3. Maciej Juryńczyk, **Paweł Jakuszyk**, Iwona Kurkowska-Jastrzębska, Jacqueline Palace “Increasing role of imaging in differentiating MS from non-MS and defining indeterminate borderline cases” *Neurologia i neurochirurgia polska*, 56(3), 210–219. https://doi.org/10.5603/PJNNS.a2021.0077.

4. Anna Żochowska*, **Paweł Jakuszyk***, Maria M. Nowicka, Anna Nowicka, “Are covered faces eye-catching for us? The impact of masks on attentional processing of self and other faces during the COVID-19 pandemic”, *Cortex*, Volume 149, 2022, Pages 173-187, ISSN 0010-9452, https://doi.org/10.1016/j.cortex.2022.01.015.

5. Anna Żochowska, **Paweł Jakuszyk**, Maria M. Nowicka, Anna Nowicka, “The self and a close-other: differences between processing of faces and newly acquired information”, *Cerebral Cortex*, Volume 33, Issue 5, 1 March 2023, Pages 2183–2199, https://doi.org/10.1093/cercor/bhac201.